ROBUST DATA-DRIVEN FIXED-ORDER H_∞ CONTROLLER SYNTHESIS USING CONVEX OPTIMIZATION

KONVEKS OPTİMİZASYON KULLANARAK VERİYE DAYALI SABİT DERECELİ GÜRBÜZ H_∞ KONTROLCÜ SENTEZİ

ERSİN DAŞ

Assoc. Prof. Dr. SELAHATTİN ÇAĞLAR BAŞLAMIŞLI

Supervisor

Submitted to

Graduate School of Science and Engineering of Hacettepe University

as a Partial Fulfillment to the Requirements

for the Award of the Degree of Doctor of Philosophy

in Mechanical Engineering.

2019

This thesis is dedicated to the Republic of Turkey.

ABSTRACT

ROBUST DATA-DRIVEN FIXED-ORDER H_∞ CONTROLLER SYNTHESIS USING CONVEX OPTIMIZATION

ERSİN DAŞ

Doctor of Philosophy, Department of Mechanical Engineering

Supervisor: Assoc. Prof. Dr. Selahattin Çağlar BAŞLAMIŞLI

October 2019, 111 pages

The main objective of this thesis study is to develop fixed-order (low-order) structured controller design methods for frequency domain non-parametric uncertain systems using convex optimization. The majority of the available controller synthesis methods are based on the mathematical model of the system dynamics. The performance of these model based control methods entirely relies on the accuracy of the model. Model uncertainty, due to unmodeled system dynamics, nonlinearities and operating point changes, are almost inevitable and may cause controller performance degradation due to the fact that there is always a trade-off between performance of the closed loop system and robustness. Therefore, model based methods may impede desired high performance requirements of today's industrial complex dynamical systems.

In this thesis, a novel robust data-driven fixed-order H_∞ controller design method based on convex optimization is proposed for linear single input single output systems. Linear time-invariant systems represented by non-parametric frequency domain data and linearly parameterized controllers are considered. The proposed approach renders the need for a mathematical model of the controlled plant unnecessary. First, a semi-definite convex optimization algorithm, which is based on the concept of the Chebyshev center of a set of points, is proposed to simultaneo-

usly compute a minimal uncertainty bound and corresponding nominal model from the experimental data. Thanks to this algorithm, multiple measurements can be considered in the robust control design method instead of one set of measurement with minimal uncertainty bound. Then, a new sufficient robust performance condition is derived using Nyquist stability theorem and μ synthesis methods on the Nyquist plot.

Low-order controllers such as lead-lag compensators and proportional integral derivative (PID) controller are much desired in today's industrial process due to their engineering advantages. Therefore, a convex optimization method is developed which optimizes the coefficients of the fixed-order controllers while guaranteeing internal stability and robustness. Furthermore, the proposed method allows formulating closed-loop model matching objective and control input constraints by convex functions. An extension of the one degree of freedom controller design algorithm is proposed to synthesise two degree of freedom controllers for reference tracking of the non-parametric systems. The presented theoretical design approaches are experimentally verified on position control of an electromechanical actuation systems of an air vehicle.

Keywords: Data-driven control, Robust H_∞ control, Convex optimization, Model matching, 2-DOF control, Laguerre basis function

ÖZET

KONVEKS OPTİMİZASYON KULLANARAK VERİYE DAYALI SABİT DERECELİ GÜRBÜZ H_∞ KONTROLCÜ SENTEZİ

ERSİN DAŞ

Doktora, Makine Mühendisliği Bölümü

Tez Danışmanı: Doç. Dr. Selahattin Çağlar BAŞLAMIŞLI

Ekim 2019, 111 sayfa

Bu tez çalışmasının temel amacı, frekans düzleminde parametrik olmayan sistemler için sabit dereceli (düşük mertebeli) kontrolcü sentezleme metodu geliştirmektir. Mevcut kontrolcü sentez yöntemlerinin çoğu, sistem dinamiğinin matematiksel modeline dayanmaktadır. Bu model tabanlı kontrol yöntemlerinin performansı büyük oranda modelin doğruluğuna bağlıdır. Modellenemeyen sistem dinamikleri, doğrusalsızlıklar ve çalışma noktası değişiminden kaynaklanan model belirsizlikleri neredeyse kaçınılmazdır ve kapalı çevrim sistemin performansı ve gürbüzlüğü arasında bir denge olduğu için kontrolcü performansının düşmesine neden olabilir. Bu nedenle, model tabanlı yöntemler günümüzün karmaşık yapılı endüstriyel dinamik sistemlerinin istenen yüksek performans gereksinimlerini sağlamasını engelleyebilir.

Bu tez çalışmasında, tek giriş tek çıkışlı doğrusal sistemler için konveks optimizasyon temelli ve veriye dayalı, sabit dereceli yeni bir H_∞ kontrolcü tasarım metodu önerilmiştir. Frekans düzleminde parametrik olmayan doğrusal zamanla değişmeyen sistemler ve doğrusal olarak parametrelenebilir kontrolcüler ele alınmıştır. Önerilen yaklaşım, kontrol edilen sistemin matematiksel modeline duyulan ihtiyacı gereksiz kılmaktadır. İlk olarak, minimum belirsizlik bandı ve ilgili nominal modelin birlikte seçimine yönelik, bir noktalar kümesinin Chebyshev merkezi konseptine dayanan yarı tanımlı konveks optimizasyon algortiması önerilmiştir. Gürbüz kontrolcü tasarımında çoklu ölçüm verileri, tek bir ölçüm verisi yerine bu algoritma sayesinde minimum be-

lelirsizlik bandı ile temsil edilerek kullanılabilir. Daha sonra, Nyquist kararlılık teoremi ve μ sentezi metotları kullanılarak gürbüz performans kriteri için Nyquist grafiği üzerinde yeni bir yeterli koşul türetilmiştir.

İleri-geri kompanzatörler ve PID gibi düşük mertebeli kontrolcüler, sahip oldukları mühendislik avantajlarından dolayı günümüz endüstrisinde daha çok tercih edilirler. Bu nedenle, hem iç kararlılık ve gürbüzlüğü garanti eden hem de sabit dereceli kontrolcü parametrelerini optimize eden bir konveks optimizasyon algoritması geliştirilmiştir. Bunun yanısıra, kapalı çevrim model eşleme problemi ve kontrol girdisi kısıtı önerilen yöntemde konveks fonkiyonlar ile uygulanabilmektedir. Tek serbestik dereceli kontrolcü tasarım algoritması, parametrik olmayan sistemlerin referans takibi için iki serbestlik dereceli kontrolcü sentezine genişletilmiştir. Sunulan teorik yaklaşımlar bir hava aracının elektromekanik eyletim sistemi üzerinde denyesel olarak doğrulanmıştır.

Anahtar Kelimeler: Veriye dayalı kontrol, Gürbüz H_∞ kontrol, Konveks optimizasyon, Model eşleme, 2-DOF kontrol, Laguerre temel fonskiyonu

ACKNOWLEDGMENTS

First of all, I would like to thank Allah for giving me the ability to complete this thesis.

I would like to express my sincere appreciation to my thesis advisor Assoc. Prof. Dr. S. Çağlar BAŞLAMIŞLI who guided me and gave me a lot of advice and corrections. I have learnt a lot from him and I could not complete this thesis if he did not give technical contributions. It was a great pleasure to work with him.

I would like to extend my appreciation to exam committee members, Prof. Dr. Mehmet Önder EFE, Asst. Prof. Dr. Bilsay SÜMER, Assoc. Prof. Dr. Yiğit YAZICIOĞLU and Prof. Dr. Hitay ÖZBAY for their contributions to my thesis.

I would also like to thank my colleagues Olcay ŞENEL, Dr. Mete AYDEMİR, Hamza KAMİŞLİ, Burak DENİZHAN, Murat KELEŞ, İsmail CANTÜRK and Selen İNCEGÖZ for their being good friends and their supports.

I am thankful to my family who raised me and always gave me their moral and material support for my whole life.

I am thankful to my beloved wife, Rahime, because of her endless support, toleration, patience understanding.

Finally, I also thank to TÜBİTAK SAGE for all the opportunities that they gave me throughout my thesis work.

TABLE OF CONTENTS

LIST OF FIGURES

LIST OF SYMBOLS AND ABBREVIATIONS

$\bar{\sigma}$	Maximum singular value
β	Confidence parameter
Δ	Uncertainty matrix
Δ_p	Fictitious performance block
$\frac{\partial f}{\partial x}$	Multidimensional partial derivative operator
ϵ	Risk parameter
γ	Disturbance attenuation level
λ_{ds}	d-axis flux linkage
λ_{qs}	q-axis flux linkage
λ_m	Flux linkage amplitude
$\mathbb{B}$	Ball
$\mathbb{E}$	Ellipsoid
μ	Structured singular value
ω	Exogenous input vector
ω_Δ	Perturbation output
$\overline{\nabla}$	Multidimensional gradient
$\overline{x}$	Vector of decision variables
$\overline{x}_c$	Chebyshev center
ψ	Vector of Laguerre basis functions
τ_d	Derivative time constant
θ	Deflection angle of the rotational systems
$\tilde{S}$	Perturbed sensitivity function
$\tilde{S}_{max}$	$\tilde{S}$ with the possible maximum magnitude
$\widehat{\phi}$	Spectral density function
$\widehat{G}_N$	Estimated linear plant model
$\widehat{R}$	Correlation function
ξ	Time scaling factor of the Laguerre functions
ζ	Damping ratio

G_{nom}^{opt}	Optimal nominal model
W_2^{opt}	Optimal multiplicative uncertainty model
B_e	Equivalent viscous damping
d_i	Input disturbance
d_o	Output disturbance
d_p	Number of optimization variables
e	Error signal
F	Feasible domain
$f(\overline{x})$	Objective function
F_e	equivalent Coulomb friction
G	Lapalace-domain system model
g	Time-domain system model
$g(\overline{x})$	Inequality constraints function
G_{nom}	Nominal system model
H	Hessian operator
$h(\overline{x})$	Equality constraints function
i_{ds}	d-axis current
i_{qs}	q-axis current
J_e	Equivalent moments of inertia
K	Controller
k	Vector of controller parameters
K_{ff}	Feedback controller
K_{ff}	Feedforward controller
$K_p,\ K_i,\ K_d$	Proportional gain, integral gain and derivative gain
K_t	Torque constant of the motor
L_{ds}	d-axis inductance
L_{qs}	q-axis inductance
L_d	Desired loop-gain
$M_e,\ N_e$	Coprime factor of a plant model

N	Number of samples
N_g	Mechanical reduction ratio
P	Generalized plant
Q	Q-parameter trasnfer function
r	Reference input
r_s	Stator resistance
s	Laplace transformvariable
S	Sensitivity function
T	Complementary sensitivity function
T_e	Electromagnetic torque
T_d	Reference model
T_L	Load torque
T_s	Sampling period
u	Input signal
v	Measurement noise
w	Frequency
W_A	Additive uncertainty weight
W_e	Error weighting function
W_M	Multiplicative uncertainty weight
w_r	Electrical angular velocity
W_1	Performance weighting function
W_2	Uncertainty weighting function
w_n	Natural frequency
W_u	Control signal weighting function
$X_e,\ Y_e$	Coprime factor of controller
y	Output signal
z	Performance variable
z_Δ	Perturbation input
z_Δ	Perturbation input

BLDC	Brushless DC
CAS	Control actuation system
CbT	Correlation-based tuning
DAQ	Data acquisition
DOF	Degree of freedom
EMA	Electromechanical actuator
ETFE	Empirical transfer function estimate
FDRC	frequency-domain robust control toolbox
FRF	Frequency response function
IFT	Iterative feedback tuning
ILC	Iterative learning control
KYP	Kalman-Yakubovich-Popov
LFT	Linear fractional transformation
LL	Lazy learning
LMI	Linear matrix inequality
LTI	Linear time invariant
MFAC	Model-free adaptive control
MIMO	Multiple input multiple output
MISO	Multiple input single output
PID	Proportional integral derivative
PRBS	Pseudo random binary sequence
QFT	Quantitative feedback theory
SDP	Semidefinite programming
SIP	Semi-infinite programming
SISO	Single input single output
SSV	Structured singular value
TVC	Thrust vector control
UC	Unfalsified control
VRFT	Virtual reference feedback tuning

1. INTRODUCTION

In this chapter, motivations, state of the art, contributions and organization of thesis are presented.

1.1 Motivation

Although the basic theorems about classical feedback control were introduced by Nyquist [1] and Bode [2] in the 20^{th} century, the first application of the feedback control systems is related to flow rate control of a water clock which was invented by Ctesibius of Alexandria in 3^{rd} century B.C. [3]. Since digital computers have become easily accessible, it is possible nowadays to implement advanced control algorithms in daily life and industrial processes. Therefore, researchers follow their studies in this field to propose new methods for feedback control systems.

It is well known that the principal aim of automatic control systems is to conveniently shape the feedback loop. Most of the available model based control methods in the literature such as PID control, H_∞ control, adaptive control, optimal control, and backstepping control require an accurate mathematical description of system dynamics under interest. The performance of these model based control methods entirely relies on the accuracy of the model. The mathematical models of physical systems are generally built based on laws of physics and system identification methods. As these modelling approaches provide mathematical descriptions of the real process; model uncertainty, due to noise and disturbance inputs, unmodeled dynamics, nonlinearities and operating point changes are almost always present and may cause controller performance degradation due to the fact that there is always a trade-off between performance of the closed loop system and robustness. Furthermore, it may be difficult to build a reliable parametric model from a set of measurements since this approach requires prior information about the model structure. Therefore, model based methods may impede desired closed loop performance requirements of today's industrial complex process.

Thanks to the developments in information science, alternative control methods called data-driven control have been proposed [4]. Unlike model based controller de-

sign methods, the controller synthesis in data-driven control methods is performed by using the input-output signals of the system without the need for a plant transfer function. Furthermore, analysis of the control system is also examined using the measured input-output data only. Thus, the need for a parametric plant model is eliminated and the controller structure is independent of the mathematical expression of the system. Data-driven control methods are more useful than model based control methods especially for systems which are difficult to model or have high-order complex transfer functions.

Three items, namely, a parametric model of the system, user-defined weighting functions and an uncertainty model, are required for model-based robust H_∞ control framework. The order of the resulting full-order robust controller is equal to the order of the augmented plant, i.e., the sum of the order of the three above mentioned function. Therefore, as the order of the system model or user-defined weighting functions increase, the order of the H_∞ controller also increases. These unstructured controllers may be as very high-order, which complicates implementation and readjustment.

Fixed-order (low-order) controllers such as lead-lag compensators and PID controller are preferred in practical industrial control applications because of their easily adjustable structures, practicality and low processing requirements on embedded system. The H_∞ control problem leads to an NP-hard non-convex problem, which is difficult to solve, in controller parameter space if a fixed-order controller structure is considered instead of a full-order controller in state space algorithms which are formed by two algebraic Ricatti equations [5], or linear matrix inequalities (LMI) [6] based solution algorithms [7]. Therefore, fixed-order H_∞ control problem remains an open problem in control theory.

The designed controller should be robust to the external disturbances and uncertainties such as changing environmental condition, operating point change, undefined system dynamics, materiel life and aging. Classical uncertainty modelling approach in robust control theory is generally calculated from a set of frequency response data. However, this approach produces a considerably large uncertainty magnitude. On the other hand, because of the contradictory features of performance and ro-

bustness, it is desirable that magnitude of the uncertainty models be as small as possible. Furthermore, the modelling of the uncertainty depends on a nominal model of the system.

In the feedback-only (1-DOF) control system structure for reference tracking, the controller acts only on the error signal. There are algebraic limitations on this control scheme. Since sum of the sensitivity function and complementary sensitivity function equals to unity, the designed controller cannot achieve required magnitude values for these dependent functions at frequency points of interest. It is well known that the tracking error minimization and noise attenuation are related to the complementary sensitivity function. On the other hand, the sensitivity function determines the effect of the output disturbance on the measured output of the control system. Therefore; there is a trade-off between reference tracking accuracy and disturbance rejection constraints [7]. Above mentioned performance limitations in the feedback-only control scheme can be eliminated by using a two degree of freedom (2-DOF) control system configuration, including a feedforward path [8].

To sum up, the following control challenges are addressed in this study:

- The stabilization and robust control of uncertain non-parametric systems using data-driven techniques;
- Robust fixed-order H_∞ controller synthesis using convex optimization;
- Optimal uncertainty modelling;
- High precision reference tracking.

1.2 State of the Art

In this section, some of the relevant data-driven control methods and fixed-order controller design approaches are briefly presented.

1.2.1 Data-driven Control Methods

Data-driven control methods have been developed to deal with modelling issues by synthesizing controllers using only a set of time domain or frequency domain measu-

rements instead of a parametric model. This advantage has made these methods a popular research topic within the automatic control community in recent years [9]. The fundamental goal of such methods is to directly synthesize controllers through experimentally obtained data, particularly for high precision control applications and high order dynamical systems with unavailable mathematical models.

Data-driven control methods can be divided into three main groups according to the usage of input-output data as

- Online data-based control methods;
- Off-line data-based control methods;
- hybrid (based on both online and off-line) data-based control methods;

Model-free adaptive control (MFAC) [10] and unfalsified control (UC) [11] methodologies are included in the first group. Iterative feedback tuning (IFT) [12], correlation-based tuning (CbT) [13], virtual reference feedback tuning (VRFT) [14]) and noniterative data-driven model reference control [15] methods can be examined in the off-line data-driven group. Iterative learning control (ILC) [16] and lazy learning (LL) [17] are examples of Hybrid data-driven control method.

1.2.2 Fixed-order H_∞ Controller Design Methods

Robust control theory, which includes the H_∞ and μ concepts, has been developed to take into account the dynamic uncertainties in controller design algorithms. In model based H_∞ control method, both plant and uncertainties are represented by transfer functions. As the order of transfer functions increase to satisfy high accuracy system modelling, the order of the synthesized full-order robust H_∞ controller also increases. In addition, the total order of user-defined weighting functions increases the order of the controller. This disadvantage is one of the limitations of robust H_∞ control.

Restricting the order of a controller turns the H_∞ controller design into an NP-hard non-convex problem [18]. Recently, nonsmooth optimization [19], meta-heuristic approach [20], Kalman-Yakubovich-Popov (KYP) Lemma [21, 22], inner convex appro-

ximation [23], convex-concave optimization [24], regional pole assignment [25] and exact gradient methods [26] have been adopted in fixed-order controller design problem with H_∞ criterion. Furthermore, the results of studies [27, 28] to solve this non-convex problem by using non-smooth optimization techniques have been incorporated into *hinfstruct* function of MATLAB and *HIFOO* toolbox, respectively. However, these techniques cannot be used for data-driven controller synthesis (i.e., they are model based control algorithm), and, hence, they introduce some conservatism into the designed closed-loop control systems due to uncertainty of the used parametric model.

1.2.3 Data-driven Fixed-order H_∞ Controller Design Methods

To avoid model identification and design fixed-order (structured) controllers from the input/output set of measurements in the data-driven approach, frequency domain H_∞ control framework can be considered. In such approaches, the controller synthesis problem is generally transformed into an inner constrained convex optimization problem, where H_∞ norm criteria can be used to formulate constrained optimization problem, to obtain a local solution in the frequency domain.

Quantitative feedback theory (QFT) [29] uses Nichols chart of the plant to synthesize fixed-order robust controllers. However, this method is mostly based on trial and error. In [30], a linear programming approach for linearly parameterized fixed-order controller synthesis is proposed. Robustness margins such as gain, phase and modulus margin are imposed as constraints in the Nyquist diagram. Although the method is also suitable for multiple models, performance requirements are limited to the selection of an interval for crossover frequency. This approach was later improved to synthesize a data-driven linearly parameterized robust controller via convex optimization for an uncertain model in [31] by the introduction of a desired loop gain model. However, this method leads to a conservative solution and narrowing of the solution space of the non-convex control problem due to the convexification approach. Another contribution to frequency domain data-driven synthesis of fixed-order controller for non-parametric systems is presented in [32]. In their work, the authors used a line to constrain the critical point of the Nyquist diagram for nominal stability or nominal performance requirement. The effectiveness

of the obtained controller largely depends on the selection of this constraint line. A non-linear optimization based solution approach for tuning fixed-order controllers is presented in [33], [34]. This method to necessitates the non-parametric response of the system that is provided by closed-loop tests. The most important reason limiting the use of this method is the need for three different initial controllers to obtain the frequency response of the controlled plant. A convex-concave procedure for robust PID controller design with a low-pass measurement filter is proposed in [35], but this study does not consider unstructured uncertainty. In [36], a robust data-driven digital controller design method for two degree of freedom RST controller is presented, where only the measurement process based uncertainty is taken into account. Frequency-domain approaches to suppress vibrations of flexible structures via lower order controllers are presented in [37, 38] for single input single output (SISO) and multiple input single output (MISO) systems respectively, where a non-convex H_∞ controller synthesis problem is solved for the mixed sensitivity objective. Another non-convex optimization algorithm based frequency domain data-driven fixed-order controller synthesis approach is introduced in [39] to solve H_∞ control problem for control signal limited linear time invariant (LTI) systems using non-parametric data. However, model uncertainties and robust performance constraints are not considered in the optimization problem of this study. In [40], the authors propose a frequency domain control design for stable multiple input multiple output (MIMO) systems for structured controllers based on nonsmooth trust-region bundle method. They also developed a new adaptive frequency gridding method to solve the fixed-order control problem with a finite number of frequency points.

1.3 Contributions of the Thesis

In this study, a fixed-order H_∞ controller synthesis method for non-parametric SISO systems is introduced by using linearly parameterized Laguerre basis functions in the frequency domain using convex optimization. In order to make the data-driven structured H_∞ approach more applicable and to reduce the conservatism of the method, this thesis study addresses the aforementioned limitations of the available methods. First, unstructured multiplicative model uncertainty bound is minimized by selecting the nominal model and uncertainty circle via the concept of Chebys-

hev center of a set of points at the corresponding frequency points on the Nyquist plot. Therefore, this algorithm reduces the conservatism and improves the robust performance of the proposed method. Thanks to this approximation, multiple measurements can be considered in the robust control design algorithm instead of one set of measurement with minimal uncertainty bound. Second, this study applies the robust data-driven fixed-order H_∞ controller synthesis methodology to linear plants with control input constraints. Physical systems usually have input signal constraints, because the power supplies cannot provide infinitely large control input. Two inequality constraints are added to the optimization based control design problem to account for this limit in the convex optimization framework. Third, in this thesis, the objective function of the convex optimization problem is formulated as a closed-loop model matching problem. Due to the fact that the model matching does not guarantee internal stability, a novel robust performance condition is derived and considered using an affine constraint on the Nyquist plot. Therefore, designed closed-loop control system is stable and experimentally obtained dynamical characteristics of the interested system matches predefined system dynamics in the H_∞ norm sense. Then, an extension of the 1-DOF feedback controller design algorithm is proposed to synthesize 2-DOF controllers for reference tracking of the non-parametric systems. Furthermore, another new method to synthesize data-driven structured H_∞ controller for SISO LTI plants by using generalized plant dynamics obtained from closed-loop test and control parameters written in diagonal form is presented. Finally, the proposed algorithms are verified experimentally with application to the control of electromechanical systems of an air vehicle.

1.4 Organization of the Thesis

Chapter 2 introduces the notation, frequency response identification methods, class of controllers, convex optimization method, and other basic definitions which are used throughout this study.

Chapter 3 proposes a new data-driven fixed-order H_∞ controller design method based on convex optimization for linear single input single output systems. A semi-definite convex optimization algorithm is proposed to simultaneously compute a minimal uncertainty model and an optimal nominal model from the experimental

data. Then, the H_∞ robust performance condition, control input constraints and the closed-loop model matching objective are described by convex functions with respect to the parameters of the controller. Finally, the usefulness and efficiency of the proposed approach are verified experimentally with application to the control of a flexible nozzle type electromechanical thrust vector control (TVC) system. Modelling of electromechanical actuation systems also given in this chapter.

Chapter 4 presents a novel data-driven controller design approach to synthesize two degree of freedom robust fixed-order H_∞ controllers for reference tracking by using convex optimization techniques. A structured 2-DOF robust controller synthesis approach based on constrained convex optimization problem is introduced with closed loop model matching objective and control input constraints for non-parametric perturbed model in the frequency domain. The theoretical design approach is experimentally verified on the full-closed loop feedback position control of an electromechanical control actuation system (CAS).

Chapter 5 suggests a novel method to synthesize data-driven structured H_∞ controller for LTI SISO plants by using the generalized plant obtained from closed-loop test and control parameters written in diagonal form. Based on the user defined weighting functions, the fixed-order H_∞ controller synthesis optimization algorithm is defined on the Nyquist plot to calculate the parameters of the controller. PD type position controller synthesis for an electromechanical CAS is realized by the proposed method.

Chapter 6 concludes the thesis and gives suggestions for future works.

2. PRELIMINARIES

This chapter introduces the notation, frequency response identification methods, class of controllers, convex optimization methods and other basic definitions that are used throughout this study.

2.1 Notation

The set of all real matrices, complex matrices and non-negative real matrices are denoted as $\mathbb{R}^{p\times q}$, $\mathbb{C}^{p\times q}$, ${\mathbb{R}_+}^{p\times q}$, respectively. The set of all real and all complex numbers are represented without the superscript p and q. The notation $G(s)$, $G(z)$ and $G(jw)$ represent the transfer function of the system G in the Laplace domain, z-domain and frequency domain, respectively. For the real and imaginary components of the input argument we use the $\Re(\cdot)$ and $\Im(\cdot)$ symbols, respectively. $\mathbf{RH}_\infty$ consists real rational proper stable models [41]. The superscript $(\cdot)^*$ represents the feasible solution of the optimization problem.

2.2 Norms of Signals and Systems

An LTI system G can be considered as a mapping from input data to output data, i.e., $u(t) \in X^{n_u}$ to $y(t) \in X^{m_y}$ by means of the convolution and defined as

$$\begin{aligned} G:\ X^{n_u} &\mapsto X^{m_y} \\ u(t) \mapsto y(t) &= \int_{-\infty}^{\infty} g(t-\tau)u(\tau)d\tau = g(t) * u(t) \end{aligned} \tag{2.1}$$

where $g(t)$ is the impulse response of the model. The system G is called single input single output (SISO) if $n_u = m_y = 1$ and multiple input multiple output (MIMO) if $n_u > 1$ or $m_y > 1$. The system model $g(t)$ is strictly causal if $g(t) = 0$ while $t \leq 0$. We consider strictly causal plants throughout this thesis study.

The Laplace transform of the causal $g(t)$ is defined as

$$\mathscr{L}\{g(t)\} = G(s) = \int_0^{\infty} g(\tau)e^{-s\tau}d\tau \tag{2.2}$$

where $\mathscr{L}\{\cdot\}$ is the Laplace transformation operator and $s \in \mathbb{C}$ is the Laplace variable. Finally, by means of the Laplace transformation, the output of the Laplace domain model is given by

$$Y(s) = G(s)U(s) \tag{2.3}$$

where $U(s)$ and $Y(s)$ are the Laplace domain representation of the input and output signals, respectively [42].

In this thesis study, causal LTI SISO systems are considered.

The norms gives strength, length or size of a vector (signal). Therefore, following definitions for signal norms, system spaces, vector norms and system norms used in defining fundamental concepts of robust control theory prevail.

Definition 2.1. ***(2-norm of a signal)*** *The 2-norm of a signal $u(t)$ is the square root of the integral of its square from $-\infty$ to ∞ and associated with the energy of the signal:*

$$\|u(t)\|_2 := \left(\int_{-\infty}^{\infty} u(t)^2 dt \right)^{1/2}. \tag{2.4}$$

Definition 2.2. ***(2-norm of a vector)*** *The 2-norm of a vector x gives the Euclidean distance on $\mathbb{R}^n$:*

$$\|x\|_2 := \left(\sum_{i=1}^{N} \left|x_i\right|^2 \right)^{1/2}, \ i = 1, \ 2, \ \ldots \ N. \tag{2.5}$$

Definition 2.3. ***(2-norm of a system)*** *The 2-norm of a frequency domain causal system $G(jw)$ is the total area under its magnitude plot from $w = 0$ to $w = \infty$:*

$$\|G\|_2 := \left(\frac{1}{2\pi} \int_{0}^{\infty} \left|G(jw)\right|^2 dw \right)^{1/2}. \tag{2.6}$$

Definition 2.4. ***($\mathcal{L}_2$ space)*** *The $\mathcal{L}_2$ space is Hilbert space of matrix-valued complex*

functions on $j\mathbb{R}$ (imaginary axis) such that the 2-norm is finite [43]:

$$\mathcal{L}_2 = \{G : \ \|G\|_2 < \infty\}. \tag{2.7}$$

Definition 2.5. ***(∞-norm of a signal)*** *The ∞-norm of a signal $u(t)$ is the supremum (the least upper bound) of its absolute value:*

$$\|u(t)\|_\infty := \sup_t \big|u(t)\big| \tag{2.8}$$

Definition 2.6. ***(∞-norm of a vector)*** *The ∞-norm of a vector x gives the maximum of its absolute value:*

$$\|x\|_\infty := \max_i \big|x_i\big|, \ i = 1, \ 2, \ \dots \ N. \tag{2.9}$$

Definition 2.7. ***(∞-norm of a system)*** *The ∞-norm of a causal system G is the peak value (maximal gain) of its magnitude plot in the frequency domain:*

$$\|G\|_\infty := \sup_{\Re(s)>0} [G(s)] = \sup_{w\in\mathbb{R}} [G(jw)] \tag{2.10}$$

and it is submultiplicative such that

$$\|GH\|_\infty \leq \|G\|_\infty \|H\|_\infty \tag{2.11}$$

which is an important property for robust stability analysis by small gain theorem [41].

Definition 2.8. ***($\mathcal{L}_\infty$ space)*** *The $\mathcal{L}_\infty$ space is a Banach space of matrix-valued functions, which are bounded on $j\mathbb{R}$ such that $\|G\|_\infty$ is finite [43]:*

$$\mathcal{L}_2 = \{G : \ \|G\|_\infty < \infty\}. \tag{2.12}$$

Definition 2.9. ***($\mathcal{H}_\infty$ space)*** *The $\mathcal{H}_\infty$ space is a closed subspace of $\mathcal{L}_\infty$ space with functions that analytic on the right half plane with a finite ∞-norm.*

2.3 Robust Controller Synthesis and Analysis

Any interconnected feedback control system can be rearranged as a linear fractional transformation (LFT). Generalized control system configuration with LFT structure for robust control system design and analysis is given in Figure. 2.1.

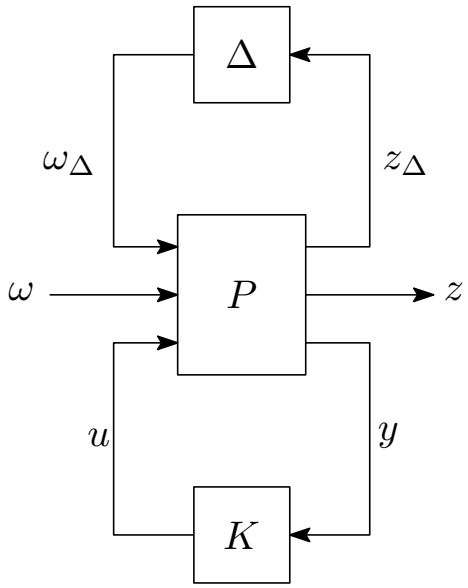

Figure. 2.1. Generalized control system configuration.

This framework can be obtained by separating controller K and uncertainty Δ blocks from feedback interconnection. In Figure. 2.1; P denotes the generalized plant, ω is the exogenous input vector comprising of reference command, sensor noise, output disturbance, z is the performance variable of interest, y denotes the measured outputs, (or error signal), u denotes the control signal, ω_Δ represents the output of the perturbation block, and z_Δ represents the input of the perturbation block.

P represents the mathematical relations between $\begin{bmatrix}\omega_\Delta & \omega & u\end{bmatrix}^T$ and $\begin{bmatrix}z_\Delta & z & y\end{bmatrix}^T$. P matrix can be partitioned in matrix form as

$$\begin{bmatrix} z_\Delta \\ z \\ y \end{bmatrix} = \left[\begin{array}{c|c} P_{11} & P_{12} \\ \hline P_{21} & P_{22} \end{array}\right] \begin{bmatrix} \omega_\Delta \\ \omega \\ u \end{bmatrix} = \left[\begin{array}{cc|c} P_{11}^{(11)} & P_{11}^{(12)} & P_{12}^{(11)} \\ P_{11}^{(21)} & P_{11}^{(22)} & P_{12}^{(21)} \\ \hline P_{21}^{(11)} & P_{21}^{(12)} & P_{22}^{(11)} \end{array}\right] \begin{bmatrix} \omega_\Delta \\ \omega \\ u \end{bmatrix} \tag{2.13}$$

where $\omega_\Delta \mapsto z_\Delta$ is the uncertainty channel and $\omega \mapsto z$ is the performance channel.

The closed loop system transfer function $T_{z\omega}$, which represents the transfer function from the exogenous inputs to the performance variables, can be written by using upper and lower LFT on the uncertainty block and controller as

$$\begin{aligned} z &= (T_{z\omega})\omega \\ z &= F_u\Big(F_l(P,K),\Delta\Big)\omega \\ z &= F_l\Big(F_u(P,\Delta),K\Big)\omega \end{aligned} \tag{2.14}$$

where

$$\begin{aligned} F_l(P,K) &= M = P_{11} + P_{12}K\big(I - P_{22}K\big)^{-1}P_{21} \\ F_u(P,\Delta) &= N = P_{22} + P_{21}\Delta\big(I - P_{11}\Delta\big)^{-1}P_{12}. \end{aligned} \tag{2.15}$$

For the H_∞ controller synthesis methods, the generalized control system configuration can be modified into the controller synthesis framework (Figure. 2.2) with $\Delta = 0$ block (without uncertainty channel) and following generalized plant P:

$$\begin{bmatrix} z \\ y \end{bmatrix} = \begin{bmatrix} P_{11}^{(22)} & P_{12}^{(21)} \\ P_{21}^{(12)} & P_{22}^{(11)} \end{bmatrix} \begin{bmatrix} \omega \\ u \end{bmatrix} \tag{2.16}$$

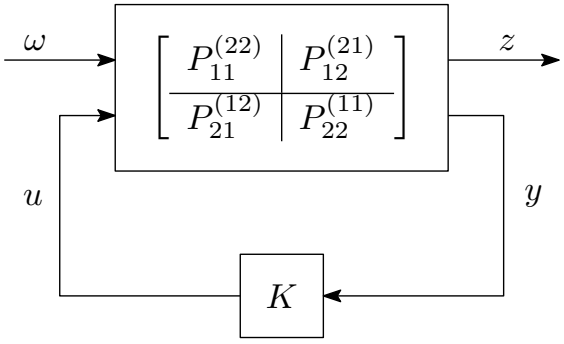

Figure. 2.2. Controller synthesis framework.

All of the transfer functions from exogenous inputs to performance outputs, i.e., $T_{z\omega}$

can be written by using lower LFT as

$$z = F_l\left(\begin{bmatrix} P_{11}^{(22)} & P_{12}^{(21)} \\ P_{21}^{(12)} & P_{22}^{(11)} \end{bmatrix}, K\right)\omega$$
$$T_{z\omega} = P_{11}^{(22)} + P_{12}^{(21)}K\big(I - P_{22}^{(11)}K\big)^{-1}P_{21}^{(12)}. \tag{2.17}$$

The model based H_∞ control design method aims to find a suboptimal controller K that minimizes effects of the exogenous inputs ω on performance output z. In other words, optimal H_∞ control problem is: find all admissible, i.e., it internally stabilizes the system, controller K such that

$$\|T_{z\omega}\|_\infty = \sup_{\Re(s)>0}[T_{z\omega}(s)] = \sup_{w\in\mathbb{R}}[T_{z\omega}(jw)] \tag{2.18}$$

is minimized. However, computing an optimal H_∞ controller is not simple [41]. To overcome this difficulty, a sub-optimal control problem can be considered [5]. This sub-optimal H_∞ control problem is: find all admissible controller K such that

$$\|T_{z\omega}\|_\infty < \gamma \tag{2.19}$$

where $\gamma > 0$. Classical solution techniques of sub-optimal H_∞ controller synthesis problem are based on the state space algorithms which are formed by two algebraic Ricatti equations [5].

For the robustness analysis methods, the H_∞ controller K can be considered as another known component of generalized system configuration. Therefore, the controller can be included into the system structure using lower LFT as given in the first part of the (2.15) and (2.17). Then, the generalized control system configuration can be modified into the robustness analysis framework, i.e., $(M-\Delta)$ structure as shown in Figure. 2.3.

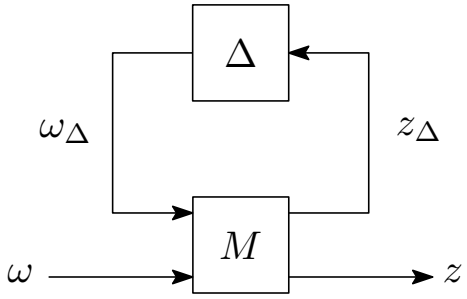

Figure. 2.3. Controller analysis framework.

In robust stability or robust performance analysis, the system model is described with perturbations. Multiplicative uncertainty and additive uncertainty are the most commonly used methods for uncertain model description. For additive uncertainty (Figure. 2.4) modelling approach, the nominal (parameter) model is assumed to be in the set:

$$\mathbf{M} := P + \Delta W_A,\ \|\Delta\|_\infty < 1 \tag{2.20}$$

Similarly, the nominal (parameter) model is assumed to be in the set

$$\mathbf{M} := P(I + \Delta W_M),\ \|\Delta\|_\infty < 1 \tag{2.21}$$

for multiplicative uncertainty (Figure. 2.5).

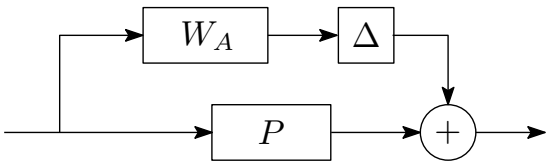

Figure. 2.4. Additive uncertainty.

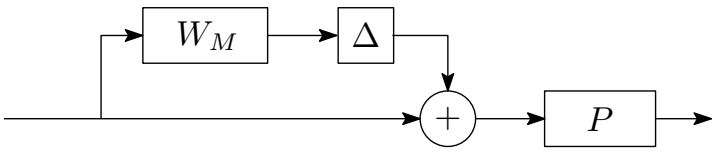

Figure. 2.5. Multiplicative uncertainty.

The functions W_A and W_M are stable, strictly proper transfer functions, i.e., $W_A\, W_M\, \Delta \in$

$\mathbf{RH}_\infty$, which define the magnitude of the uncertainty at each interested frequency point.

Structured singular value, which is denoted by μ or SSV, is a measure of the destabilizing structured uncertainty matrix Δ. Additionally, a fictitious block $\|\Delta_F\|_\infty < 1$ can be used for representation of the performance channel (robust performance analysis). By using the special structure of the Δ matrix, μ value of a system matrix M is defined as the inverse of the smallest norm of a perturbation matrix that causes the instability. This definition can be written as

$$\mu_\Delta(M) = \frac{1}{min\{\bar{\sigma}(\Delta) : det(I - M\Delta) = 0\}} \tag{2.22}$$

where $\bar{\sigma}$ is the maximum singular value of the $\Delta \in \mathbb{C}^{n\times n}$ matrix. There is no exact solution for $\mu_\Delta(M)$. However, the upper and lower limits of the perturbation matrix that cause the instability can be approximated [41].

2.4 Linearly Parameterized Controllers

Linearly parameterized fixed-order controllers can be modelled with stable orthogonal basis functions as

$$K(s,k) = k\psi(s) \tag{2.23}$$

where $k = \begin{bmatrix} k_0 & k_1 \dots k_n \end{bmatrix} \in \mathbb{R}^{1\times n}$ is the gain matrix of the controller and $\psi(s)^T = \begin{bmatrix} 1 & \psi_1(s) \dots \psi_n(s) \end{bmatrix} \in \mathbf{RH}_\infty$ is the matrix of transfer functions. These basis functions can be formed by using Laguerre functions, Kautz functions or generalized orthonormal basis functions [44]. In this thesis, we consider the Laguerre basis functions, also known as Laguerre filters, given by

$$\psi_i(s) = \frac{\sqrt{2\xi}(s-\xi)^{i-1}}{(s+\xi)^i} \tag{2.24}$$

for $i = 1, \dots, n$ with $\xi > 0$ which is called the time scaling factor of the Laguerre functions. The poles of these functions are at the same location ξ. All functions except $\psi_1(s)$, which is a low-pass filter, are formed with all-pass filters in series with a first order filter [45]. The block diagram of the Laplace domain structure of the

n^{th}-order Laguerre model based controller is shown in Figure. 2.6.

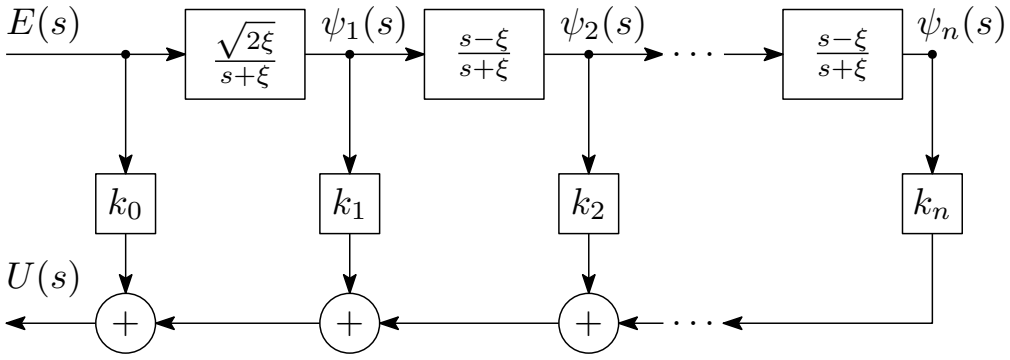

Figure. 2.6. Structure of the linearly parameterized controllers.

In Figure. 2.6, the controller input signal $E(s)$ is filtered by Laguerre functions. Then, the control signal of the plant $U(s)$ is obtained by multiplication of each filtered outputs by their respective controller parameters k_i as

$$U(s) = \left[k_0 + k_1\psi_1(s) + \cdots + k_n\psi_n(s)\right] E(s). \tag{2.25}$$

Time domain representation of the Laguerre functions can be obtained by using inverse Laplace transform as follows:

$$\psi_i(t) = \mathscr{L}^{-1}\left(\frac{\sqrt{2\xi}(s-\xi)^{i-1}}{(s+\xi)^i}\right) = \sqrt{2\xi}\frac{e^{\xi t}}{(i-1)!}\frac{d^{i-1}}{dt^{i-1}}\left(t^{i-1}e^{-2\xi t}\right) \tag{2.26}$$

where $\psi_i(t)$, $i = 1,\ 2,\ \ldots$ is an orthonormal set satisfying following properties:

$$\int_0^\infty \psi_i^2(t)dt = 1 \tag{2.27}$$

$$\int_0^\infty \psi_i(t)\psi_j(t)dt = 0,\ i \neq j. \tag{2.28}$$

Any analytical function $g(t)$ can be written as

$$g(t) = \sum_{i=1}^{N} a_i\psi_i(t) \tag{2.29}$$

where a_i is the coefficient of the Laguerre expansion and given by

$$a_i = \int_0^\infty \psi_i(t) g(t) dt. \tag{2.30}$$

Although the Laguerre expansion has an infinite number of a_i and $\psi_i(t)$, one can approximate the function $g(t)$ with a sufficient number of a_i and $\psi_i(t)$ terms, i.e., $i = 1,\ 2,\ \ldots,\ N$.

Example 2.1: Consider the following stable second order stable system model.

$$G(s) = \frac{2}{(2s+1)(3s+2)} \tag{2.31}$$

The impulse response of this function can be approximated using Laguerre expansion for $i = 1,\ 2,\ 3,\ 4$. For the sake of simplicity, the time scaling factor ξ assumed as $\xi = 1$. Then, the Laguerre coefficients can be obtained using (2.30) as

$$\begin{aligned} a_1 &= 0.188 \\ a_2 &= -0.289 \\ a_3 &= 0.141 \\ a_4 &= -0.051. \end{aligned} \tag{2.32}$$

The time domain impulse response of the resulting $1^{st},\ 2^{nd},\ 3^{rd},\ 4^{th}$ order Laguerre models and $g(t)$ are given in Figure. 2.7.

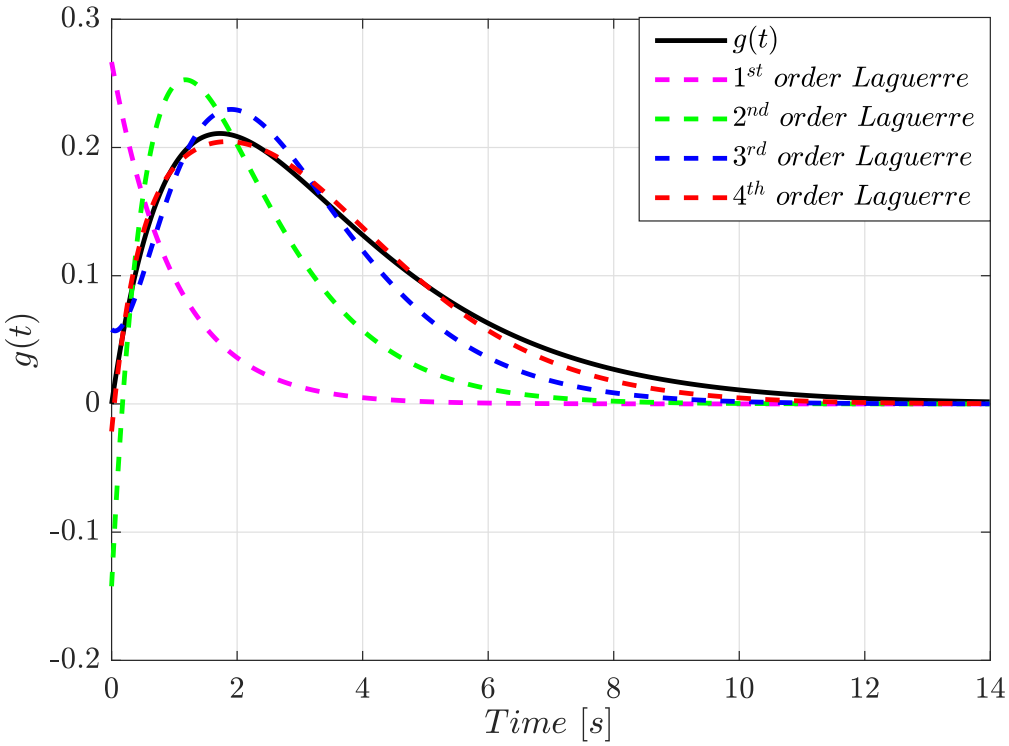

Figure. 2.7. $1^{st},\ 2^{nd},\ 3^{rd},\ 4^{th}$ order Laguerre expansions of the $g(t)$.

As can be seen from the figure, as the order of the Laguerre model increases, Laguerre expansion approximates the response of real system model.

2.4.1 PID Controller

The continuous-time PID controller also can be written in linearly parameterized form as

$$K_{PID}(s) = k\psi(s) = \begin{bmatrix} K_p & K_i & K_d \end{bmatrix} \begin{bmatrix} 1 \\ 1/s \\ s/(\tau_d s + 1) \end{bmatrix} \tag{2.33}$$

where $k = \begin{bmatrix} K_p & K_i & K_d \end{bmatrix} \in \mathbb{R}_+^{1\times 3}$ are the proportional gain, integral gain and derivative gain, respectively. The $\tau_d \in \mathbb{R}_+$ parameter of the PID controller is the derivative time constant, which is assumed to be fixed.

Note that, the basic idea behind using linearly parameterized type controllers is to represent transfer functions constituting the control objective function as a convex function with respect to the optimization parameter k.

2.5 Frequency Response Identification

2.5.1 FRF Estimation From Open-loop Data

The complex value $G(jw)$, which is $G(z)\big|_{z=e^{jw}}$, gives full information about the system in steady-state case if the system is stable and the input is sinusoidal. Therefore, $G(jw)$ is called the frequency response function (FRF) of the plant. This approach may not be feasible for some systems in all situations because one can not sequentially implement all possible sinusoidal inputs. An extension of the direct FRF method is the empirical transfer function estimate (ETFE) [46] that estimates FRF from normal inputs instead of sinusoidal ones. If the system is disturbance free and has zero boundary conditions, the estimate of $G(jw)$, which is denoted by $\widehat{G}_N(jw)$, can be calculated by dividing the periodogram of the system output $y[k]$ to the periodogram of the input signal $u[k]$ as follows:

$$\widehat{G}_N(jw) = \left[\frac{1}{\sqrt{N}}\sum_{t=1}^{N} y[t]e^{-jwt}\right]\left[\frac{1}{\sqrt{N}}\sum_{t=1}^{N} u[t]e^{-jwt}\right]^{-1} \tag{2.34}$$

where N is the number of available measurement samples for each experiment, t is the time instant, $w \in [0, \pi/T_s]$ and T_s is the sampling period.

On the other hand, experimental systems often contain measurement noise. An experimental test setup could produce an output such as

$$y[t] = G(z)u[t] + v[t] \tag{2.35}$$

where $v[t]$ is the random measurement noise, and $u[t]$ and $y[t]$ are uncorrelated. Since the $u[t]$ signal is not entirely random, $y[t]$ is a quasi-stationary signal. Estimation of the auto-correlation function of $u[t]$ can be defined as

$$\widehat{R}_u^N(\tau) := \frac{1}{N}\sum_{k=0}^{N-1} u[k]u[k-\tau],\ |\tau| \leq N-1. \tag{2.36}$$

Similarly, estimated cross-correlation function between $u[k]$ and $y[k]$ is given by

$$\widehat{R}_{yu}^{N}(\tau) := \frac{1}{N}\sum_{t=0}^{N-1} y[t]u[t-\tau],\ |\tau| \leq N-1. \tag{2.37}$$

The spectral density of $u[t]$ and the cross spectral density between $u[t]$ and $y[t]$ are defined by

$$\widehat{\phi}_u(jw) = \sum_{\tau=-\infty}^{\infty} W_M(\tau)\widehat{R}_u^N(\tau)e^{-jw\tau} \tag{2.38}$$

$$\widehat{\phi}_{yu}(jw) = \sum_{\tau=-\infty}^{\infty} W_M(\tau)\widehat{R}_{yu}^N(\tau)e^{-jw\tau} \tag{2.39}$$

where $W_M(\tau)$ is the lag window that is used for smoothing the estimated FRF. Finally, $\widehat{G}_N(jw)$ can be estimated from these spectral density functions as

$$\widehat{G}_N(jw) = \frac{\widehat{\phi}_{yu}(jw)}{\widehat{\phi}_u(jw)}. \tag{2.40}$$

2.5.2 FRF Estimation From Closed-loop Data

During the synthesis of data-driven robust controller, the non-parametric spectral model of system is needed in the frequency domain instead of a well defined transfer function of the system. The FRF, which consists of a finite number of data points of the system, can be derived from the parametric model or the spectral analysis of the input/output data. The stability and performance characteristics of the discussed system are examined using non-parametric model in what follows.

The FRF data of an LTI system can be obtained by using closed-loop system identification techniques. Especially for systems that are unstable, motion constrained or with with high security requirements or unreachable feedback loop; closed-loop identification is generally preferred [47]. Closed-loop identification methods can be divided into three main groups: direct, indirect and joint input-output approach [46]. In order to derive the FRF model of the experimental devices of this study, the direct approach is selected. In this method, the input $r(t)$, error $e(t)$, control input $u(t)$,

output $y(t)$ and the transfer function of the controller $K(jw)$ in the feedback system, which are shown in Figure. 2.8, are assumed to be known.

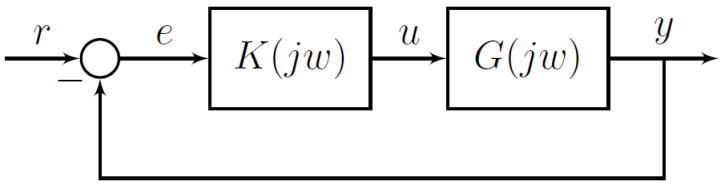

Figure. 2.8. Feedback system.

The mathematical relationships between $r(t)$ and $y(t)$, and $r(t)$ and $e(t)$ are given by

$$y(jw) = T(jw)r(jw) \tag{2.41}$$

$$e(jw) = S(jw)r(jw) \tag{2.42}$$

where $S(jw)$ is the sensitivity function and $T(jw)$ is the complementary sensitivity function such that $S(jw) + T(jw) = I$.

The generalized plant P is generated by writing arithmetic relations between the input and output signals defined in the remainder where the controller $K(s)$ is separated from the system as

$$z = P_{11}\omega + P_{12}u \tag{2.43}$$

$$e = P_{21}\omega + P_{22}u \tag{2.44}$$

where ω is the exogenous input and z is the performance variable of interest. P matrix can be partitioned as

$$\begin{bmatrix} z \\ e \end{bmatrix} = \begin{bmatrix} P_{11} & P_{12} \\ P_{21} & P_{22} \end{bmatrix} \begin{bmatrix} \omega \\ u \end{bmatrix} \tag{2.45}$$

$$\left[P\right] = \begin{bmatrix} P_{11} & P_{12} \\ P_{21} & P_{22} \end{bmatrix} = \begin{bmatrix} 0 & G \\ I & -G \end{bmatrix} \tag{2.46}$$

where P represents the transfer function from $\begin{bmatrix} \omega & u \end{bmatrix}^{\mathrm{T}}$ to $\begin{bmatrix} z & e \end{bmatrix}^{\mathrm{T}}$ and $z \in \mathbb{R}^{n_z}$, $e \in \mathbb{R}^{n_e}$, $\omega \in \mathbb{R}^{n_\omega}$, $u \in \mathbb{R}^{n_u}$. The general control configuration with P is derived by following the steps given in Figure. 2.9 and Figure. 2.10 for the closed-loop system in Figure. 2.8, respectively.

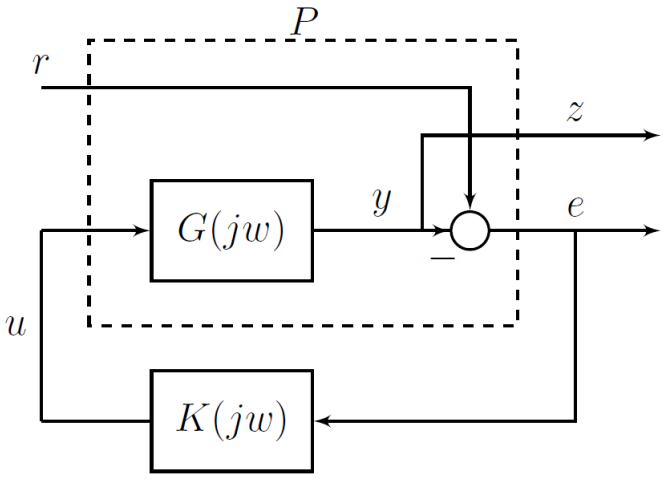

Figure. 2.9. Construction of the generalized plant.

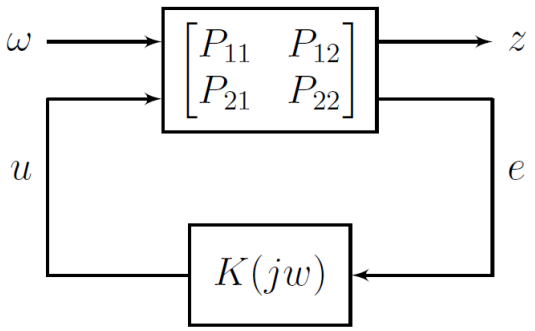

Figure. 2.10. Generalized control system configuration.

The transfer function of $T_{z\omega}$, which represents the transfer function from generalized input to generalized output of the system, can be written as

$$T_{z\omega} = \frac{z}{\omega} = \frac{P_{11} - P_{11}KP_{22} + P_{12}KP_{21}}{1 - KP_{22}} \tag{2.47}$$

for the SISO system in Figure. 2.8, is also given in (2.41). The definition of generalized plant parameters $P_{11},\ P_{12},\ P_{21},\ P_{22}$ in the above equations is required for μ analysis and H_∞ controller synthesis. For the SISO system given in Figure. 2.8, only P_{12} and P_{22} are unknown and equal to G and $-G$, respectively. For this reason, definition of the FRF data of the open-loop plant G is sufficient for the identification of P.

In direct closed-loop identification, $T(jw)$ is excited by $\omega(t)$ input signal and corresponding outputs $u(t)$, $z(t)$ signals for N time samples are measured. The applied $\omega(t)$ should be a rich signal to be able to continuously excite the system within the frequency range of interest. Usually, Pseudo Random Binary Sequence (PRBS), white noise and chirp signals are preferred input signals [48]. Then $G(jw)$ can be obtained by applying the Blackman-Tukey spectral analysis method [46]. In the first step of this method, covariance of $u(t)$ and cross-covariance of $u(t)$ and $z(t)$ can be calculated by using

$$\hat{R}_u^N(\tau) = \frac{1}{N}\sum_{t=1}^{N} u(t+\tau)u(t) \tag{2.48}$$

$$\hat{R}_{zu}^N(\tau) = \frac{1}{N}\sum_{t=1}^{N} z(t+\tau)u(t) \tag{2.49}$$

equations for N measured samples, respectively. Fourier transforms of these functions can be calculated using

$$\hat{\phi}_u(jw) = \sum_{\tau=-M}^{M} \hat{R}_u^N(\tau)W_M(\tau)e^{-jw\tau} \tag{2.50}$$

$$\hat{\phi}_{zu}(jw) = \sum_{\tau=-M}^{M} \hat{R}_{zu}^N(\tau)W_M(\tau)e^{-jw\tau} \tag{2.51}$$

equations where $W_M(\tau)$ is the Hanning window with a width of M. This window is designed as a function of frequency and is chosen small around the bandwidth and large of higher frequencies [37]. Finally, FRF of open-loop plant $G(jw)$ is obtained

by using

$$G(jw) = \frac{\hat{\phi}_{zu}(jw)}{\hat{\phi}_{u}(jw)} \tag{2.52}$$

equation and FRF of P matrix can be calculated by using (2.46) with known $G(jw)$.

2.6 Convex Optimization

Optimization is the methodology of computing the feasible solution that minimizes or maximizes the cost function $f(x)$ with or without constraints. Optimization problems are mainly divided into two groups as unconstrained optimization problem and constrained optimization problem.

Definition 2.10. ***(Unconstrained optimization)*** *An unconstrained optimization problem can be written as*

$$\min_{\overline{x} \in X} \; f(\overline{x}) \tag{2.53}$$

where $\overline{x} = \begin{bmatrix} x_1 & x_2 \dots x_n \end{bmatrix}^T \in \mathbb{R}^n$ *is the vector of optimization variables, the function* $f(\overline{x})\colon \mathbb{R}^n \to \mathbb{R}$ *is called the objective or cost function of the optimization problem and* X *is an n-dimensional subset.*

Definition 2.11. ***(Constrained optimization)*** *Constrained optimization problem is a mathematical problem which consists of minimizing a objective function* $f(x)$ *subject to equality or inequality constraints. A mathematical optimization problem can be formulated as*

$$\begin{aligned} \min_{\overline{x} \in X} \quad & f(\overline{x}) \\ s.t. \quad & g(\overline{x}) \leq 0 \\ & h(\overline{x}) = 0 \end{aligned} \tag{2.54}$$

Here, $\overline{g}(\overline{x}) = \begin{bmatrix} g_1(\overline{x}) & g_2(\overline{x}) \dots g_m(\overline{x}) \end{bmatrix}^T$ *is the vector of the inequality constraint functions. Similarly,* $\overline{h}(\overline{x}) = \begin{bmatrix} h_1(\overline{x}) & h_2(\overline{x}) \dots h_l(\overline{x}) \end{bmatrix}^T$ *is the vector of the equality constraint functions. The vector* $\overline{x}$ *is a feasible solution of the constrained optimization problem (2.54) if and only if* $g(\overline{x}) \leq 0,\ h(\overline{x}) = 0$ *and* $\overline{x} \in X$*.*

Definition 2.12. ***(Ball)*** $\mathbb{B}(\overline{x}^*, \epsilon)$ *is a ball at point* $\overline{x}^*$ *with radius* ϵ *such that*

$$\mathbb{B}(\overline{x}^*, \epsilon) = \{\overline{x}^* \mid \|\overline{x} - \overline{x}^*\|_2 \leq \epsilon\}. \tag{2.55}$$

Note that, the set of points

$$\mathbb{B}(\overline{x}_c, r_c) = \{\overline{x} \mid \|\overline{x} - \overline{x}_c\|_2 \leq r_c\} = \{\overline{x}_c + r_c\overline{\rho} \mid \|\overline{\rho}\|_2 \leq 1\} \tag{2.56}$$

constitutes a Chebyshev ball with respect to the Euclidean norm around the Chebyshev center $\overline{x}_c$ *with radius* $r_c > 0$*. This ball definition is generally used in the optimization algorithm to define the bound of the error.*

Definition 2.13. ***(Ellipsoid)*** *Similarly, ellipsoid has the form*

$$\mathbb{E}_p = \{\overline{x} \mid (\overline{x} - \overline{x}_c)^T P_e^{-1}(\overline{x} - \overline{x}_c) \leq 1\} = \{\overline{x}_c + A_p\overline{\rho} \mid \|\overline{\rho}\|_2 \leq 1\} \tag{2.57}$$

where P_e *is a symmetric positive definite (SPD) matrix* $\left(P_e = P_e^T \succ 0\right)$*, and* A_p *is a square nonsingular matrix [49, 50].*

Definition 2.14. ***(Positive-semidefinite)*** *An* $n\times$ *symmetric matrix* A_s *is called positive-semidefinite if*

$$x^T A_s x \geq 0, \ \ \forall x \in \mathbb{R}^n \tag{2.58}$$

and it is denoted as

$$A_s \succeq 0 \tag{2.59}$$

where the special inequality $\succeq$ *means positive semidefinite with non-negative eigenvalues.*

Definition 2.15. ***(Local minimum)*** *A vector* $\overline{x}^* \in F$
is a local minimum of the optimization problem if

$$\exists \epsilon > 0 \ \Rightarrow f(\overline{x}^*) \leq f(\overline{y}), \ \forall \overline{y} \in \mathbb{B}(\overline{x}^*, \epsilon) \cap F; \tag{2.60}$$

is a strict local minimum of the optimization problem if

$$\exists \epsilon > 0 \ \Rightarrow f(\overline{x}^*) < f(\overline{y}),\ \forall \overline{y} \in \mathbb{B}(\overline{x}^*, \epsilon) \cap F,\ \overline{y} \neq \overline{x}^*; \tag{2.61}$$

is a global minimum of the optimization problem if

$$f(\overline{x}^*) \leq f(\overline{y}),\ \forall \overline{y} \in F; \tag{2.62}$$

is a strict global minimum of the optimization problem if

$$f(\overline{x}^*) < f(\overline{y}),\ \forall \overline{y} \in F,\ \overline{y} \neq \overline{x}^* \tag{2.63}$$

where F is the feasible domain, which is a subset of X, and defined as

$$F = X \cap \left\{ \overline{x} \in X \middle| g_1(\overline{x}) \leq 0 \dots g_m(\overline{x}) \leq 0,\ h_1(\overline{x}) = 0 \dots h_l(\overline{x}) = 0 \right\}. \tag{2.64}$$

Example 2.2: Consider the following constrained optimization problem in standard form [51]:

$$\begin{aligned} \min_{x_1, x_2 \in \mathbb{R}^2} \quad & f(x_1, x_2) = (x_1 - 3)^2 + (x_2 - 2)^2 \\ \text{s.t.} \quad & g_1(x_1, x_2) = x_1 + x_2 - 7 \leq 0 \\ & g_2(x_1, x_2) = x_1 - 0.25 x_2^2 \leq 0 \\ & h_1(x_1, x_2) = 2x_1 + x_2 - 8 = 0 \\ & h_2(x_1, x_2) = (x_1 - 1)^2 + (x_2 - 4)^2 = 0 \\ & \overline{x} \in X = \left\{ \overline{x} \in \mathbb{R}^2 \ \middle|\ 0 \leq x_1 \leq 10,\ 0 \leq x_2 \leq 10 \right\} \end{aligned} \tag{2.65}$$

The feasible domain of $\overline{x}$ such that the constraints are satisfied is given by $F = X \cap \left\{ \overline{x} \in X \middle| g_1(\overline{x}) \leq 0,\ g_2(\overline{x}) \leq 0,\ h_1(\overline{x}) = 0,\ h_2(\overline{x}) = 0 \right\} = \left\{ (1, 6)^* \right\}$. Figure. 2.11 shows the graphical representation of this constrained optimization problem with level curves (countours of the objective function $f(x_1, x_2)$).

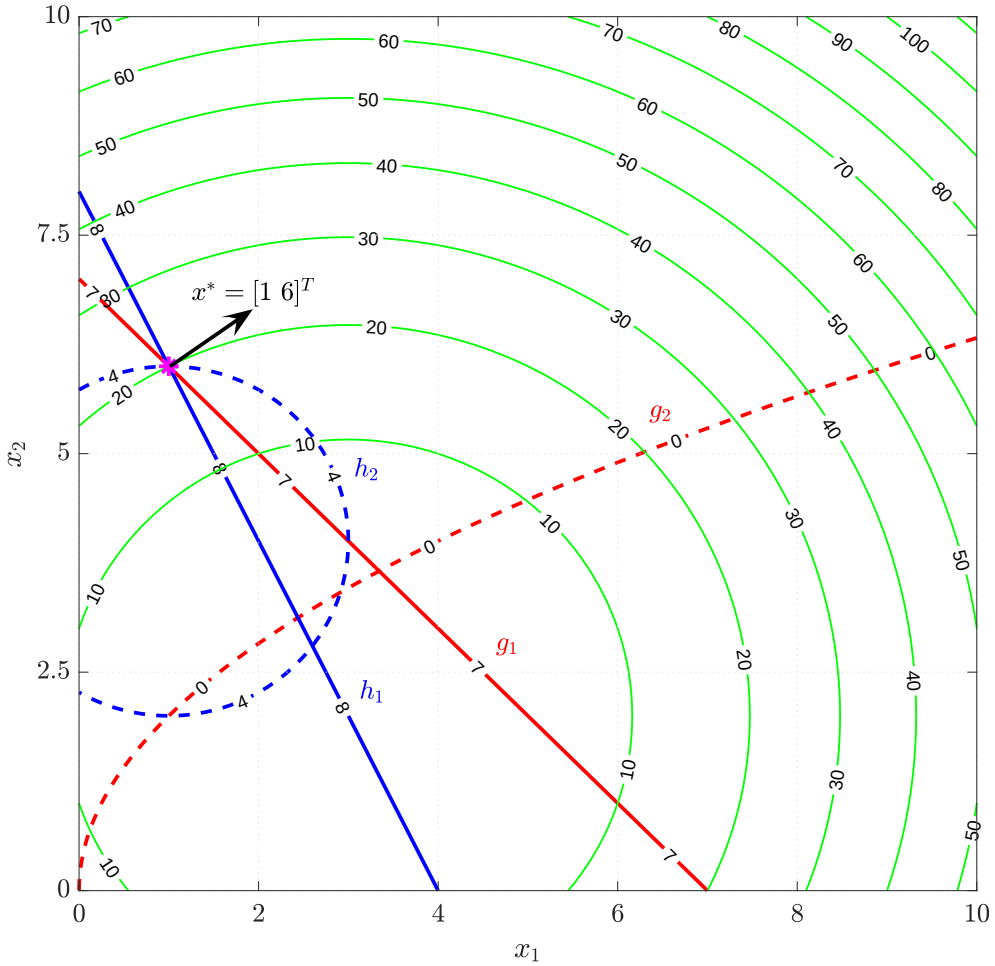

Figure. 2.11. Graphical representation of given constrained optimization example.

As can seen from Figure. 2.11, the intersection of two equality constraints defines two possible solutions to the optimization problem as $(x_1 = 1,\ x_2 = 6)$ and $(x_1 = 2.6,\ x_2 = 2.8)$. However, the point $(2.6,\ 2.8)$ does not satisfies the second inequality constraint, i.e., $g_2(x_1, x_2)$. Therefore, the point $(1,\ 6)$, which satisfies all constraints, is a uniquely feasible solution of the given optimization problem.

A convex optimization problem can be defined as a problem of minimizing a convex function over a convex set. In this framework, the basic definitions and theorems required for convex optimization method are given below.

Definition 2.16. ***(Infimum)*** *The infimum or the greatest lower bound of the function* $f(x)$ *is denoted as*

$$\inf_{\overline{x} \in X} \ f(\overline{x}) \tag{2.66}$$

and defined by

$$\inf_{\overline{x}\in X} \ f(\overline{x}) \ \leq f(\overline{x}), \ \forall \overline{x} \in X \tag{2.67}$$

where X is a subset of the feasible decision variables.

Definition 2.17. ***(Supremum)*** *The supremum or the least upper bound of a function $f(x)$ is denoted as*

$$\sup_{\overline{x}\in S} \ f(\overline{x}) \tag{2.68}$$

and defined by:

$$\sup_{\overline{x}\in S} \ f(\overline{x}) \ \geq f(\overline{x}), \ \forall \overline{x} \in X. \tag{2.69}$$

Definition 2.18. ***(Affine set)*** *A set $X \subseteq \mathbb{R}^n$ is said to be affine if*

$$\lambda \overline{x}_1 + (1-\lambda)\overline{x}_2 \in X, \ \forall \overline{x}_1, \overline{x}_2 \in X, \ \lambda \in \mathbb{R} \tag{2.70}$$

where $\lambda x_1 + (1-\lambda)x_2$ constitutes a line segment.

Definition 2.19. ***(Affine function)*** *A function $f(\overline{x})\colon \mathbb{R}^n \to \mathbb{R}^m$ defined on X is affine, i.e., linear function plus a constant term $(a^T\overline{x}+b)$, if it satisfies the following equality:*

$$f(\lambda \overline{x}_1 + (1-\lambda)\overline{x}_2) = \lambda \overline{x}_1 + (1-\lambda)\overline{x}_2, \ \forall \overline{x}_1, \overline{x}_2 \in X, \ \lambda \in \mathbb{R} \tag{2.71}$$

where $a \in \mathbb{R}^n \times \mathbb{R}^m, \ b \in \mathbb{R}^m$ and $dom \ f = X \subseteq \mathbb{R}^n$.

Definition 2.20. ***(Convex set)*** *A set $X \subseteq \mathbb{R}^n$ is said to be convex if*

$$\lambda \overline{x}_1 + (1-\lambda)\overline{x}_2 \in X, \ \forall \overline{x}_1, \overline{x}_2 \in X, \ \lambda \in [0,1]. \tag{2.72}$$

In other words, line segment between $x_1 \in X$ and $x_2 \in X$ lies in set X.

Definition 2.21. ***(Convex function)*** *A function $f(\overline{x})\colon \mathbb{R}^n \to \mathbb{R}$ is convex if $dom \ f = X \subseteq \mathbb{R}^n$ is a convex set and $f(\overline{x})$ satisfies the following Jensen's Inequality [52]:*

$$f(\lambda \overline{x}_1 + (1-\lambda)\overline{x}_2) \leq \lambda \overline{x}_1 + (1-\lambda)\overline{x}_2, \ \forall \overline{x}_1, \overline{x}_2 \in X, \ \lambda \in [0,1]. \tag{2.73}$$

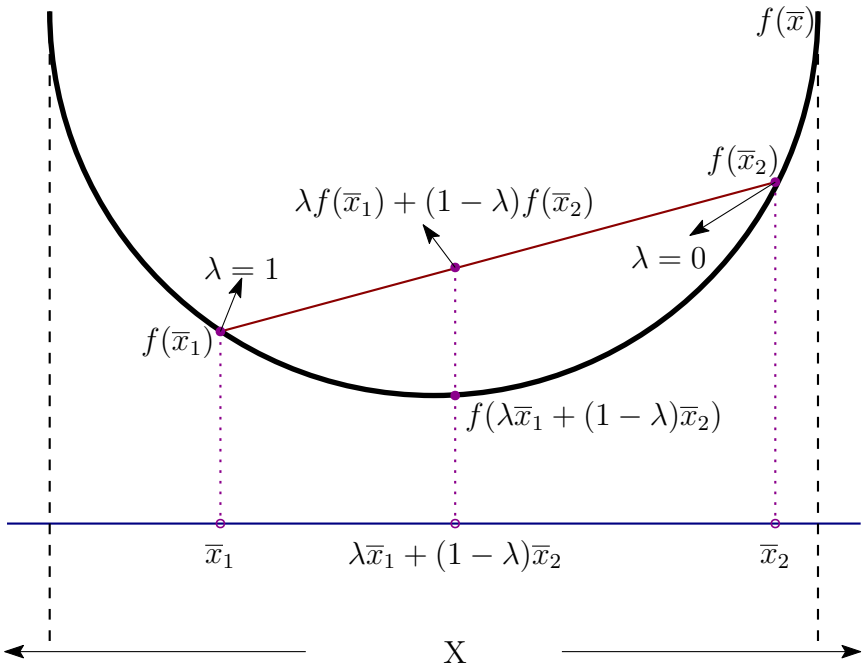

Figure. 2.12. A graphical interpretation of the Jensen's Inequality.

A graphical interpretation of the Jensen's Inequality, which means that the line segment between any chosen two points on the $f(\overline{x})$ graph lies above the graph of $f(\overline{x})$, is given in Figure. 2.12. Note that, an affine function $a^T\overline{x} + b$ with convex domain, i.e., $domf \ : \ convex$, satisfies the Jensen's Inequality as

$$f(\lambda \overline{x}_1 + (1-\lambda)\overline{x}_2) = \lambda \overline{x}_1 + (1-\lambda)\overline{x}_2, \ \forall \overline{x}_1, \overline{x}_2 \in X, \ \lambda \in [0,1] \tag{2.74}$$

Hence, affine functions are convex.

First and second order conditions for convexity of a function are given by following theorems, respectively.

Theorem 2.1. *[49]: Assume that $f(\overline{x})$ is differentiable $(\overline{\nabla} f(\overline{x}) \ exists \ \forall \overline{x} \in dom \ f)$ and $dom \ f$ is convex and open then $f(\overline{x})$ is a convex function if and only if first-order Taylor expansion of $f(\overline{x})$ is a global underestimator such that*

$$f(\overline{x}) \geq f(\tilde{x}) + \overline{\nabla} f(\tilde{x})^T (\overline{x} - \tilde{x}), \ \forall \overline{x}, \tilde{x} \in dom \ f \tag{2.75}$$

where $\overline{\nabla} f(\tilde{x})$ is the gradient vector of $f(\overline{x})$ at point $\tilde{x}$ and defined as

$$\overline{\nabla} f(\tilde{x}) = \begin{bmatrix} \dfrac{\partial f(\tilde{x})}{\partial x_1} \\ \vdots \\ \dfrac{\partial f(\tilde{x})}{\partial x_n} \end{bmatrix}_{n\times 1} . \tag{2.76}$$

Theorem 2.2. *[50]: If $f(\overline{x})$ is twice differentiable $(H(\overline{x})\ exists\ \forall \overline{x} \in dom\ f)$ and $dom\ f$ is convex and open then $f(\overline{x})$ is a convex function if and only if*

$$H(x) \succeq 0,\ \forall \overline{x} \in dom\ f \tag{2.77}$$

where $H(\overline{x})$ is the Hessian (matrix) of $f(\overline{x})$ such that

$$\Big[H(\overline{x})\Big]_{ij} = \overline{\nabla}^2 f(\overline{x}) = \overline{\nabla}\ \overline{\nabla}^T f(\overline{x}) = \left[\frac{\partial^2 f(\overline{x})}{\partial x_i \partial x_j}\right]_{n\times n},\ i,j \in 1,\dots n. \tag{2.78}$$

The most useful characteristic of convex functions can be explained by following theorem:

Theorem 2.3. *[49]: Assume that X is a convex set, $f(\overline{x})\colon X \to \mathbb{R}$ is a convex function with (strict) local minimum $\tilde{x}$. Then, $\tilde{x}$ is a (strict) global minimum of $f(\overline{x})$ over X.*

Proof. (Proof by contradiction) Suppose $\tilde{x}$ is not a (strict) global minimum, i.e., $\exists \overline{y} \in X,\ f(\overline{y}) < f(\tilde{x})$. Let

$$z(\lambda) \cong \lambda\tilde{x} + (1-\lambda)\overline{y},\ 0 \le \lambda \le 1, \tag{2.79}$$

hence, $z \in X$ and

$$\begin{aligned} f(z(\lambda)) = f(\lambda\tilde{x} + (1-\lambda)\overline{y}) &\le \lambda f(\tilde{x}) + (1-\lambda) f(\overline{y}) \\ &< \lambda f(\tilde{x}) + (1-\lambda) f(\tilde{x}) = f(\tilde{x}),\ \forall\lambda, \end{aligned} \tag{2.80}$$

meaning that $f(z(\lambda)) < f(\tilde{x}),\ \forall\lambda \in (0,1)$.
$\Rightarrow \tilde{x}$ is not a local minimum (contradiction). □
Theorem 2.3 gives the main property of convex functions for optimization: Any local minimum of a convex function is a global minimum.

Definition 2.22. ***(Constrained convex optimization problem)*** *Finally, a constrained convex optimization problem can be written as following form:*

$$\begin{aligned} \min_{\overline{x}\in X} \quad & f(\overline{x}) \\ s.t. \quad & g(\overline{x}) \leq 0 \\ & h(\overline{x}) = 0 \end{aligned} \tag{2.81}$$

Here, $f(\overline{x}),\ g(\overline{x}),\ h(\overline{x})$ *are convex functions and* $dom\ f$ *is convex.*

Example 2.3: This example is a classical H_∞ robust performance problem using convex optimization method. The main goal of this example is to find a controller $K(s)$ that minimizes the performance objective, i.e., $\||W_1 S| + |W_2 T|\|_\infty$, for a given model G and weighting functions W_1 and W_2, where

$$\begin{aligned} S &= \frac{1}{1+GK} \\ T &= \frac{GK}{1+GK}. \end{aligned} \tag{2.82}$$

All stabilizing controllers can be approximated by coprime factorization as follows:

$$\begin{aligned} G &= N_e M_e^{-1} \\ N_e X_e + M_e Y_e &= 1 \\ K &= \frac{X_e + M_e Q_e}{Y_e + N_e Q_e}. \end{aligned} \tag{2.83}$$

S and T can be rewritten as

$$\begin{aligned} S &= M_e(Y - N_e Q_e) \\ T &= N_e(X + M_e Q_e) \end{aligned} \tag{2.84}$$

which are affine with respect to Q_e. Hence, robust performance objective can be

modified as

$$\left|W_1 M_e(Y - N_e Q_e)\right| + \left|W_2 N_e(X + M_e Q_e)\right| < \gamma \quad \forall w \in \mathbb{R} \cup \{\infty\} \tag{2.85}$$

Note that, (2.85) is a set of convex constraints. Now, assume that Q_e is affine with respect to optimization variables $a_1,\ a_2,\ \ldots, a_n$, then (2.85) is also affine with respect to these variables. A possible choice of Q_e can be written as follows:

$$Q_e(s) = \frac{a_1 s^n + \cdots + a_n + b}{(s+c)^n} \tag{2.86}$$

where b and c are constant. The resulting convex optimization problem with an infinite number of constraints can be written as

$$\begin{aligned} &\min_{a_1,\ a_2,\ \ldots, a_n} \quad \gamma \\ &\text{s.t.} \ \ \left|W_1 M_e(Y - N_e Q_e)\right| + \left|W_2 N_e(X + M_e Q_e)\right| - \gamma < 0 \end{aligned} \tag{2.87}$$

This convex optimization problem can be solved numerically by gridding frequency points.

2.7 Comments

This section has essentially introduced frequency response identification methods, class of controllers, convex optimization methods, and other definitions which are used for the solution of data-driven fixed-order robust control problems. In Chapter 3, Chapter 4 and Chapter 5, the control problems will be solved using these methods and definitions.

3. ROBUST DATA-DRIVEN FIXED-ORDER H_∞ CONTROLLER SYNTHESIS: MODEL MATCHING APPROACH

This chapter concerned with the robust fixed-order H_∞ controller design problem for frequency domain non-parametric uncertain SISO systems. The proposed controller synthesis algorithm consist of two steps: First, a convex optimization method that is based on the concept of Chebyshev center of a set of points for the computation of optimal uncertainty models is proposed. In the second step, a sufficient condition is derived for robust performance constraints using the Nyquist stability theory and μ synthesis method. Then, a fixed-order H_∞ controller design algorithm based on convex optimization is introduced using linearly parameterized Laguerre basis functions with closed-loop model matching objective and control input constraints for identified non-parametric perturbed models. For comparison purpose, the performance of the presented method is compared with the available frequency-domain robust control toolbox (FDRC) [53] on the experimental test setup. Finally, the usefulness and efficiency of the proposed approach is verified experimentally with application to the control of a TVC system.

3.1 Closed-loop transfer functions

The frequency domain system and controller are connected in the one degree-of-freedom feedback control structure given in Figure. 3.1, defined by following equations:

$$e = r - y - v \tag{3.1}$$

$$u = K(jw)(r - y - v) \tag{3.2}$$

$$y = G(jw)(u + d_i) + d_o \tag{3.3}$$

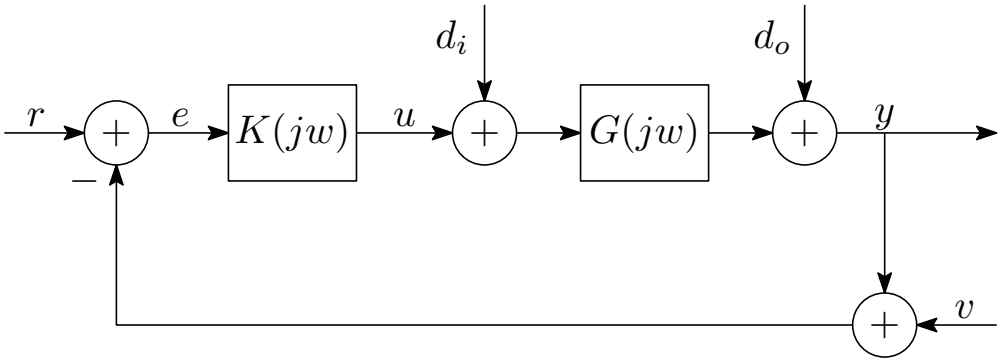

Figure. 3.1. Classical unity feedback interconnection.

where r is the reference input, e is the error, d_i is the input disturbance, v is the measurement noise and d_o is the output disturbance. The main objective of the H_∞ control theory is to synthesize a stabilizing controller that satisfies selected constraints on several closed-loop transfer functions. We will be interested in three sensitivity functions that are defined below:

Sensitivity function: The sensitivity function is the transfer function from the output disturbance to the plant output and is defined as

$$S(jw,k) = \frac{y}{d_o} = \frac{1}{1 + G(jw)K(jw)} \tag{3.4}$$

where $L(jw) = G(jw)K(jw)$ is the loop transfer function [7].

Complementary sensitivity function: The complementary sensitivity function is the transfer function from the reference input to the plant output and is defined as

$$T(jw,k) = \frac{y}{r} = \frac{G(jw)K(jw)}{1 + G(jw)K(jw)} \tag{3.5}$$

also, one have $S(jw) + T(jw) = I$.

Q-parameter: The Q-parameter function is the transfer function from the reference input to the control input and is defined as

$$Q(jw,k) = \frac{u}{r} = \frac{K(jw)}{1 + G(jw)K(jw)} \tag{3.6}$$

which is used as an indicator of the actuator effort [24].

3.2 Computing Optimal Multiplicative Uncertainty Models

In this section, a convex optimization method that is based on the concept of Chebyshev center of a set of points for the computation of optimal non-parametric uncertainty models is proposed. This approach simultaneously defines the optimal nominal frequency domain plant dynamics and minimal, least conservative uncertainty weighting function such that all $G_i(jw_n)$ exist within the uncertainty tube around the nominal model $G_{nom}(jw_n)$. The main objective is to find smallest uncertainty weighting function magnitude, which covers all of the available experimental data, and optimal nominal model at each frequency point.

In order to account for model uncertainty, we will assume that system dynamics of plant is represented by a set $\mathbf{M}$ of possible models. The number of frequency-domain models in the set $\mathbf{M}$ is m and the number of frequency points is N; therefore, the multiple model set $\mathbf{M}$ can be represented with unstructured multiplicative uncertainty frequency response function $W_2(jw)$ or unstructured additive uncertainty frequency response function $W_2^A(jw)$ by

$$\mathbf{M} : \tilde{G}(jw) := G_i(jw_n)\big(1 + W_{2i}(jw_n)\Delta\big) \tag{3.7}$$

$$\mathbf{M} : \tilde{G}(jw) := G_i(jw_n) + W_{2i}^A(jw_n)\Delta \tag{3.8}$$

respectively for $\Delta \in \mathbf{RH}_\infty,\ \|\Delta(jw)\|_\infty \leq 1\ \forall w,\ i = 1, \ldots, m;\ n = 1, \ldots, N$. In these equations, $\tilde{G}(jw)$ denotes the perturbed real plant dynamics. The functions $W_2(jw)$ and $W_2^A(jw)$ are stable, strictly proper transfer functions which define the magnitude of the uncertainty at each interested frequency point.

Modelling of the uncertainties is an essential part of the robust H_∞ control theory. A set of frequency domain data measured from experimental plant at different operating conditions is used to define the uncertainty model of the system. Because of the contradictory features of performance and robustness, it is desirable that magnitude of the uncertainty weighing function be as small as possible. A classical way

to define $W_2(jw)$ is given in [54] as

$$\left|\frac{G_i(jw_n) - G_{nom}(jw_n)}{G_{nom}(jw_n)}\right| \leq W_2(jw_n) \tag{3.9}$$

where $G_{nom}(jw_n)$ denotes the nominal model. One simple method for computing $G_{nom}(jw_n)$ is to calculate the average of the experimental data at each frequency point as

$$G_{nom}^{avg}(jw_n) := \frac{1}{m}\sum_{i=1}^{m} G_i(jw_n) \tag{3.10}$$

for $n = 1, \ldots, N$.

Multiplicative uncertainty optimization tries to minimize the magnitude of the terms $W_2(jw_n)G_{nom}(jw_n)$. For this cost function, the nominal model and multiplicative uncertainty function appear as products. Hence, this is a non-convex objective function with respect to $W_2(jw_n)$ and $G_{nom}(jw_n)$. However, in the additive uncertainty case the objective function is convex because the optimization algorithm attempts to minimize the magnitude of $W_2^A(jw_n)$ only. Therefore, one way to calculate a multiplicative uncertainty with minimum amplitude for a SISO system by convex semidefinite programming (SDP) is to solve convex optimization problem for additive uncertainty and then calculate the equivalent multiplicative weighting function using

$$W_2(jw_n) = \frac{W_2^A(jw_n)}{G_{nom}(jw_n)} \tag{3.11}$$

which is evident from (3.7) and (3.8).

An optimal multiplicative uncertainty model $W_2^{opt}(jw_n)$, which covers the data $G_i(jw_n)$ at frequency point w_n, and the optimal nominal model $G_{nom}^{opt}(jw_n)$ can be computed by forming a Chebyshev ball in the complex plane.

Definition 3.1. ***(Chebyshev ball)*** *The set of points*

$$\mathbb{B}(\overline{x}_c, r_c) = \{\overline{x} \mid \|\overline{x} - \overline{x}_c\|_2 \leq r_c\} = \{\overline{x}_c + r_c\overline{\rho} \mid \|\overline{\rho}\|_2 \leq 1\} \tag{3.12}$$

forms a Chebyshev ball with respect to the Euclidean norm around Chebyshev cen-

ter $\overline{x}_c$ with radius r_c [49, 50].

Proposition 3.1. *An optimal multiplicative uncertainty model $W_2^{opt}(jw_n)$ which contains the experimental data around the optimal nominal model $G_{nom}^{opt}(jw_n)$ can be calculated by the solution of the following convex optimization problem for optimal additive uncertainty model at each frequency point of interest:*

$$\begin{aligned} &\min_{G_{nom}(jw_n),\ |W_2^A(jw_n)|} |W_2^A(jw_n)| \\ s.t.\ &\begin{bmatrix} \Re(G_i(jw_n)) \\ \Im(G_i(jw_n)) \end{bmatrix} \in \mathbb{B}\left(\begin{bmatrix} \Re(G_{nom}(jw_n)) \\ \Im(G_{nom}(jw_n)) \end{bmatrix}, W_2^A(jw_n) \right) \end{aligned} \tag{3.13}$$

for $i = 1, \ldots, m;\ n = 1, \ldots, N$ and using (3.11) as

$$|W_2^{opt}(jw_n)| = \frac{|W_2^{A_{opt}}(jw_n)|}{|G_{nom}^{opt}(jw_n)|}. \tag{3.14}$$

Proof. Frequency response of $G_i(jw_n)$ can be represented by a complex number as

$$G_i(jw_n) = \Re\big(G_i(jw_n)\big) + j\Im\big(G_i(jw_n)\big) = x_{1n_i} + jx_{2n_i} \tag{3.15}$$

where the vector $\overline{x}_{n_i}$ defined as $\begin{bmatrix} x_{1n_i} & x_{2n_i} \end{bmatrix}^T$. Using the definition of Chebyshev ball, optimal additive uncertainty modelling problem can be formulated as:

$$\begin{aligned} &\min_{\overline{x}_{cn},\ \delta} \ \delta \\ &\text{s.t. } \|\overline{x}_{n_i} - \overline{x}_{cn}\|_2 - \delta \leq 0 \end{aligned} \tag{3.16}$$

for $i = 1, \ldots, m;\ n = 1, \ldots, N$. Solution algorithm of this convex optimization problem gives:

$$\begin{aligned} G_{nom}^{opt}(jw_n) &= \Re(x_{cn}^*) + j\Im(x_{cn}^*) \\ |W_2^{A_{opt}}(jw_n)| &= \delta^* \end{aligned} \tag{3.17}$$

which concludes the proof with (3.11). □

Remark 3.1. *The optimization (3.13) is a SDP convex optimization problem since both of the its objective function and its inequality constraint function are convex.*

Remark 3.2. *We assume that the uncertainty structure is in multiplicative form for the optimal uncertainty modelling approach in rest of the study. Obviously, the same convex optimization method can be applied to other uncertainty models (such as inverse additive uncertainty structure, ...).*

3.3 Model Matching Problem

A closed-loop model matching problem is an objective function based optimal control problem, i.e., it concerns the synthesis of the controller such that obtained closed-loop system is stable and matches as closely possible a chosen reference stable model. This predefined reference model $T_d(jw)$ is generally a low-order model that includes the desired dynamic behaviour of the controlled plant [55]. Using the FRF of the system and the linearly parameterized controller, the closed-loop model matching problem can be defined as

$$\begin{aligned} &\min_k \| W_m \left(T(jw,k) - T_d \right) \|_\infty \\ &= \min_k \left\| W_m \left(\frac{G(jw)K(jw)}{1+G(jw)K(jw)} - T_d \right) \right\|_\infty \\ &= \min_k \left\| W_m \left(\frac{G(jw)k\psi(jw)(1-T_d) - T_d}{1+G(jw)k\psi(jw)} \right) \right\|_\infty \end{aligned} \tag{3.18}$$

in the H_∞ sense where $W_m(jw)$ is the FRF of a stable penalty function weighting the frequency domain requirements. A block diagram representation of the closed-loop model matching problem is given in Figure. 3.2.

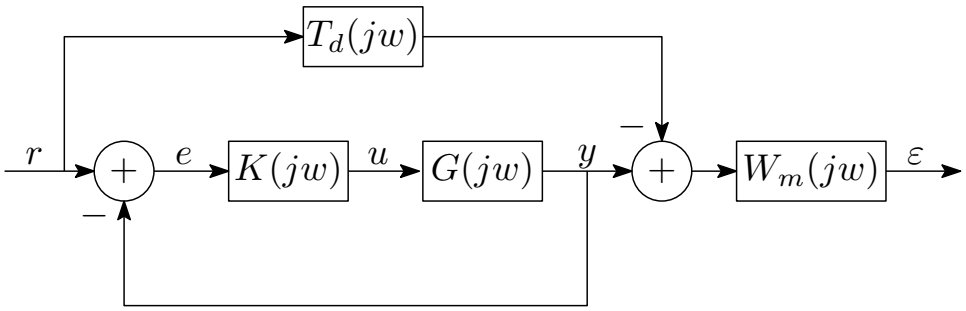

Figure. 3.2. Block diagram representation of the model matching problem.

The objective function of the optimization problem (3.18) is not a convex function with respect to the controller parameters k, because the denominator of this function includes design parameters. In order to approximate this non-convex optimization problem to a convex optimization problem, one approach is to replace the term $G(jw)k\psi(jw)$ in the denominator with the desired loop gain $L_d(jw)$ and formulate the sub-optimal control problem as

$$\min_k \left\| W_m \left(\frac{G(jw)k\psi(jw)(1-T_d) - T_d}{1 + L_d(jw)} \right) \right\|_\infty \tag{3.19}$$

where the desired loop-gain $L_d(jw)$ is given by

$$L_d(jw) = \frac{T_d(jw)}{1 - T_d(jw)}. \tag{3.20}$$

Note that objective function (3.19) $f : \mathbb{R}^{1\times n} \to \mathbb{C}$ is affine with respect to the k that is, linear function plus a constant term:

$$f(k) = \frac{W_m G(jw)\psi(jw)(1-T_d)}{1 + L_d(jw)} k - \frac{W_m T_d}{1 + L_d(jw)} \tag{3.21}$$

therefore, it can be considered as convex function.

3.4 Derivation of the Robust Performance Conditions

Due to the fact that the model matching does not guarantee internal stability, a sufficient condition for closed-loop stability can be derived and represented by a convex constraint on the Nyquist plot. Furthermore, the robust performance (RP) condition

is identical to robust stability (RS) condition with a fictitious uncertainty block, which is a full matrix [7].

Robust performance conditions can be derived based on a block diagram representation of the proposed control system which is shown in Figure. 3.3, where $W_1(jw)$ is the performance weighting function, ω is the exogenous input, z is the performance variable of interest and $\Delta_p(jw)$ is a fictitious bock defined through the performance channel such that $\|\Delta_p(jw)\|_\infty \leq 1$. This configuration is similar to the structured singular value, which is denoted by the μ or SSV, based analysis technique of robust performance criterion with fictitious block $\Delta_p(jw)$. Note that, for notation purposes, the dependence in jw will be omitted throughout the rest of the thesis and it will be used only if necessary.

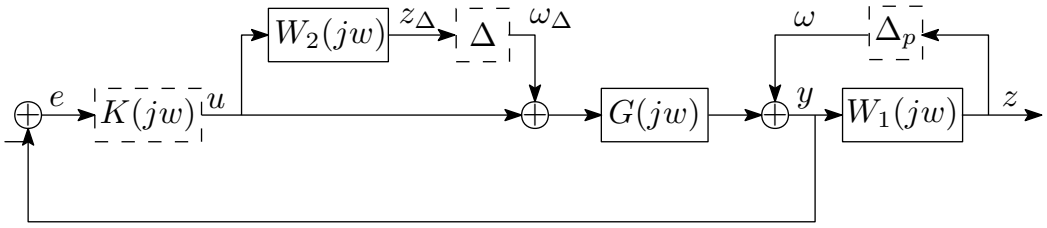

Figure. 3.3. Block diagram for robust performance constraints with two complex blocks.

The augmented plant P is constructed by separating the controller $K(jw)$, $\Delta_p(jw)$ and $\Delta(jw)$ from the control system in Figure. 3.3. P matrix can be partitioned in matrix form as

$$\begin{bmatrix} z_\Delta \\ z \\ e \end{bmatrix} = \left[\begin{array}{cc|c} P_{11}^{(11)} & P_{11}^{(12)} & P_{12}^{(11)} \\ P_{11}^{(21)} & P_{11}^{(22)} & P_{12}^{(21)} \\ \hline P_{21}^{(11)} & P_{21}^{(12)} & P_{22}^{(11)} \end{array}\right] \begin{bmatrix} \omega_\Delta \\ \omega \\ u \end{bmatrix}$$

$$\Big[P\Big] = \left[\begin{array}{cc|c} 0 & 0 & W_2 \\ W_1G & W_1 & W_1G \\ \hline -G & -I & -G \end{array}\right] \tag{3.22}$$

where P represents the transfer function from $\begin{bmatrix}\omega_\Delta & \omega & u\end{bmatrix}^{\mathrm{T}}$ to $\begin{bmatrix}z_\Delta & z & e\end{bmatrix}^{\mathrm{T}}$. With the

augmented plant P, the control system given by Figure. 3.3 can be transformed to an equivalent configuration given in Figure. 3.4.

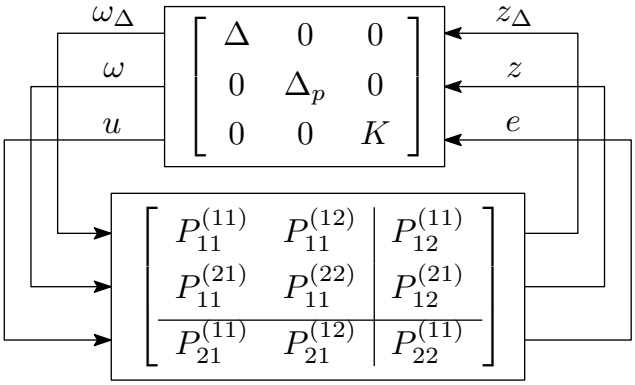

Figure. 3.4. Modification of the control problem for robust performance condition.

Lemma 3.1. *The closed-loop SISO system given by Figure. 3.3 and Figure. 3.4 satisfies the robust performance condition for a given internally stable plant G if and only if Nyquist plot of*

$$Q_{RP}(k, \Delta, \Delta_p, jw) = I - \Delta_p W_1 + \Delta W_2 GK + GK \tag{3.23}$$

function does not encircle the origin of the complex plane for $\forall w \in \mathbb{R} \cup \{\infty\},\ \Delta_p, \Delta \in \mathbf{RH}_\infty,\ \|\Delta_p\|_\infty, \|\Delta\|_\infty \leq 1$.

Proof. Loop gain of the positive feedback control system shown in Figure. 3.4 is given by

$$L_{pf} = \left[\begin{array}{cc|c} P_{11}^{(11)} & P_{11}^{(12)} & P_{12}^{(11)} \\ P_{11}^{(21)} & P_{11}^{(22)} & P_{12}^{(21)} \\ \hline P_{21}^{(11)} & P_{21}^{(12)} & P_{22}^{(11)} \end{array}\right] \begin{bmatrix} \Delta & 0 & 0 \\ 0 & \Delta_p & 0 \\ 0 & 0 & K \end{bmatrix}. \tag{3.24}$$

Generalized Nyquist stability theorem for given positive feedback system with stable

plant can be written as

$$\begin{aligned} & det\Big(I - L_{pf}\Big) \neq 0 \\ & \Leftrightarrow 1 - P_{11}^{(11)}\Delta \\ & + \Big(P_{11}^{(11)}P_{11}^{(22)}\Delta - P_{11}^{(12)}P_{11}^{(21)}\Delta - P_{11}^{(22)}\Big)\Delta_p \\ & + \Big(P_{11}^{(11)}P_{22}^{(11)}\Delta - P_{12}^{(11)}P_{21}^{(11)}\Delta - P_{22}^{(11)}\Big)K \\ & + \Big(P_{11}^{(22)}P_{22}^{(11)} - P_{12}^{(21)}P_{21}^{(12)} - P_{11}^{(11)}P_{11}^{(22)}P_{22}^{(11)}\Delta \\ & + P_{11}^{(11)}P_{12}^{(21)}P_{21}^{(12)}\Delta + P_{11}^{(12)}P_{11}^{(21)}P_{22}^{(11)}\Delta \\ & + P_{11}^{(12)}P_{12}^{(21)}P_{21}^{(11)}\Delta - P_{12}^{(11)}P_{11}^{(21)}P_{21}^{(12)}\Delta \\ & + P_{12}^{(11)}P_{11}^{(22)}P_{21}^{(11)}\Delta\Big)\Delta\Delta_p \neq 0. \end{aligned} \tag{3.25}$$

Then, substituting the components of matrix P in (3.22) into the (3.25) we obtain:

$$I - \Delta_p W_1 + \Delta W_2 GK + GK \neq 0 \tag{3.26}$$

which is the statement of the Lemma. □

Perturbed sensitivity function $\tilde{S}$ can be written as

$$\tilde{S} = \frac{1}{1 + GK(1 + W_2\Delta)} \tag{3.27}$$

with multiplicative uncertainty. The maximum magnitude of the $\tilde{S}$ occurs if $\Delta = 1$ and the phase angle of the terms (W_2GK) and $(1+GK)$ have opposite signs. Therefore, $\tilde{S}$ with the possible maximum magnitude is given by

$$\tilde{S}_{max} = \frac{1}{|1 + GK| - |W_2GK|}. \tag{3.28}$$

The necessary and sufficient condition for robust performance criterion of the clas-

sical unity negative feedback system (Figure. 3.3) is given by [54]

$$\begin{aligned} &\big|W_1 S\big| + \big|W_2 T\big| < 1 \\ \Leftrightarrow &\left|\frac{W_1}{1+GK}\right| + \left|\frac{W_2 GK}{1+GK}\right| < 1,\ \forall w \in \mathbb{R} \cup \{\infty\}. \end{aligned} \tag{3.29}$$

Multiplying both sides of (3.29) by $(1+GK)$ gives

$$\begin{aligned} &\big|W_1\big| + \big|W_2 GK\big| < \big|1+GK\big| \\ \Leftrightarrow &\frac{1}{\big|1+GK\big| - \big|W_2 GK\big|} < \frac{1}{\big|W_1\big|} \end{aligned} \tag{3.30}$$

and it is clear that, left hand side of the second part of (3.30) is equal to S_{max}; therefore, the robust performance condition holds if and only if

$$\|\tilde{S}_{max}\|_\infty < \frac{1}{|W_1|},\ \forall w \in \mathbb{R} \cup \{\infty\}. \tag{3.31}$$

In Figure. 3.4; $\omega_\Delta \to z_\Delta$ is the uncertainty channel and $\omega \to z$ is the performance channel. Using these channels, robust stability, nominal performance (NP) and nominal stability (NS) conditions can be defined as follows:

Definition 3.2. ***(Robust stability)*** *Robust stability condition is a special form of robust performance condition with $\Delta_p = 0$ fictitious performance block and depicts the stability of system for all perturbed models. Therefore, the closed-loop control system given by Figure. 3.4 with $\Delta_p = 0$ block satisfies the RS condition for an internally stable system if and only if Nyquist plot of*

$$\begin{aligned} &det\left(I - \left[\begin{array}{c|c} P_{11}^{(11)} & P_{12}^{(11)} \\ \hline P_{21}^{(11)} & P_{22}^{(11)} \end{array}\right] \begin{bmatrix} \Delta & 0 \\ 0 & K \end{bmatrix}\right) \neq 0 \\ &\Leftrightarrow 1 - P_{11}^{(11)}\Delta \\ &+\Big(P_{11}^{(11)} P_{22}^{(11)}\Delta - P_{12}^{(11)} P_{21}^{(11)}\Delta - P_{22}^{(11)}\Big)K \neq 0 \end{aligned} \tag{3.32}$$

function does not encircle the origin of the complex plane. Then, substituting the component of matrix P into the (3.32) we obtain the RS condition for control system

given by Figure. 3.4 as:

$$I + \Delta W_2 GK + GK \neq 0;\ \forall w, \Delta \in \mathbf{RH}_\infty,\ \|\Delta\|_\infty \leq 1. \tag{3.33}$$

Definition 3.3. ***(Nominal performance)*** *Nominal performance condition can be considered as a special form of robust performance condition with nominal model ($\Delta = 0$) and defines the performance requirements with no model uncertainty. Then,*

$$\begin{aligned} NP \Leftrightarrow det\left(I - \left[\begin{array}{c|c} P_{11}^{(22)} & P_{12}^{(21)} \\ \hline P_{21}^{(12)} & P_{22}^{(11)} \end{array}\right]\left[\begin{array}{cc} \Delta & 0 \\ 0 & K \end{array}\right]\right) \neq 0 \\ \Leftrightarrow 1 - P_{11}^{(11)}\Delta \\ + \left(P_{11}^{(11)}P_{22}^{(11)}\Delta - P_{12}^{(11)}P_{21}^{(11)}\Delta - P_{22}^{(11)}\right)K \neq 0 \end{aligned} \tag{3.34}$$

and the closed-loop control system given by Figure. 3.4 with $\Delta = 0$ block satisfies the NP condition for an internally stable system if and only if

$$I - \Delta_p W_1 + GK \neq 0;\ \forall w, \Delta_p \in \mathbf{RH}_\infty,\ \|\Delta_p\|_\infty \leq 1. \tag{3.35}$$

Definition 3.4. ***(Nominal stability)*** *Nominal stability condition defines the internal stability of requirement of control system with no model uncertainty. Then,*

$$NS \Leftrightarrow det\left(I - P_{22}^{(11)}\right) \neq 0 \tag{3.36}$$

$$\tag{3.37}$$

and the closed-loop control system given by Figure. 3.4 with $\Delta = 0,\ \Delta_p = 0$ blocks satisfies the NS condition if and only if

$$I + GK \neq 0;\ \forall w. \tag{3.38}$$

Note that, internally stable system requirement for RP, RS and NP conditions can be satisfied if and only if given control system satisfies the NS condition. Therefore, NS condition is a prerequisite for RP, RS and NP conditions [7].

Remark 3.3. *We consider only the RP condition throughout the rest of this thesis.*

However, in some control applications, synthesis or analysis of the control system may be required according to the RS, NP or NS conditions. In such cases, the above definitions may be useful.

Constraint functions of the fixed-order H_∞ control problem can be derived using Nyquist plot based on the robust performance condition given by (3.23). The fact that frequency dependent $Q_{RP}(k, \Delta, \Delta_p, jw)$ polynomial does not encircle the origin of the Nyquist plot constitutes the main constraint function of optimization problem. This robust performance condition inequality can be modified as

$$\Delta W_2 GK + GK \neq -I + \Delta_p W_1 \tag{3.39}$$

where Δ and Δ_p blocks represent two different balls in complex plane such that $\|\Delta\|_\infty, \|\Delta_p\|_\infty \leq 1$. Note that, when $\|\Delta_p\|_\infty = 1$ (worst-case) right hand side of (3.39) defines a circle, which is called performance circle, with radius $|W_1|$ and center $(-1, j0)$ in the Nyquist diagram. Similarly, if Δ block satisfies the worst-case condition ($\|\Delta\|_\infty = 1$), left hand side of (3.39) defines another circle, which is called robustness circle, with radius $|W_2 GK|$ and center $\big(\Re(GK), \Im(GK)\big)$ (Figure. 3.5). Therefore, robust performance condition given by (3.23) is satisfied if and only if the performance circle and the robustness circle do not intersect each other in complex plane for all frequencies w. This statement holds if and only if the performance circle and robustness circle does not have intersection. Hence, robust performance constraint can be adapted to the robust H_∞ control problem by preventing the intersection of these circles via a frequency dependent line.

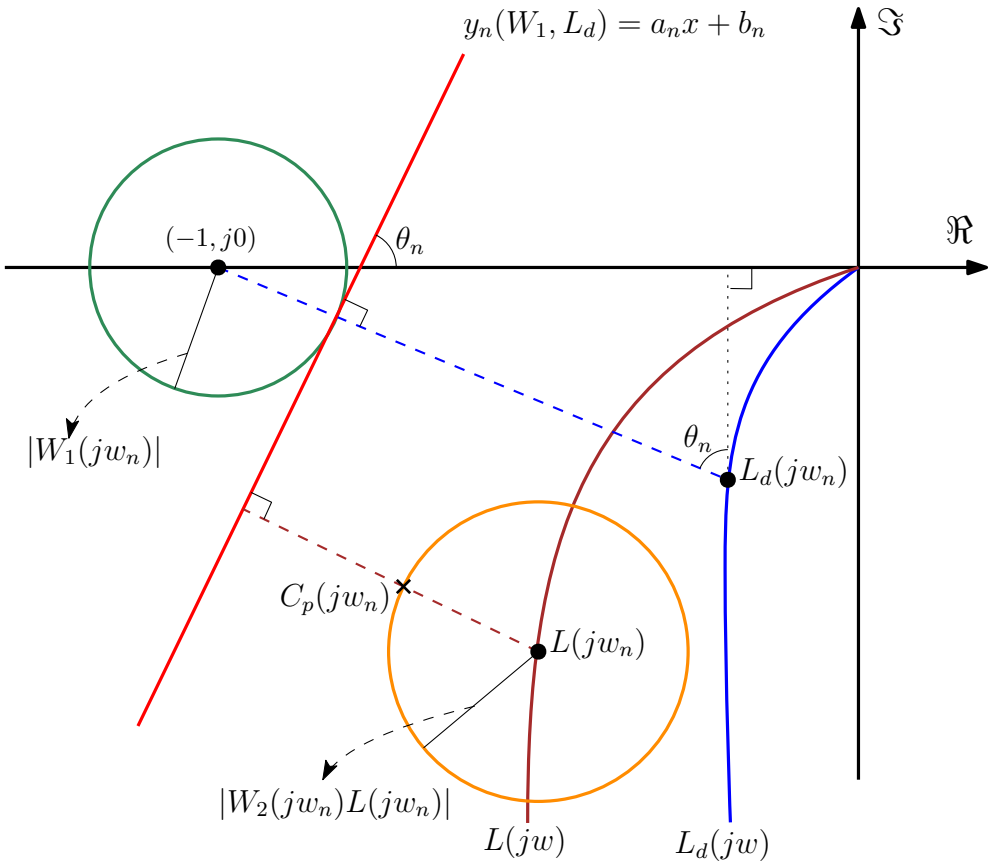

Figure. 3.5. Graphical representation of the robust performance constraint.

The robust performance condition given by (3.23) is satisfied if robustness circle lies below the line $y_n(W_1, L_d) = a_n x + b_n$ in Nyquist diagram as shown in Figure. 3.5. In order to represent robust performance condition as a convex constraint in optimization problem, parameters of the line can be defined with respect to L_d. Constructed line tangent to the performance circle and orthogonal to the line from the $(-1, j0)$ point to L_d as shown in Figure. 3.5. The frequency dependent parameters of this line can be defined using geometrical relationships in Figure. 3.5 as

$$a_n = \frac{1 - \Re(L_d)}{\Im(L_d)} \tag{3.40}$$

$$b_n = \frac{a_n\big(sin(\theta_n) - |W_1|\big)}{sin(\theta_n)} \tag{3.41}$$

where θ_n is the slope of the line and given by

$$\theta_n = tan^{-1}\left(\frac{1-\Re(L_d)}{\Im(L_d)}\right). \tag{3.42}$$

Now, consider the nearest critical point $C_p(jw_n)$ from the robustness circle to the line $y_n(W_1, L_d) = a_n x + b_n$ in Figure. 3.5. Then, the robustness circle lies below the line if and only if $C_p(jw_n)$ exists below the line for all frequencies w. Therefore, the representation of the robust performance constraint in H_∞ controller synthesis problem with a sufficient condition is given by following proposition:

Proposition 3.2. *Closed-loop control system given by Figure. 3.3, satisfies the robust performance condition (3.23) if*

$$\begin{gathered}\Im(k\psi G) - a_n\Re(k\psi G) \\ +|W_2 k\psi G|\big(a_n sin(\theta_n) + cos(\theta_n)\big) - b_n \leq 0\end{gathered} \tag{3.43}$$

for $\forall w \in \mathbb{R} \cup \{\infty\}$.

Proof. The point $C_p(jw_n)$ lies below the line if

$$C_p(jw_n) \leq y_n = a_n x + b_n \tag{3.44}$$

in the Nyquist plot. Real and imaginary parts of the the critical point $C_p(jw_n)$ in Figure. 3.5 can be defined with respect to the origin of the Nyquist plot as

$$\begin{aligned}\Re\big(C_p(jw_n)\big) &= \Re(k\psi G) - |W_2 k\psi G| sin(\theta_n) \\ \Im\big(C_p(jw_n)\big) &= \Im(k\psi G) + |W_2 k\psi G| cos(\theta_n)\end{aligned} \tag{3.45}$$

respectively. Then, substituting real part of this equation into the (3.44) yields:

$$\begin{gathered}\Im(k\psi G) - a_n\Re(k\psi G) \\ +|W_2 k\psi G|\big(a_n sin(\theta_n) + cos(\theta_n)\big) - b_n \leq 0\end{gathered} \tag{3.46}$$

for $\forall w \in \mathbb{R} \cup \{\infty\}$, which is the statement of the proposition. □

Remark 3.4. *Since RS, NP and NS conditions are specific forms of RP condition, these conditions can be derived by making the necessary arrangements, which are given by Definition 1, Definition 2, Definition 3 respectively, in (3.43).*

3.5 Control Input Constraints

One of the most important obstacles of physical real systems is the saturation characteristics of the actuators. Real time control systems usually have control input limits, because the power sources cannot provide infinitely large control input. In order to take into account available input limits in the convex optimization problem, in this subsection we derive the control input constraints for fixed-order H_∞ control synthesis scheme.

The block diagram representation of the closed loop control system with control signal weighting function W_u is shown in Figure. 3.6.

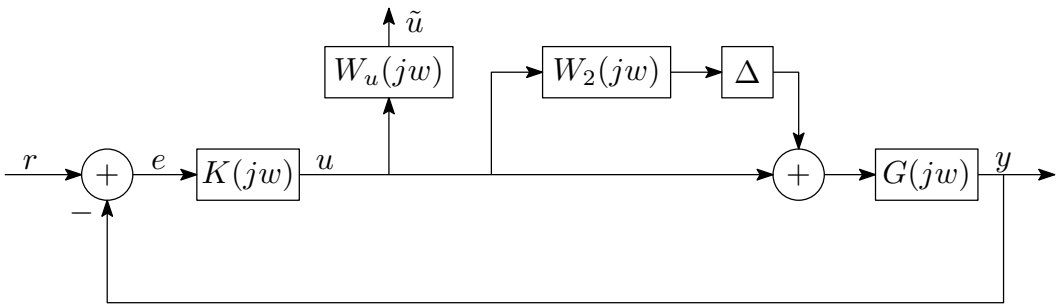

Figure. 3.6. Closed-loop control system with control input constraint.

By using this figure, Q-parameter transfer function from the reference input to the control input with multiplicative type model uncertainty of the plant given by

$$\tilde{Q} = \frac{u}{r} = \frac{k\psi}{1 + Gk\psi(1 + W_2\Delta)}. \tag{3.47}$$

Then, control input constraint can be written as

$$
\begin{aligned}
&|W_u\tilde{Q}| - \tilde{u}_{max} \leq 0 \\
&\Leftrightarrow \left| \frac{W_u k\psi}{1 + Gk\psi(1 + W_2\Delta)} \right| \leq \tilde{u}_{max} \\
&\Leftrightarrow -\tilde{u}_{max} \leq \frac{W_u k\psi}{1 + Gk\psi(1 + W_2\Delta)} \leq \tilde{u}_{max}
\end{aligned}
\tag{3.48}
$$

for $\forall w \in \mathbb{R} \cup \{\infty\}$, where $\tilde{u}_{max}$ is the upper bound of the weighted control input signal in frequency domain. The maximum control input occurs at minimum loop-gain condition; therefore, the worst-case control input generated when $\Delta = 1$ and the phase angle of the terms $(W_2 Gk\psi)$ and $(1 + Gk\psi)$ have opposite signs. Hence,

$$
\begin{aligned}
&|W_u\tilde{Q}_{max}| - \tilde{u}_{max} \leq 0 \\
&\Leftrightarrow -\tilde{u}_{max} \leq \frac{|W_u k\psi|}{|1 + Gk\psi| - |W_2 Gk\psi|} \leq \tilde{u}_{max} \\
&\Leftrightarrow \begin{bmatrix} -\tilde{u}_{max}(|1 + Gk\psi| - |W_2 Gk\psi|) - |W_u k\psi| \\ -\tilde{u}_{max}(|1 + Gk\psi| - |W_2 Gk\psi|) + |W_u k\psi| \end{bmatrix} \leq \begin{bmatrix} 0 \\ 0 \end{bmatrix}
\end{aligned}
\tag{3.49}
$$

which are the control input constraint functions of the fixed-order H_∞ control problem. Notice that these constraint functions are convex (affine) with respect to the controller parameters k.

3.6 Optimization Problem

In order to satisfy the robust performance condition, the control input constraints and the closed-loop model matching objective, the fixed-order H_∞ controller design problem can be formulated as constrained convex optimization problem with respect to the controller parameters. According to the these requirements, a convex optimization problem is arranged for the optimal synthesis of the fixed-order H_∞ controller

as follows:

$$\begin{aligned}
\min_{k} \quad & \left\| \frac{W_m G\psi(1-T_d)}{1+L_d}k - \frac{W_m T_d}{1+L_d} \right\|_\infty \\
\text{s.t.} \quad & \Im(k\psi G) - a_n \Re(k\psi G) - b_n \\
& + |W_2 k\psi G| \big(a_n sin(\theta_n) + cos(\theta_n)\big) \leq 0; \\
& -\tilde{u}_{max}(|1+Gk\psi| - |W_2 Gk\psi|) - |W_u k\psi| \leq 0; \\
& -\tilde{u}_{max}(|1+Gk\psi| - |W_2 Gk\psi|) + |W_u k\psi| \leq 0
\end{aligned} \tag{3.50}$$

for $\forall w \in \mathbb{R} \cup \{\infty\}$.

This optimization problem involves an infinite number of constraints; therefore, it is a convex semi-infinite programming (SIP) problem. In order to transform this SIP problem into SDP problem, which can be solved numerically using available convex optimization techniques and solvers, finite number of frequency points $w_n (n = 1, 2, \ldots N)$ are considered. The parameters of the linearly parameterized robust controller are determined efficiently by solving the above SDP convex optimization problem in sampled frequency range.

Practically, the number of points in the frequency range of interest should be large enough. However, ensuring that defined conditions are satisfied at a finite number of frequency points does not mean that the conditions are also satisfied at all frequencies. A randomized scenario approach [56] can be used to compute the minimum number of frequency point to guarantee the constraints with a chosen probability level. According to the scenario approach, if the number of scenarios N satisfies

$$N \geq \frac{2}{\epsilon}\left(d_p - 1 + ln\frac{1}{\beta}\right) \tag{3.51}$$

condition for d_p number of optimization variables, risk parameter $\epsilon \in (0, 1)$, and confidence parameter $\beta \in (0, 1)$, then, constraints hold with a probability level $\geq 1 - \beta$.

3.7 Performance Weighting Function Selection

Deviations from the predefined reference model are inevitable due to the uncertainties in the system dynamics. Therefore, it is useful to determine the performance weighting function with respect to worst-case reference model matching requirement. Since the objective function of the optimization problem related to the complementary sensitivity function, the worst-case desired closed-loop transfer function T_d^1 can be considered as

$$T_d^1 = \frac{w_n^2}{s^2 + 2\zeta w_n s + w_n^2} \tag{3.52}$$

where w_n is the natural frequency and ζ is the damping ratio. In order to chose the performance weighting function W_1, we consider the loop-gain of a standard second-order system as

$$L_d^1 = \frac{T_d^1}{1 - T_d^1} = \frac{w_n^2}{s^2 + 2\zeta w_n s} \tag{3.53}$$

then, ideal sensitivity function can be defined as

$$S_d^1 = \frac{1}{1 + L_d^1} = \frac{s^2 + 2\zeta w_n s}{s^2 + 2\zeta w_n s + w_n^2}. \tag{3.54}$$

Note that

$$\left|S_d^1\left(jw_n/\sqrt{2}\right)\right| = 1 \tag{3.55}$$

$$M_s := \|S_d^1\|_\infty = \frac{\beta_s\sqrt{\beta_s^2 + 4\zeta^2}}{\sqrt{(1-\beta_s^2)^2 + 4\zeta^2\beta_s^2}} \tag{3.56}$$

$$w_b \approx \frac{w_n}{\sqrt{2}} \tag{3.57}$$

where $\beta_s = \sqrt{0.5 + 0.5\sqrt{1 + 8\zeta^2}}$, w_b is the cut-off frequency of S_d^1 and M_s is the peak gain of S_d^1 at $w_{max} = \beta_s w_n$ frequency point [41]. Sensitivity function S is a good indicator of control performance. Therefore, performance weighting function can be

defined with respect to S. A possible choice of performance weigh W_1 is given as

$$W_1 = \left(\frac{s/M_s^{1/\nu} + w_b}{s + w_b \varrho^{1/\nu}} \right)^{\nu} \tag{3.58}$$

where ϱ bounds the steady-state error for $\nu \geq 1$ [41].

Note that, predefined reference model in (3.18) can be chosen as given in (3.52) as well. However, for a feasible choice of performance weighting function W_1, the natural frequency of T_d^1 should be smaller than the natural frequency of reference model T_d in (3.18). Otherwise, there will be a contradiction between robust performance and model matching achievement.

3.8 Experimental Implementation

In this section, proposed controller design methodology is applied to the position control of an electromechanical TVC system.

3.8.1 Thrust Vector Control System

Several guided air vehicle platforms generally need steering mechanism in order to direct their course especially during the exoatmospheric flight conditions. TVC system is used to control the flight of the vehicle by changing the direction of main thrust vector.

In this study, a flexible joint nozzle type TVC system is used as an experimental test bench that consists of two electromechanical actuator (EMA) (Figure. 3.7).

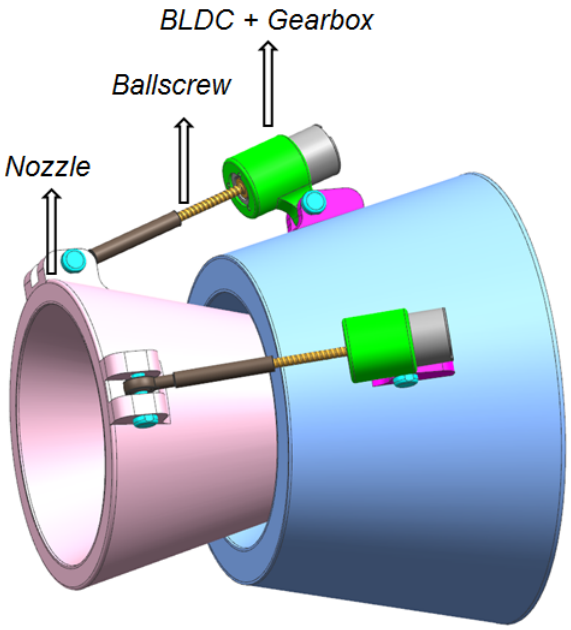

Figure. 3.7. Flexible joint nozzle type TVC system.

The EMA configuration, which is composed of a brushless DC (BLDC) electric motor, planetary gear train, a ballscrew and a digital position sensor, is presented in this figure.

3.8.2 Modelling of Electromechanical Actuation Systems

The use of electromechanical-based actuation systems in the defence, aerospace and robotics industries is becoming increasingly widespread. The main reasons for this increase are dynamic system behaviour performance, high power density, easy controllability, simple structure, low cost, low volume requirement and reliability of electromechanical based actuation systems [57–59].

Motion control systems are mainly composed of actuators, sensors and mechanism. The sensors measure position or velocity with faster dynamics than the closed-loop bandwidth of the motion control systems. If the position sensor is located on the motor side, i.e., non-collocated side, the motion control system is called the semi-closed loop feedback position control system. On the other hand, if the position sensor is placed on the load side, i.e., collocated side, the motion control system is called the full-closed loop feedback position control system. In high precision control applications, the sensors are generally used on load side [60].

Several guided air vehicle platforms generally use aerodynamic control surfaces or steering mechanism to direct their course. The TVC system is used to control the flight of the vehicle by changing the direction of main thrust vector. Similarly, the CAS is responsible for the motion that controls the flight of the air vehicle by changing the direction of these control surfaces.

In this thesis, a flexible joint nozzle type electromechanical TVC system (in Chapter 3) and an electromechanical type CAS (in Chapter 4 and Chapter 5) are used as an experimental test bench. These systems are consist of EMA. The EMA configurations are composed of a brushless DC (BLDC) electric motor, gear train, a mechanism and a digital position sensor.

A nominal dynamical equation of the EMA can be obtained based on the BLDC electric motor dynamics. The separate voltage equations of the q and d axis of the three-phase, two-pole BLDC motor are given by

$$v_{qs} = r_s i_{qs} + w_r \lambda_{ds} + \frac{d}{dt}\lambda_{qs} \tag{3.59}$$

$$v_{ds} = r_s i_{ds} - w_r \lambda_{qs} + \frac{d}{dt}\lambda_{ds} \tag{3.60}$$

in which $\lambda_{qs} = L_{qs} i_{qs},\ \lambda_{ds} = L_{ds} i_{ds} + \lambda_m$, where λ_m is the flux linkage amplitude generated by permanent magnets, r_s is the stator resistance, i_{qs} is the q-axis current, i_{ds} is the d-axis current, w_r is the electrical angular velocity, λ_{qs} is the q-axis flux linkage, λ_{ds} is the d-axis flux linkage, L_{qs} is the q-axis inductance and L_{ds} is the d-axis inductance. By using these voltage equations, the current equation of the q and d axis can be derived as

$$\frac{d}{dt} i_{qs} = \frac{1}{L_{qs}} (v_{qs} - w_r L_{ds} i_{ds} - w_r \lambda_m - r_s i_{qs}) \tag{3.61}$$

$$\frac{d}{dt} i_{ds} = \frac{1}{L_{ds}} (v_{ds} + w_r L_{qs} i_{qs} - r_s i_{ds}) \tag{3.62}$$

respectively [61].

The electromagnetic torque equation of the BLDC motor is given by

$$T_e = (\frac{3}{2})(\frac{p}{2})\lambda_m i_{qs} = K_t i_{qs} \tag{3.63}$$

in which p and K_t are the number of poles and torque constant of the motor, respectively. The equation of the motion of the EMA in terms of equivalent moments of inertia J_e, equivalent viscous damping B_e, equivalent Coulomb friction F_e, load torque T_L and mechanical reduction ratio N_g can be written as

$$J_e\ddot{\theta} + B_e\dot{\theta} + F_e sign(\dot{\theta}) + T_L = K_t i_{qs} N_g \tag{3.64}$$

where θ is the deflection angle of the EMA. The main control goal of this sub-system is to provide required the control surface rotation angle or thrust vector rotation angle despite disturbances, high frequency flexible dynamics and vibration. Therefore, the input of the system is i_{qs} and the output is θ.

3.8.3 Experimental Test Setup

An experimental test bench has been built up to obtain FRF's of real-time plant and validate the closed-loop control performance of the proposed robust data-driven fixed-order controller. Signal flows between the TVC system and other items of test setup are shown in Figure. 3.8.

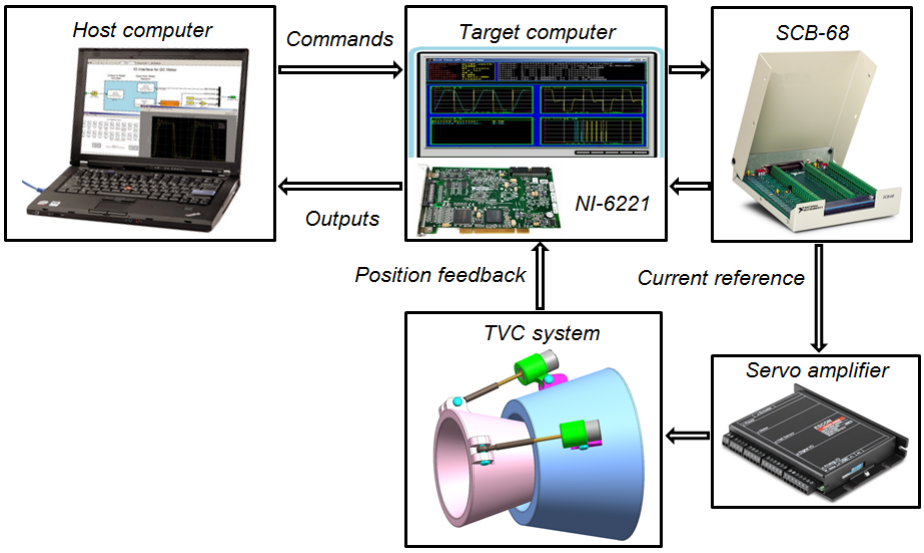

Figure. 3.8. Signal flows for experimental testing of the TVC system.

An NI 6221 data acquisition (DAQ) board is used to receive the measurement data and to send the control signal. NI SCB-68 shielded input/output (I/O) connector block is used to connect to NI 6221 DAQ cards with 68 screw terminals. The connector block also has a signal conditioning capability for filtering the signals. The EMAs are mounted on the nozzle to provide two degree of freedom rotation to TVC system. These EMA's are controlled by two separate ESCON 50/5 servo amplifier which is a commercial product of Maxon company. Real-time implementation of the control algorithm is provided by using xPC target toolbox of MATLAB software. This toolbox includes discrete time controller matrix, communication protocols and signal type converters. The synthesized fixed-order controllers are tested on the real-time hardware via xPC target toolbox. A host computer is used for off-line programming of the closed-loop control algorithm. The transfer function of the obtained controller is digitalized using bilinear transformation method. Digital closed-loop position control loop of experimental TVC system is operated at 1 kHz frequency.

3.8.4 Frequency Response Identification of TVC System

The FRF of the TVC system varies depending on the variable environmental conditions, unmodeled system dynamics, non-linear system behaviour, material life and aging. These uncertainties may cause unpredictable TVC system performance which may lead, in some cases, to the system instability. It is not always possible to guarantee required system performance under these adverse conditions with a controller synthesized using a single nominal model [59]. Therefore, in this study, frequency response identification is carried out under different working conditions in order to incorporate model uncertainties into the control system design process. Due to the schedule of environmental testing system and long temperature conditioning process, only six open-loop system identification experiment could be performed.

In order to obtain six different FRF's of the TVC system, multiple tests were carried out in the temperature range of -20 °C to 80 °C by increasing the temperature by 20 °C degrees steps at each test condition. A pseudo-random binary sequence (PRBS) signal was used as the q-axis current reference of the open-loop TVC system in the experiments to obtain the time domain response of the plant. The input q-axis current and output angle θ signals acquired from the frequency response identification

experiments are shown in Figure. 3.9.

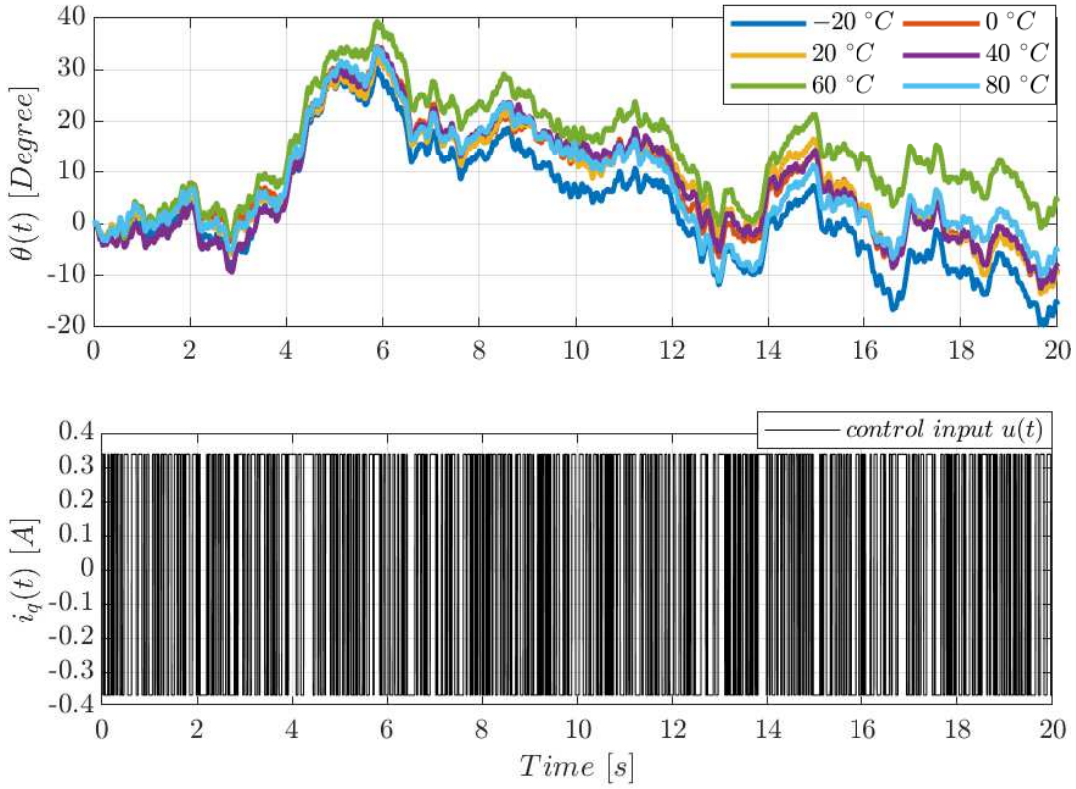

Figure. 3.9. Applied PRBS signal used for q-axis current $i_q(t)$ with the resulting output $\theta(t)$ angle.

Frequency domain experimental data was obtained with 400 logarithmically spaced frequency points, a value which is approximately calculated using (3.51) where $\epsilon = 0.05$, $\beta = 0.001$ and $d_p = 4$, between $w_l = 1\ rad/s$ and $w_u = 100\ rad/s$. FRF's of the real-time system, which are obtained with (2.40), are given in Figure. 3.10.

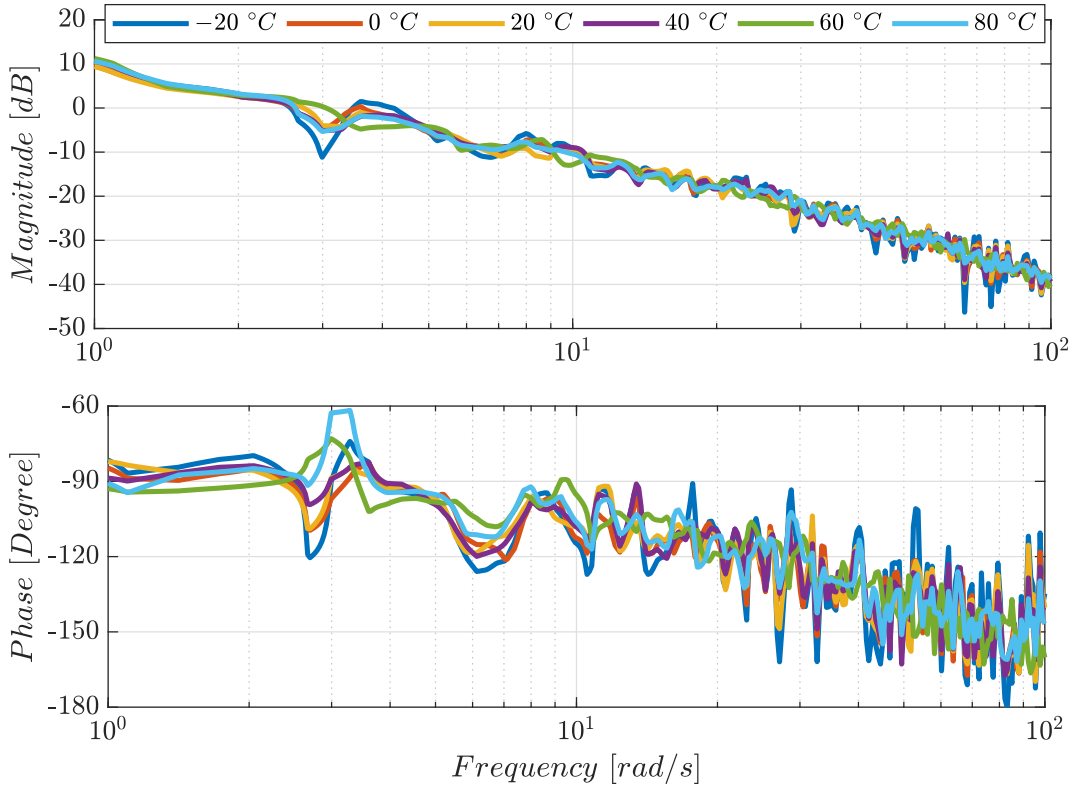

Figure. 3.10. Measured multiple FRF's of the TVC system.

3.8.5 Controller Synthesis for TVC System

The reference model for desired closed-loop control system was selected as

$$T_d = \frac{(2\pi 15)^2}{s^2 + 1.4(2\pi 15)s + (2\pi 15)^2} \tag{3.65}$$

where $\zeta = 0.7$ and $w_n = 2\pi 15\ rad/s$. Similarly, the worst-case reference model T_d^1 for the selection of the performance weight was chosen as

$$T_d^1 = \frac{(2\pi 3)^2}{s^2 + 1.4(2\pi 3)s + (2\pi 3)^2} \tag{3.66}$$

therefore, performance weighing function W_1 used to design robust controller is given by

$$W_1 = \frac{0.749s^2 + 23.081s + 177.661}{s^2 + 4.741s + 5.619} \tag{3.67}$$

which is obtained by using (3.51) with $\nu = 2,\ \varrho = 0.001$. While designing the robust controller, $\tilde{u}_{max}$, W_u and W_m were taken as 1 for the sake of simplicity and to make a fair comparison with FDRC toolbox.

The optimal nominal model (G_{nom}^{opt}) and optimal multiplicative uncertainty function (W_2^{opt}) were calculated using the semi-definite convex optimization method given by Proposition 1. This convex optimization problem was solved using CVX solver [62] which is a MATLAB-based package for convex optimization problems. For comparison purpose, another nominal model (G_{nom}^{avg}) was calculated by average method, which is given in (3.10). Additionally, corresponding multiplicative uncertainty weighing (W_2^{avg}) function was constructed by classical method, which is given in (3.9).

Obtained Nyquist plot of $G_{nom}^{opt}(jw_n)$ and $G_{nom}^{avg}(jw_n)$ are shown in Figure. 3.11 with corresponding uncertainty models.

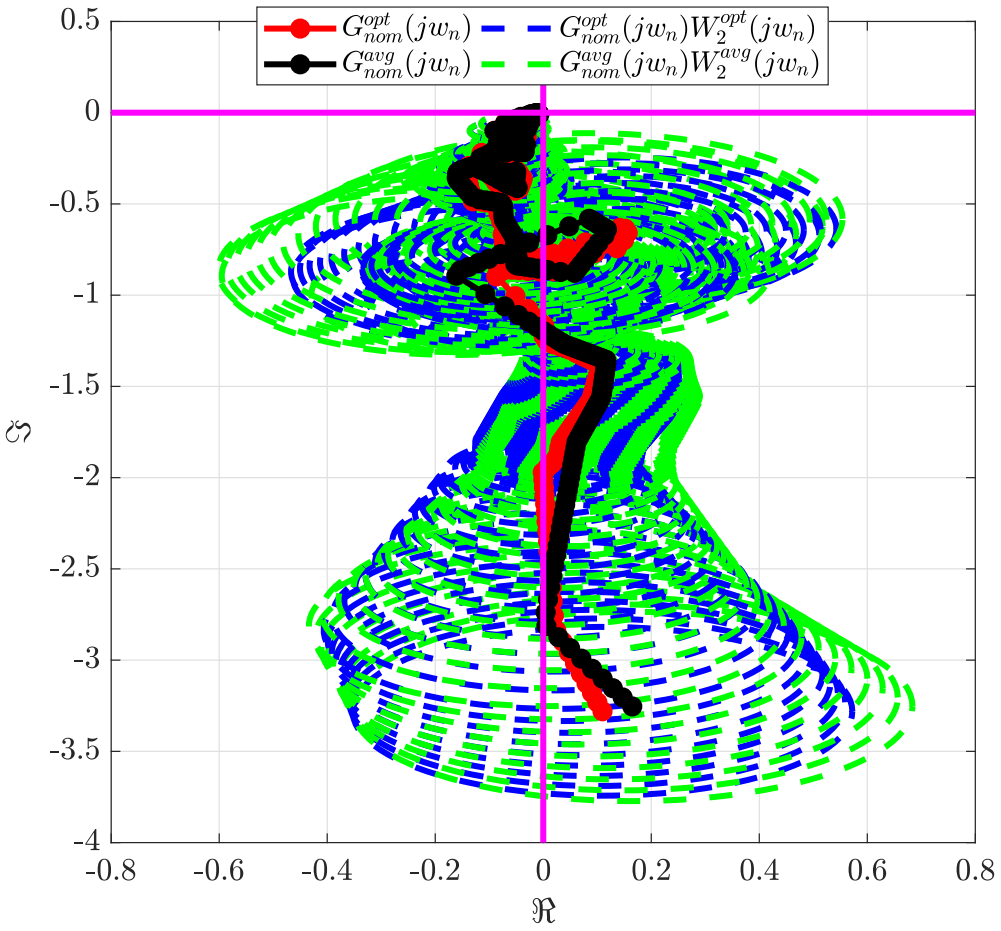

Figure. 3.11. Nyquist plot of the obtained non-parametric nominal models with optimum multiplicative uncertainty weighting bounds for proposed method and classical uncertainty bounds for average method.

The magnitude plots of the corresponding multiplicative uncertainty weighting functions are given in Figure. 3.12 for both methods.

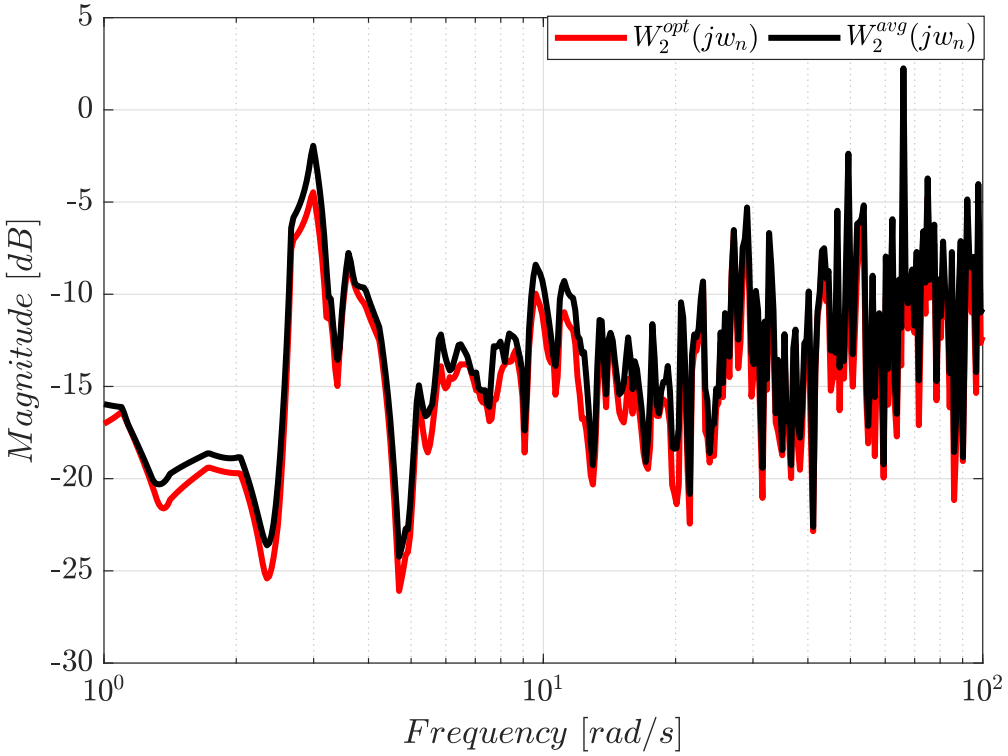

Figure. 3.12. Optimum multiplicative uncertainty weighting function for proposed method and classical method.

The obtained Chebyshev center and Chebyshev radius of a set of frequency response data points to cover all of the data at a sample point $w = 4\pi\ rad/s$ are shown in Figure. 3.13. The classical multiplicative uncertainty weighting function and average model also shown in this figure.

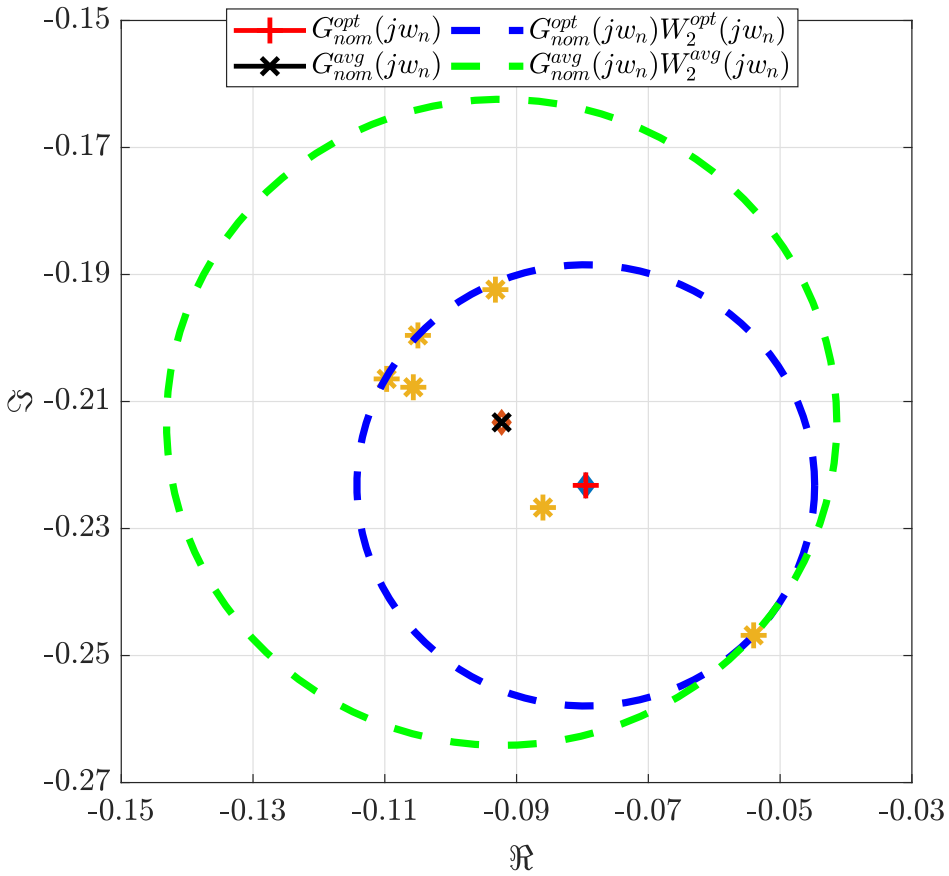

Figure. 3.13. Nyquist plot of the experimental plant response with classical uncertainty bound and optimal uncertainty bound at $w = 4\pi\ rad/s$.

Classical uncertainty modelling approach produces a considerably more conservative weighting function magnitude model than the proposed optimal uncertainty modelling method as shown in Figure. 3.11, Figure. 3.12 and Figure. 3.13. Since several data points have relatively large gain at $w = 4\pi\ rad/s$ frequency point, classical method generate larger uncertainty magnitude than the radius of optimal uncertainty function as shown in Figure. 3.13. These results demonstrate that proposed convex optimization based algorithm reduces the conservatism of uncertainty; therefore, improves the robustness of the closed-loop control system.

It is possible to increase controller order such that the H_∞ robust performance condition (3.43) is satisfied. Therefore, a third-order linearly parametrized controller transfer function was constructed for TVC system using the Laguerre basis functions,

which are given in (2.24), as

$$K = k_0 + k_1\frac{\sqrt{2\xi}}{(s+\xi)} + k_2\frac{\sqrt{2\xi}(s-\xi)}{(s+\xi)^2} + k_3\frac{\sqrt{2\xi}(s-\xi)^2}{(s+\xi)^3} \tag{3.68}$$

where $k = \begin{bmatrix} k_0 & k_1 & k_2 & k_3 \end{bmatrix}$ is the matrix of the controller parameters to be calculated using convex optimization. The pole of this controller transfer function was chosen as $\xi = 93$ by a linear search for ξ between $\xi = 1$ and $\xi = 100$. This value provided the best robust performance achievement in the search space. The controller design problem (3.50) was implemented for $N = 400$ logarithmically separated frequency points between lower frequency point $w_l = 1\ rad/s$ and upper frequency point $w_u = 100\ rad/s$ as $w = \begin{bmatrix} 1 & \dots & 100 \end{bmatrix}\ rad/s$. Then SDP convex optimization problem was solved by using CVX and optimization toolbox of MATLAB.

The coefficients matrix of the fixed-order controller were obtained as $k = \begin{bmatrix} 71.02 & -381.14 & -0.01 & 75.64 \end{bmatrix}$ and the transfer function of the obtained fixed-order robust H_∞ controller is given explicitly by

$$K(s) = \frac{71.03s^3 + 15650s^2 + 684300s + 21100000}{s^3 + 279s^2 + 25950s + 804400}. \tag{3.69}$$

The resulting robust controller satisfies the robust performance condition (3.43) such that $\|\tilde{S}_{max}(jw_n)\|_\infty = 0.96 < 1$. This result proves that the worst-case sensitivity function remains smaller than inverse of the frequency dependent performance weighting function $W_1(jw_n)$, such that

$$\|\tilde{S}_{max}(jw_n)\|_\infty < \frac{1}{|W_1(jw_n)|} \tag{3.70}$$

for $n = 1\ \dots\ 400$. Moreover, the nominal sensitivity function $S_{nom}(jw_n, K, G_{nom})$ matches the desired sensitivity function S_d as shown in Figure. 3.14.

For comparison purposes, the control problem was also solved by using FDRC toolbox to design another third-order controller. The parameters of the fixed-order controller were obtained as $k = \begin{bmatrix} 85.02 & -669.69 & -231.29 & -12.5 \end{bmatrix}$ and the transfer

function of the obtained controller is given as

$$K_F(s) = \frac{84.98s^3 + 12104s^2 + 539140s + 15204000}{s^3 + 279s^2 + 25950s + 804400}. \tag{3.71}$$

The robust performance achievement of this controller is $\|\tilde{S}_{max}^{FDRC}(jw_n)\|_\infty = 1.23$. Obtained model matching achievement by the FDRC toolbox is similar to those obtained with the proposed method as shown in Figure. 3.14.

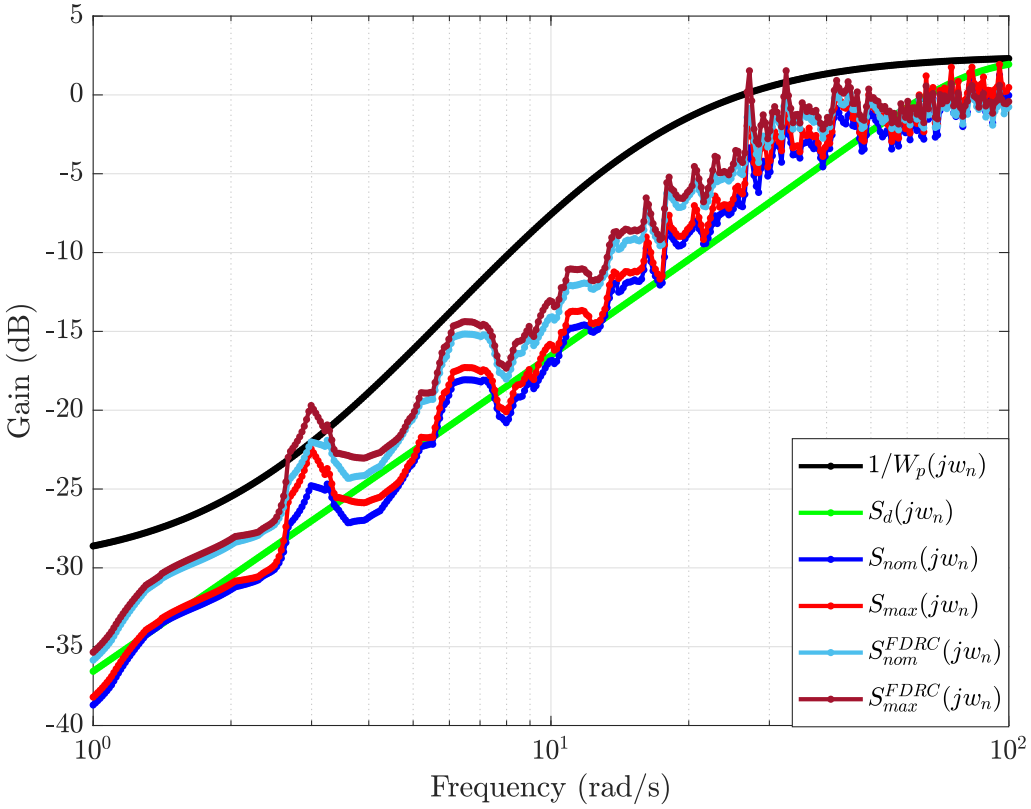

Figure. 3.14. Robust performance and model matching achievements of the designed fixed-order controllers with optimal uncertainty modelling method.

In order to investigate the robustness improvement of the proposed uncertainty modelling approach, same controller design problem was solved by using proposed method and FDRC toolbox with average nominal model (3.10) and corresponding uncertainty model (3.9). The pole of Laguerre basis function was chosen as $\xi = 66$ by a linear search for ξ between $\xi = 1$ and $\xi = 100$. The transfer functions of the obtained fixed-order robust H_∞ controllers are given by

$$K^{avg}(s) = \frac{50.79s^3 + 11150s^2 + 173700s + 8535000}{s^3 + 198s^2 + 13070s + 287500} \tag{3.72}$$

$$K_F^{avg}(s) = \frac{102s^3 + 16310s^2 + 436300s + 11860000}{s^3 + 198s^2 + 13070s + 287500} \tag{3.73}$$

for proposed method and FDRC toolbox, respectively. The robust performance achievement of these controllers are $\|\tilde{S}_{max}(jw_n)\|_\infty = 1.21$, $\|\tilde{S}_{max}^{FDRC}(jw_n)\|_\infty = 1.39$, respectively (Figure. 3.15).

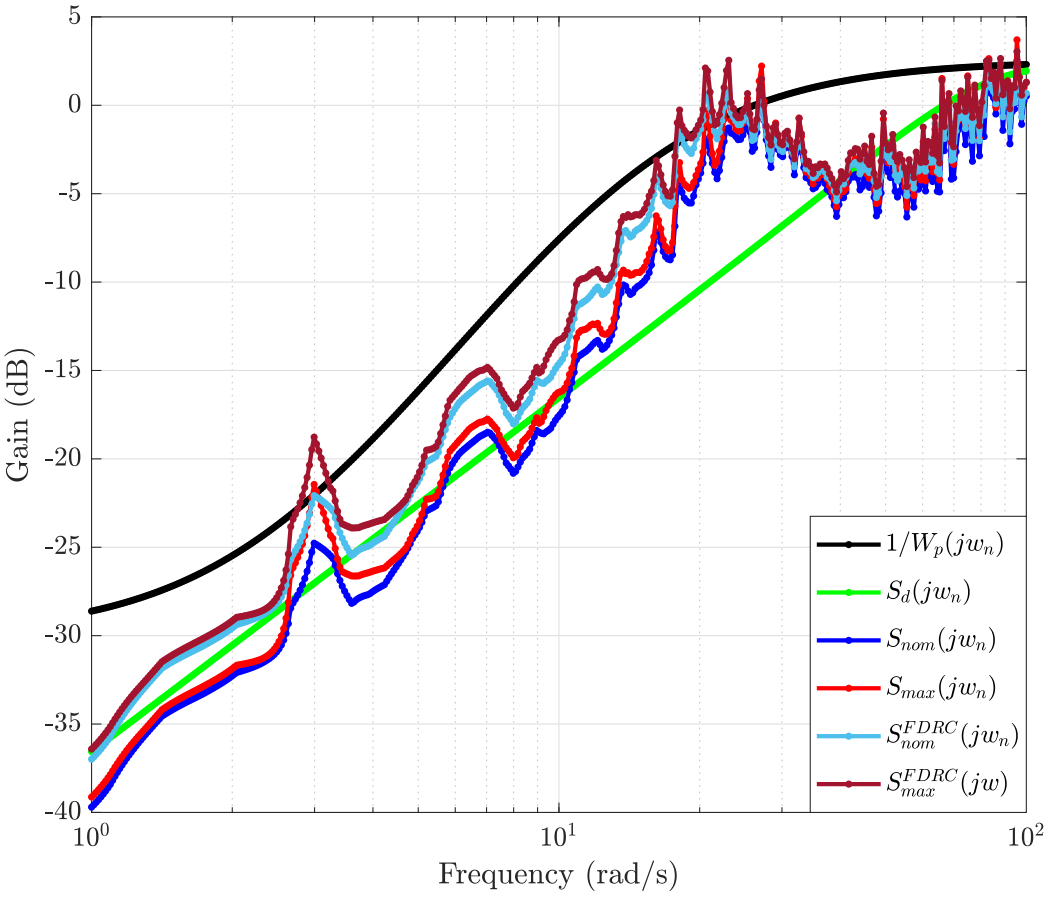

Figure. 3.15. Robust performance and model matching achievements of the designed fixed-order controllers with average method.

Therefore, robust performance achievement of the obtained controller with classical uncertainty modelling method is worse than the robustness value obtained with proposed data-driven fixed-order controller, which can be observed from Figure. 3.14 and Figure. 3.15. From these figures, it can be observed that the optimal uncertainty modelling and the optimal choice of the nominal model used for a real time system can considerably improve the desired robust performance specifications.

The controllers in (3.69) and (3.71) satisfy the control input constraints (3.48), where $\tilde{u}_{max} = 1,\ W_u = 1$, as shown in Figure. 3.16. Therefore, obtained worst-case $\tilde{Q}_{max}$-

parameter transfer function with the FDRC toolbox is similar to those obtained with the proposed method as shown in Figure. 3.16.

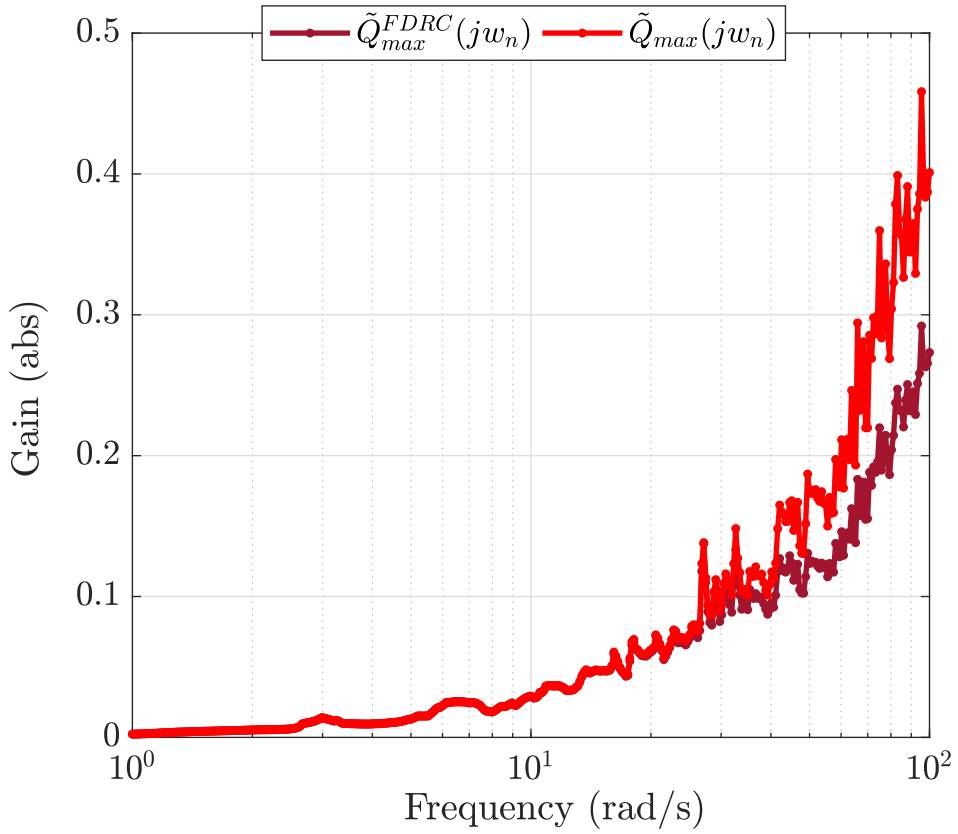

Figure. 3.16. Obtained worst-case $\tilde{Q}_{max}$-parameter transfer functions for control input constraints.

Real-time hardware in the loop tests were carried out to verify the performance of the synthesized fixed-order H_∞ controller. This controller was applied to the experimental system in the real-time hardware in the loop tests. The step response of the system in time-domain is given in Figure. 3.17. In this test a filtered step function was applied to the system to prevent sudden current consumption. As can be seen from this figure, the synthesized data-driven fixed-order H_∞ position controller satisfies the defined model matching objective. As can be seen from the position control of TVC system, which requires precise positioning, the objective of designing a data-driven, fixed-order, low-order controller in frequency domain could be achieved via proposed approach.

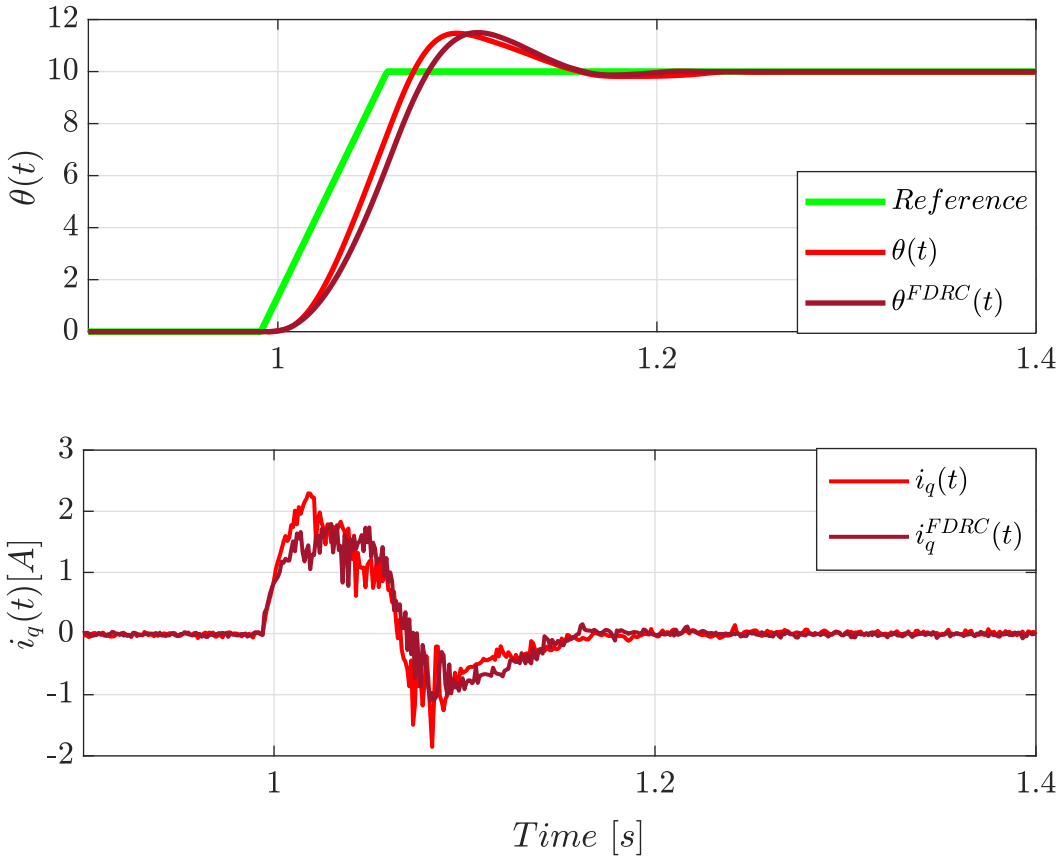

Figure. 3.17. Experimentally obtained output $\theta(t)$ angle with applied control input (current) signal $i_q(t)$.

3.9 Comments

This chapter presents a novel data-driven method to synthesize robust fixed-order H_∞ controllers by simultaneously computing minimal uncertainty bound and assigning optimal nominal model from experimental data. The proposed controller design algorithm consists of two step: First, the non-parametric frequency response of system models with minimal unstructured uncertainty model is identified from the multiple measurement data. Therefore, variations in the system dynamics are represented by minimal uncertainty circle around the optimal nominal model for the corresponding frequency points on the Nyquist diagram. In the second step, a fixed-order H_∞ controller design algorithm is introduced by using linearly parameterized Laguerre basis functions for identified non-parametric perturbed model in the frequency domain. In this algorithm, H_∞ robust performance condition, control input constraints and closed-loop model matching objective are described by convex functions with respect to the parameters of the controller. Then the control design problem

is formulated as a constrained convex optimization problem, which can be solved efficiently using convex optimization techniques to compute the parameters of the structured controllers. Moreover, the proposed method can be applied to any linearly parameterized controller structure such as PID with any convex objective function and constraint functions. An experimental flexible nozzle type electromechanical TVC system is used to validate proposed control design algorithm. The obtained results show the practicality and efficiency of the approach to synthesize fixed-order H_∞ controllers for non-parametric frequency domain perturbed plants. Furthermore, the closed-loop measurements confirm that data-driven control method with the optimal uncertainty modelling approach considerably reduces the uncertainty bound and consequently improves the robust performance.

4. TWO DEGREE OF FREEDOM ROBUST DATA-DRIVEN FIXED-ORDER H_∞ CONTROLLER SYNTHESIS USING CONVEX OPTIMIZATION

An extension of the one degree of freedom controller design algorithm, which is presented in Chapter 3, is proposed to synthesize two degree of freedom (2-DOF) controllers for reference tracking of the non-parametric systems. The theoretical design approach is experimentally verified on position control of an electromechanical CAS of an air vehicle. To improve the positioning accuracy of the actuation system, the full-closed loop feedback structure is considered. Obtained experimental results verify the usefulness and efficiency of the proposed approach.

4.1 2-DOF Control Framework and Closed-loop Transfer Functions

In the feedback-only control system structure for reference tracking, the controller acts only on the error signal. There are algebraic limitations on this control scheme. Since sum of the frequency response of sensitivity function and frequency response of complementary sensitivity function equal to unity, the designed controller cannot achieve required values for these dependent functions at frequency points of interest. The tracking error minimization and noise attenuation are related to the complementary sensitivity function. On the other hand, the sensitivity function determines the effect of the output disturbance on the measured output of the control system. Therefore; there is a trade-off between reference tracking accuracy and disturbance rejection constraints. Above mentioned performance limitations in the feedback-only (1-DOF) control scheme can be eliminated by using a 2-DOF control system configuration, including a feedforward path [8, 63, 64].

The closed loop system in Figure. 4.1, defined by following equations:

$$e = r - y - v \tag{4.1}$$

$$u = K_{ff} r + K_{fb}(r - y - v) \tag{4.2}$$

$$y = G(u + d_i) + d_o \tag{4.3}$$

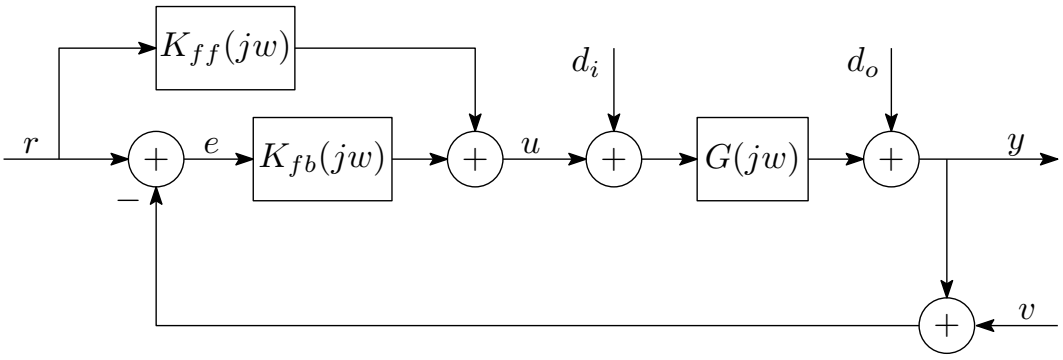

Figure. 4.1. 2-DOF feedforward control structure.

where K_{ff} is the feedforward controller, K_{fb} is the feedback controller, r is the reference input, e is the error, d_i is the input disturbance, v is the measurement noise and d_o is the output disturbance. The main objective of the H_∞ control theory is to synthesize a stabilizing controller that satisfies selected constraints on several closed-loop transfer functions. We will be interested in several closed-loop transfer functions that are defined below:

Definition 4.1. ***(Sensitivity function)*** *The sensitivity function is the transfer function from the output disturbance to the plant output and is defined as*

$$S = \frac{y}{d_o} = \frac{1}{1 + GK_{fb}} \tag{4.4}$$

where $L = GK_{fb}$ is the loop transfer function.

Definition 4.2. ***(Complementary sensitivity function)*** *The complementary sensitivity function is the transfer function from the measurement noise to the plant output and is defined as*

$$T = \frac{y}{v} = \frac{GK_{fb}}{1 + GK_{fb}} \tag{4.5}$$

also, one has $S + T = I$.

Definition 4.3. ***(Q-parameter)*** *The Q-parameter function is the transfer function*

from the reference input to the control input and is defined as

$$Q = \frac{u}{r} = \frac{K_{ff} + K_{fb}}{1 + GK_{fb}} \tag{4.6}$$

Additionally, we use the transfer function from the reference input to the measured output such that

$$T_{yr} = \frac{y}{r} = \frac{G\big(K_{ff} + K_{fb}\big)}{1 + GK_{fb}}. \tag{4.7}$$

4.2 Model Matching Problem

Using the FRF of the system and the linearly parameterized controller, the closed-loop model matching problem can be defined as

$$\begin{aligned} &\min_k \| W_m \left(T_{yr} - T_{yr}^d \right) \|_\infty \\ &= \min_k \left\| W_m \left(\frac{G\big(K_{ff} + K_{fb}\big)}{1 + GK_{fb}} - T_{yr}^d \right) \right\|_\infty \\ &= \min_k \left\| W_m \left(\frac{G\big(k_{ff}\psi_{ff} + k_{fb}\psi_{fb}\big)\big(1 - T_{yr}^d\big) - T_{yr}^d}{1 + Gk_{fb}\psi_{fb}} \right) \right\|_\infty \end{aligned} \tag{4.8}$$

in the H_∞ sense, where $k_{ff}\psi_{ff},\ k_{fb}\psi_{fb}$ are the linearly parameterized feedforward and feedback controller, respectively and $W_m(jw)$ is the FRF of a stable penalty function weighting the frequency domain requirements. A block diagram representation of the closed-loop model matching problem is given in Figure. 4.2 for 2-DOF control framework.

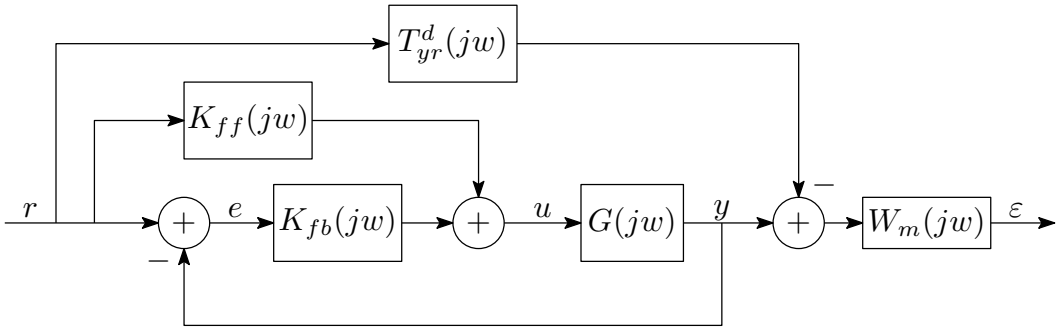

Figure. 4.2. Block diagram representation of the model matching problem in 2-DOF control framework.

The objective function of the optimization problem (4.8) is not a convex function with respect to the controller parameters $k = [k_{ff}\ k_{fb}]$, because the denominator of this function includes design parameters. In order to approximate this non-convex optimization problem to a convex optimization problem, one approach is to replace the term GK_{fb} in the denominator with the desired loop gain $L_d(jw)$ and formulate the sub-optimal control problem as

$$\min_{k} \quad \left\| W_m \left(\frac{G\big(k_{ff}\psi_{ff} + k_{fb}\psi_{fb}\big)(1 - T_{yr}^{d}) - T_{yr}^{d}}{1 + L_d} \right) \right\|_{\infty} \tag{4.9}$$

where the desired loop gain L_d is given by

$$L_d = \frac{T_d}{1 - T_d}. \tag{4.10}$$

where T_d is the desired complementary sensitivity function. Note that the objective function (4.9) $f : \mathbb{R}^{1\times n} \to \mathbb{C}$ is affine with respect to the $k = [k_{ff}\ k_{fb}]$; therefore, it can be considered as convex function.

4.3 Derivation of the Robust Performance Conditions

The controller $K_{ff}(jw)$ can be omitted because it has no effect on the closed-loop stability of the system when deriving the RP condition. For this reason, the RP conditions can be derived based on rearranged block diagram representation of the proposed control system which is shown in Figure. 4.3

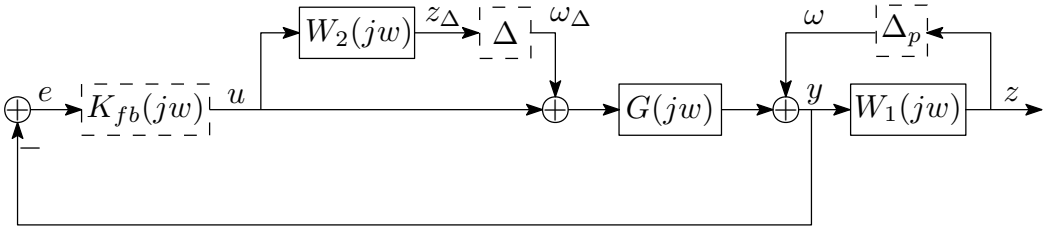

Figure. 4.3. Block diagram for robust performance constraints with two complex blocks.

Note that, this representation is the same as the 1-DOF representation given in Figure. 3.3. Therefore, the representation of the robust performance constraint in 2-DOF H_∞ controller synthesis problem with a sufficient condition is given by following

proposition:

Proposition 4.1. *Closed-loop control system given by Figure. 4.3, satisfies the robust performance condition if*

$$\begin{aligned} &\Im(k_{fb}\psi_{fb}G) - a_n\Re(k_{fb}\psi_{fb}G) \\ &+\big|W_2 k_{fb}\psi_{fb}G\big|\big(a_n sin(\theta_n) + cos(\theta_n)\big) - b_n \leq 0;\ \forall w \in \mathbb{R} \cup \{\infty\}. \end{aligned} \tag{4.11}$$

Proof of this proposition is the same as proof in 1-DOF control framework, i.e., (3.44).

4.4 Control input constraints

The block diagram representation of the closed loop control system with control signal weighting function W_u is shown in Figure. 4.4.

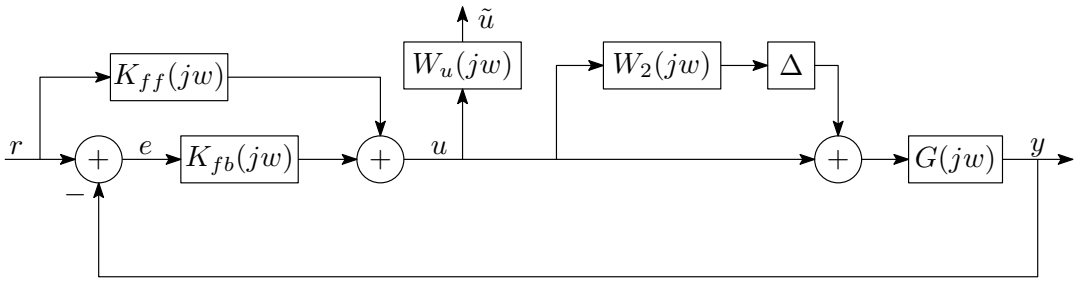

Figure. 4.4. 2-DOF closed-loop control system with control input constraint.

By using this figure, perturbed Q-parameter transfer function from the reference input to the control input with multiplicative type model uncertainty of the plant given by

$$\tilde{Q} = \frac{u}{r} = \frac{\big(k_{ff}\psi_{ff} + k_{fb}\psi_{fb}\big)}{1 + Gk_{fb}\psi_{fb}(1 + W_2\Delta)}. \tag{4.12}$$

Then, control input constraint can be written as

$$\begin{aligned} &\left|W_u\tilde{Q}\right| - \tilde{u}_{max} \leq 0 \\ \Leftrightarrow &\left|\frac{W_u\big(k_{ff}\psi_{ff} + k_{fb}\psi_{fb}\big)}{1 + Gk_{fb}\psi_{fb}(1 + W_2\Delta)}\right| \leq \tilde{u}_{max} \\ \Leftrightarrow &-\tilde{u}_{max} \leq \frac{W_u\big(k_{ff}\psi_{ff} + k_{fb}\psi_{fb}\big)}{1 + Gk_{fb}\psi_{fb}(1 + W_2\Delta)} \leq \tilde{u}_{max} \end{aligned} \tag{4.13}$$

for $\forall w \in \mathbb{R} \cup \{\infty\}$, where $\tilde{u}_{max}$ is the upper bound of the weighted control input signal in frequency domain. The maximum control input occurs at minimum loop-gain condition; therefore, the worst-case control input generated when the block $\Delta = 1$ and the phase angle of the terms $(W_2Gk_{fb}\psi_{fb})$ and $(1+Gk_{fb}\psi_{fb})$ have opposite signs. Hence,

$$\begin{aligned} &\left|W_u\tilde{Q}_{max}\right| - \tilde{u}_{max} \leq 0 \\ \Leftrightarrow &-\tilde{u}_{max} \leq \frac{\left|W_u\big(k_{ff}\psi_{ff} + k_{fb}\psi_{fb}\big)\right|}{\left|1 + Gk_{fb}\psi_{fb}\right| - \left|W_2Gk_{fb}\psi_{fb}\right|} \leq \tilde{u}_{max} \\ \Leftrightarrow &\begin{bmatrix} -\tilde{u}_{max}(|1 + Gk_{fb}\psi_{fb}| - |W_2Gk_{fb}\psi_{fb}|) - |W_u(k_{ff}\psi_{ff} + k_{fb}\psi_{fb})| \\ -\tilde{u}_{max}(|1 + Gk_{fb}\psi_{fb}| - |W_2Gk_{fb}\psi_{fb}|) + |W_u(k_{ff}\psi_{ff} + k_{fb}\psi_{fb})| \end{bmatrix} \leq \begin{bmatrix} 0 \\ 0 \end{bmatrix} \end{aligned} \tag{4.14}$$

which are the control input constraint functions of the fixed-order H_∞ control problem. Notice that these constraint functions are affine with respect to the controller parameters $k = [k_{ff}\ k_{fb}]$.

4.5 Optimization Problem

A convex SIP problem is arranged for the optimal synthesis of the 2-DOF data-driven fixed-order H_∞ controller as follows:

$$
\begin{aligned}
\min_{k} \quad & \left\| W_m \left(\frac{G\big(k_{ff}\psi_{ff} + k_{fb}\psi_{fb}\big)(1 - T_{yr}^{d}) - T_{yr}^{d}}{1 + L_d} \right) \right\|_\infty \\
\text{s.t.} \quad & \Im(k_{fb}\psi_{fb}G) - a_n\Re(k_{fb}\psi_{fb}G) \\
& \qquad + \big|W_2 k_{fb}\psi_{fb}G\big|\big(a_n sin(\theta_n) + cos(\theta_n)\big) - b_n \leq 0; \\
& -\tilde{u}_{max}\big(\big|1 + Gk_{fb}\psi_{fb}\big| - \big|W_2 G k_{fb}\psi_{fb}\big|\big) - \big|W_u\big(k_{ff}\psi_{ff} + k_{fb}\psi_{fb}\big)\big| \leq 0; \\
& -\tilde{u}_{max}\big(\big|1 + Gk_{fb}\psi_{fb}\big| - \big|W_2 G k_{fb}\psi_{fb}\big|\big) + \big|W_u\big(k_{ff}\psi_{ff} + k_{fb}\psi_{fb}\big)\big| \leq 0
\end{aligned}
\tag{4.15}
$$

for $\forall w \in \mathbb{R} \cup \{\infty\}$.

Note that, the frequency domain multiple model set $\mathbf{M}$ in (3.7) includes the time delay. Therefore, time-delay systems can be considered without any approximation in the proposed robust controller synthesis method.

4.6 Experimental Implementation

In this section, the proposed controller design methodology is applied to the position control of an electromechanical CAS.

4.6.1 Control Actuation System

Several guided air vehicle platforms generally use aerodynamic control surfaces to direct their course. The CAS is responsible for the motion that controls the flight of the air vehicle by changing the direction of these control surfaces.

Motion control systems are mainly composed of actuators, sensors and mechanism. The sensors measure position or velocity with faster dynamics than the closed-loop bandwidth of the motion control systems. If the position sensor is located on the motor side, i.e., non-collocated side, the motion control system is called the semi-closed loop feedback position control system. On the other hand, if the position sensor is placed on the load side, i.e., collocated side, the motion control system is

called the full-closed loop feedback position control system. In high precision control applications, the sensors are generally used on load side.

In this study, an electromechanical type CAS is used as an experimental test bench. The CAS configuration is composed of a BLDC electric motor, planetary gear train, a ballscrew, a mechanism and a digital position sensor on load side, i.e., collocated side. Nominal model of the CAS can be obtained based on the BLDC electric motor dynamics, which is given in Chapter 3.8.2. Signal flows between the CAS and other parts of test setup are shown in Figure. 4.5. The other components of the test setup are the same as those of Figure. 3.8.

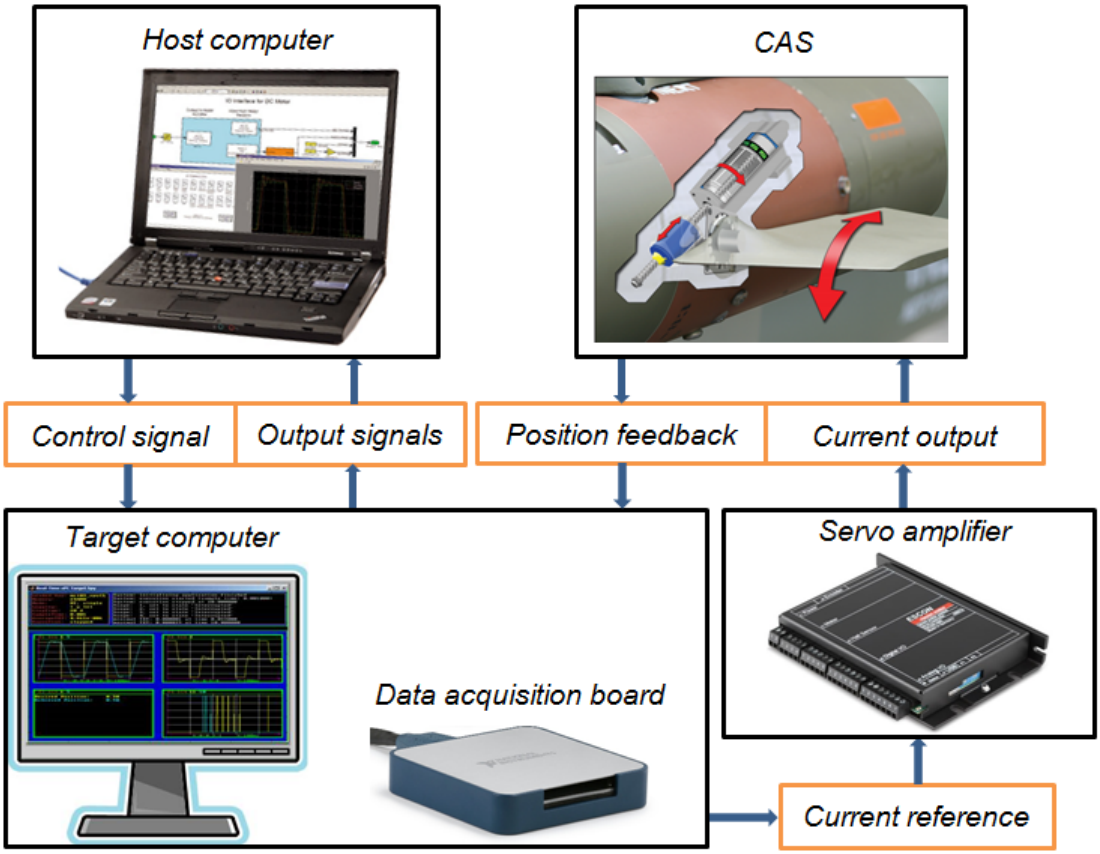

Figure. 4.5. Signal flows for experimental testing of the CAS.

4.6.2 Frequency Response Identification of CAS

In order to obtain six different FRF's of the CAS, multiple tests were carried out in the temperature range of -20 °C to 80 °C with intervals of 20 °C degrees. A modified pseudo-random binary sequence (PRBS) signal was used as the q-axis current

reference of the open-loop CAS in the experiments to obtain the time domain response of the plant. This modification was made to provide symmetrical CAS rotation in positive and negative directions. The input, i.e., q-axis current, and the output, i.e., angle θ, signals acquired from the frequency response identification experiments are shown in Figure. 4.6.

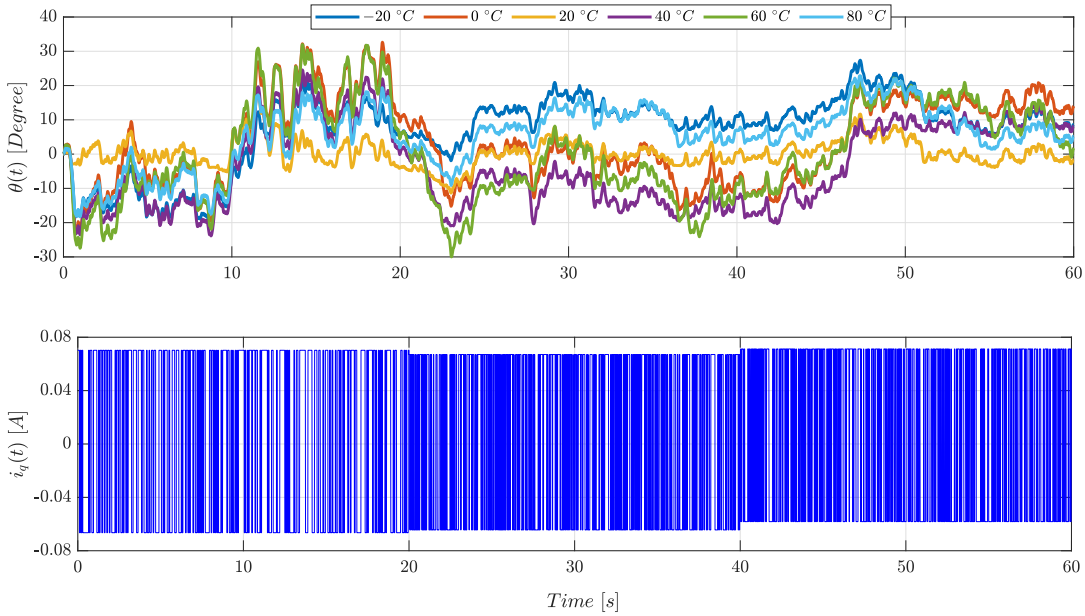

Figure. 4.6. Applied PRBS signal used for q-axis current $i_q(t)$ with the resulting output $\theta(t)$ angle.

Frequency domain experimental data was obtained with 400 logarithmically spaced frequency points, a value which is approximately calculated using (3.51) where $\epsilon = 0.1$, $\beta = 0.001$ and $d_p = 4$, between $w_l = 1\,rad/s$ and $w_u = 150\,rad/s$. Obtained FRF's of the real-time system, which are obtained with (2.40), are given in Figure. 4.7.

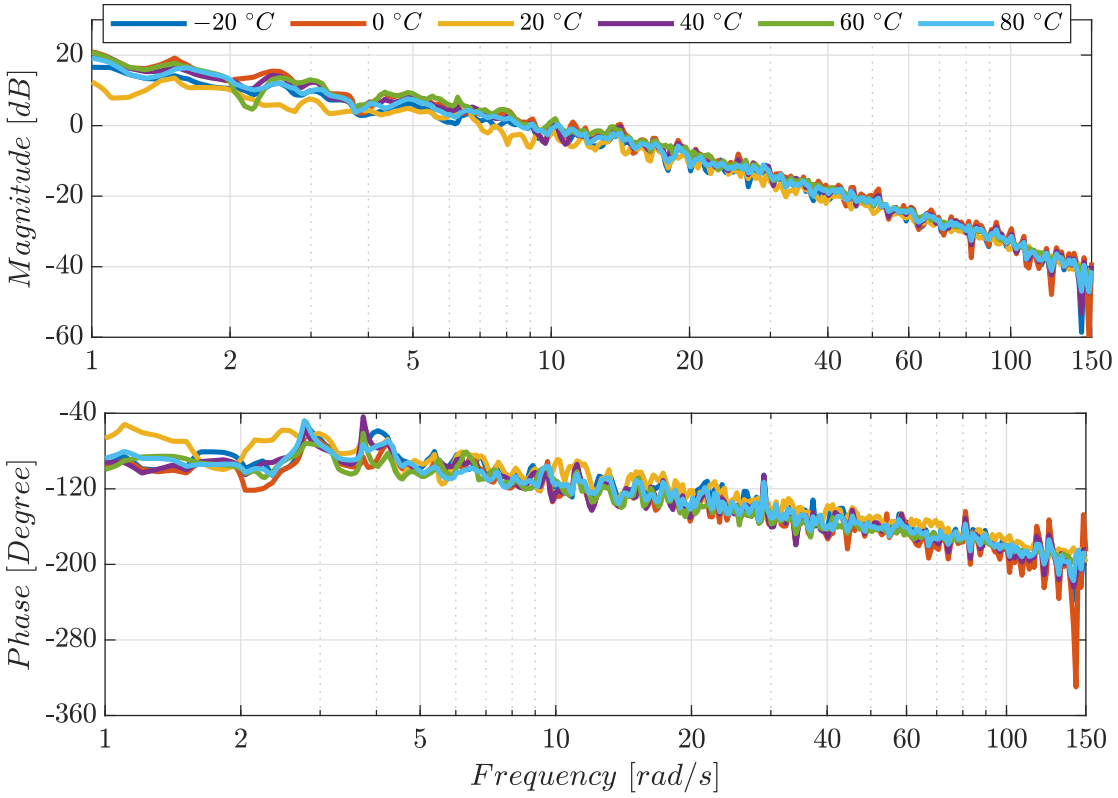

Figure. 4.7. Measured multiple FRF's of the CAS.

4.7 2-DOF Controller Synthesis for CAS

The reference model for desired closed-loop control system T_{yr}^{d} and desired nominal complementary sensitivity function T^{d} were chosen as

$$T_{yr}^{d} = \frac{(2\pi 16)^2}{s^2 + 1.2(2\pi 16)s + (2\pi 16)^2} \tag{4.16}$$

$$T^{d} = \frac{(2\pi 12)^2}{s^2 + 1.2(2\pi 12)s + (2\pi 12)^2} \tag{4.17}$$

respectively. Similarly, the worst-case complementary sensitivity function T_{d}^{1} for the selection of the performance weight was chosen as

$$T_{d}^{1} = \frac{(2\pi 3)^2}{s^2 + 0.4(2\pi 3)s + (2\pi 3)^2} \tag{4.18}$$

therefore, the performance weighing function W_1 used to design the robust controller is given by

$$W_1 = \frac{0.709s^2 + 22.46s + 177.588}{s^2 + 5.635s + 7.943} \tag{4.19}$$

which is obtained by using (3.58) with $\nu = 2,\ \varrho = 0.002,\ \zeta = 0.2,\ w_n = 2\pi 3\ rad/s$. While designing the robust controller, W_u and W_m were taken as 1 for the sake of simplicity. Upper bound of the available control input defined as $\tilde{u}_{max} = 120\ A$.

The optimal nominal model (G_{nom}^{opt}) and optimal multiplicative uncertainty function (W_2^{opt}) were calculated using the semi-definite convex optimization method given by Proposition 1. For comparison purpose, another nominal model (G_{nom}^{avg}) was calculated by average method, which is given in (3.10). Additionally, corresponding multiplicative uncertainty weighing (W_2^{avg}) function was constructed by classical method, which is given in (3.9). Obtained Nyquist plot of $G_{nom}^{opt}(jw_n)$ and $G_{nom}^{avg}(jw_n)$ are shown in Figure. 4.8 with corresponding uncertainty models. The magnitude plots of the corresponding multiplicative uncertainty weighting functions are given in Figure. 4.9 for both methods.

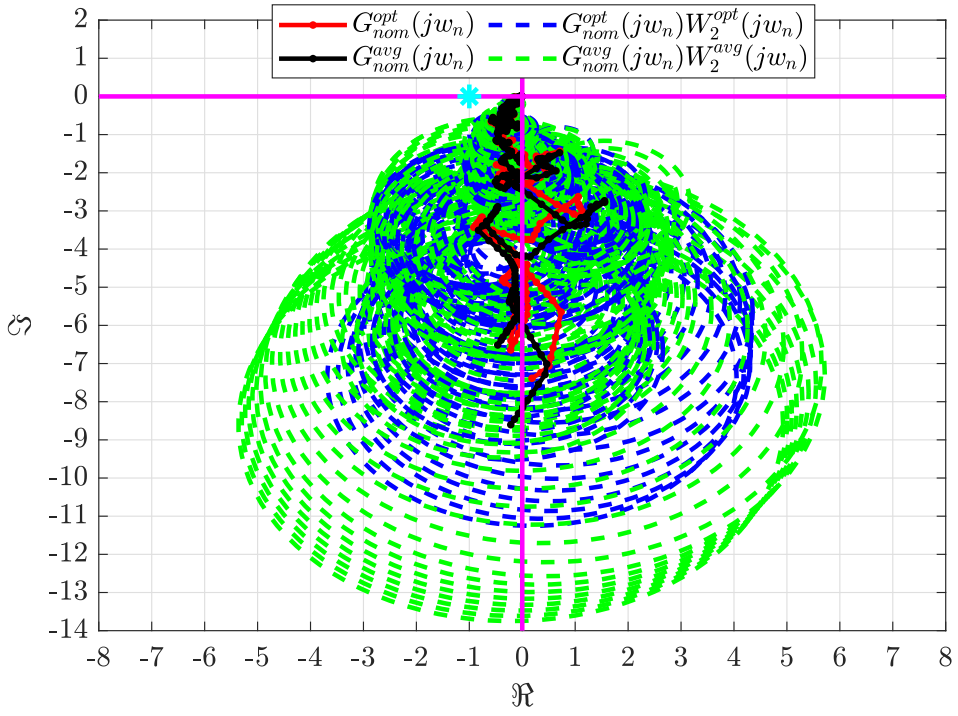

Figure. 4.8. Nyquist plot of the obtained non-parametric nominal models with optimum multiplicative uncertainty weighting bounds for proposed method and classical uncertainty bounds for average method.

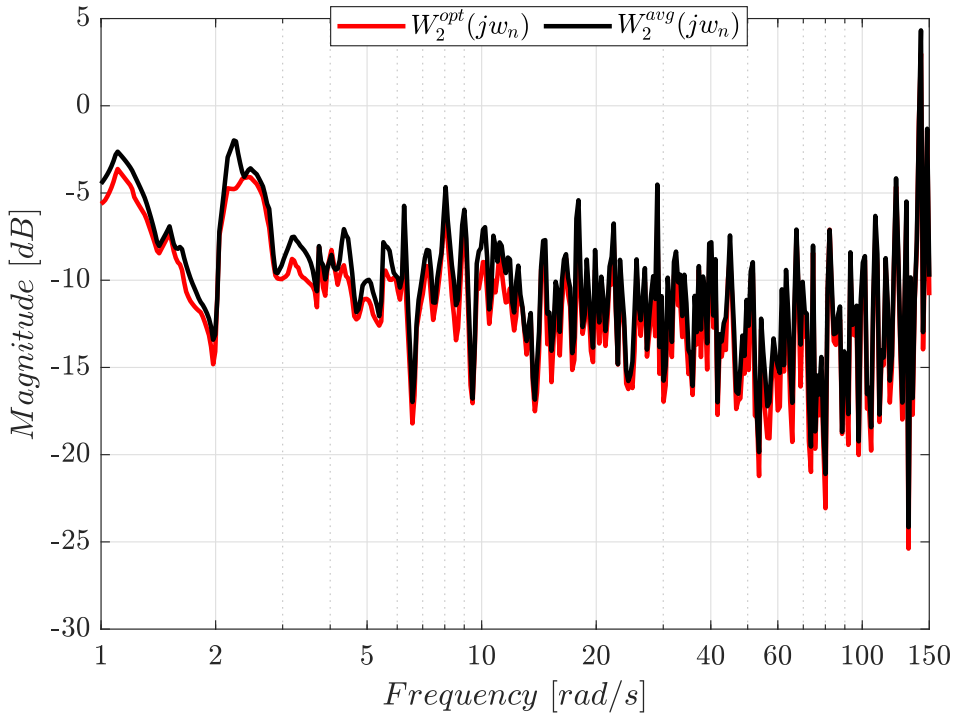

Figure. 4.9. Optimum multiplicative uncertainty weighting function for proposed method and classical method.

Third-order linearly parametrized feedback and feedforward 2-DOF controller transfer functions were constructed for CAS using the Laguerre basis functions as

$$K_{ff} = k_0^{ff} + k_1^{ff}\frac{\sqrt{2\xi}}{(s+\xi)} + k_2^{ff}\frac{\sqrt{2\xi}(s-\xi)}{(s+\xi)^2} + k_3^{ff}\frac{\sqrt{2\xi}(s-\xi)^2}{(s+\xi)^3} \tag{4.20}$$

$$K_{fb} = k_0^{fb} + k_1^{fb}\frac{\sqrt{2\xi}}{(s+\xi)} + k_2^{fb}\frac{\sqrt{2\xi}(s-\xi)}{(s+\xi)^2} + k_3^{fb}\frac{\sqrt{2\xi}(s-\xi)^2}{(s+\xi)^3} \tag{4.21}$$

where $k = \begin{bmatrix} k_0^{ff} & k_1^{ff} & k_2^{ff} & k_3^{ff} & k_0^{fb} & k_1^{fb} & k_2^{fb} & k_3^{fb} \end{bmatrix} \in \mathbb{R}^{1\times 8}$ is the matrix of the controller parameters to be calculated using convex optimization. The pole of this controller transfer function was chosen as $\xi = 87$ by a linear search for ξ between $\xi = 1$ and $\xi = 100$. This value provided the best robust performance achievement in the search space. The controller design problem (4.15) was implemented for $N = 400$ logarithmically separated frequency points between lower frequency point $w_l = 1\ rad/s$ and upper frequency point $w_u = 150\ rad/s$ as $w = \begin{bmatrix} 1 & \dots & 150 \end{bmatrix}\ rad/s$.

The coefficients matrix of the fixed-order 2-DOF controller were obtained as

$k = \begin{bmatrix} 3.28 & -20.74 & 19.91 & 19.29 & 38.85 & -231.21 & 11.36 & 61.29 \end{bmatrix}$. Then, the transfer functions of the feedforward and feedback parts of the obtained 2-DOF fixed-order robust H_∞ controller is given by

$$K^{ff}(s) = \frac{3.28s^3 + 1102s^2 - 17230s + 33200}{s^3 + 261s^2 + 22710s + 658500} \tag{4.22}$$

$$K^{fb}(s) = \frac{38.85s^3 + 8049s^2 + 210900s + 7485000}{s^3 + 261s^2 + 22710s + 658500} \tag{4.23}$$

respectively. The resulting robust controller satisfies the robust performance condition (4.11) such that $\|\tilde{S}_{max}(jw_n)\|_\infty = 0.99 < 1$. This result proves that the worst-case sensitivity function remains smaller than inverse of the frequency dependent performance weighting function $W_1(jw_n)$, such that

$$\|\tilde{S}_{max}(jw_n)\|_\infty < \frac{1}{|W_1(jw_n)|} \tag{4.24}$$

for $n = 1 \ \ldots \ 400$.

For comparison purposes, the control problem was also solved by using feedback-only, i.e., 1-DOF control method $\left(K^{ff}(s) = 0\right)$ to design a third-order controller. Controller parameters were obtained as $k = \begin{bmatrix} 55.01 & 384.52 & -77.31 & 17.59 \end{bmatrix}$. Hence, the transfer function of the obtained 1-DOF controller is given as

$$K_{1-DOF}(s) = \frac{55.01s^3 + 8498s^2 + 326200s + 7309000}{s^3 + 261s^2 + 22710s + 658500}. \tag{4.25}$$

The robust performance achievement of this data-driven fixed-order 1-DOF controller is $\|\tilde{S}^{1-DOF}_{max}(jw_n)\|_\infty = 0.99$. Obtained robust performance achievement by the 1-DOF controller is similar to those obtained with the proposed method as shown in Figure. 4.10. The robustness to unstructured uncertainty determined by the $\tilde{S}_{max}(jw_n)$; therefore, robust performance condition remain similar for both control system structure cases.

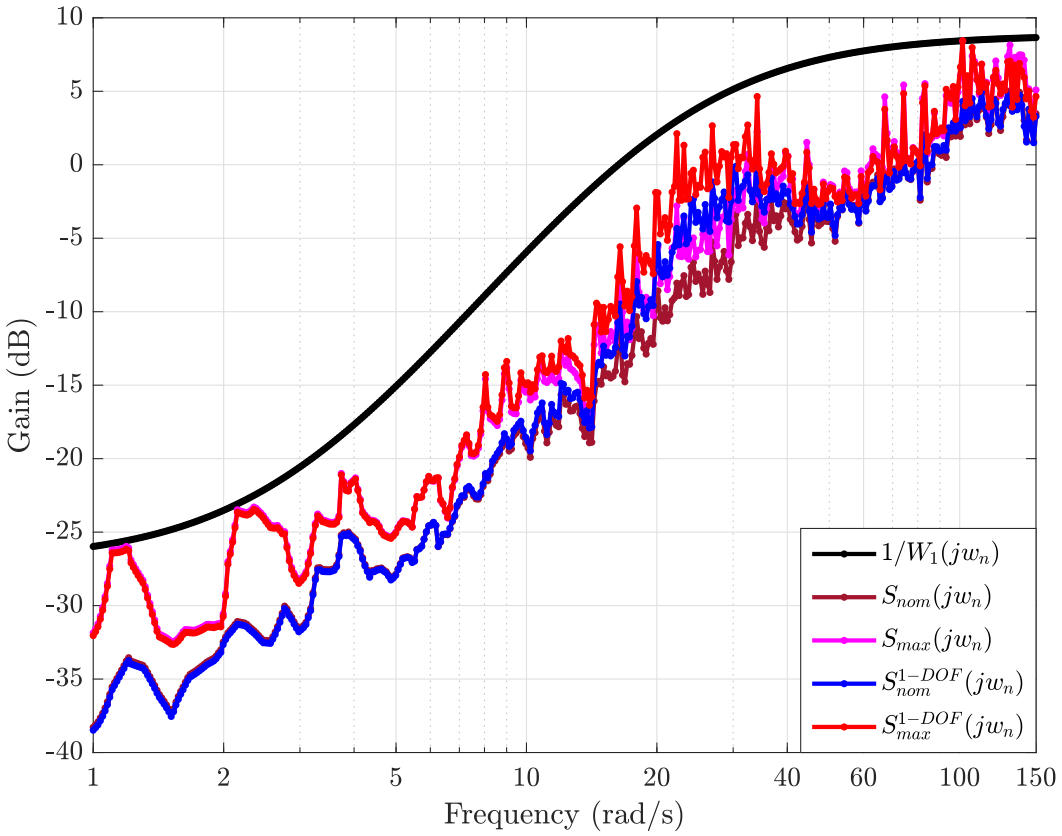

Figure. 4.10. Robust performance and model matching achievements of the designed fixed-order controllers with optimal uncertainty modelling method.

Figure. 4.11 shows the comparison of the obtained frequency domain T_{yr} function, which represents the reference tracking achievement, from fixed-order 2-DOF controller design with fixed-order 1-DOF controller design. As shown in this figure, the nominal T_{yr} transfer function, i.e., $T_{yr}(jw_n, K, G_{nom})$, matches the desired closed-loop transfer function T_{yr}^d for 2-DOF controller. Moreover, the proposed 2-DOF robust controller provides about 15% improvement in closed-loop system bandwidth (bandwidth of 1-DOF controller= $14.8\ Hz$, bandwidth of 2-DOF controller= $16.8\ Hz$), compared to 1-DOF design.

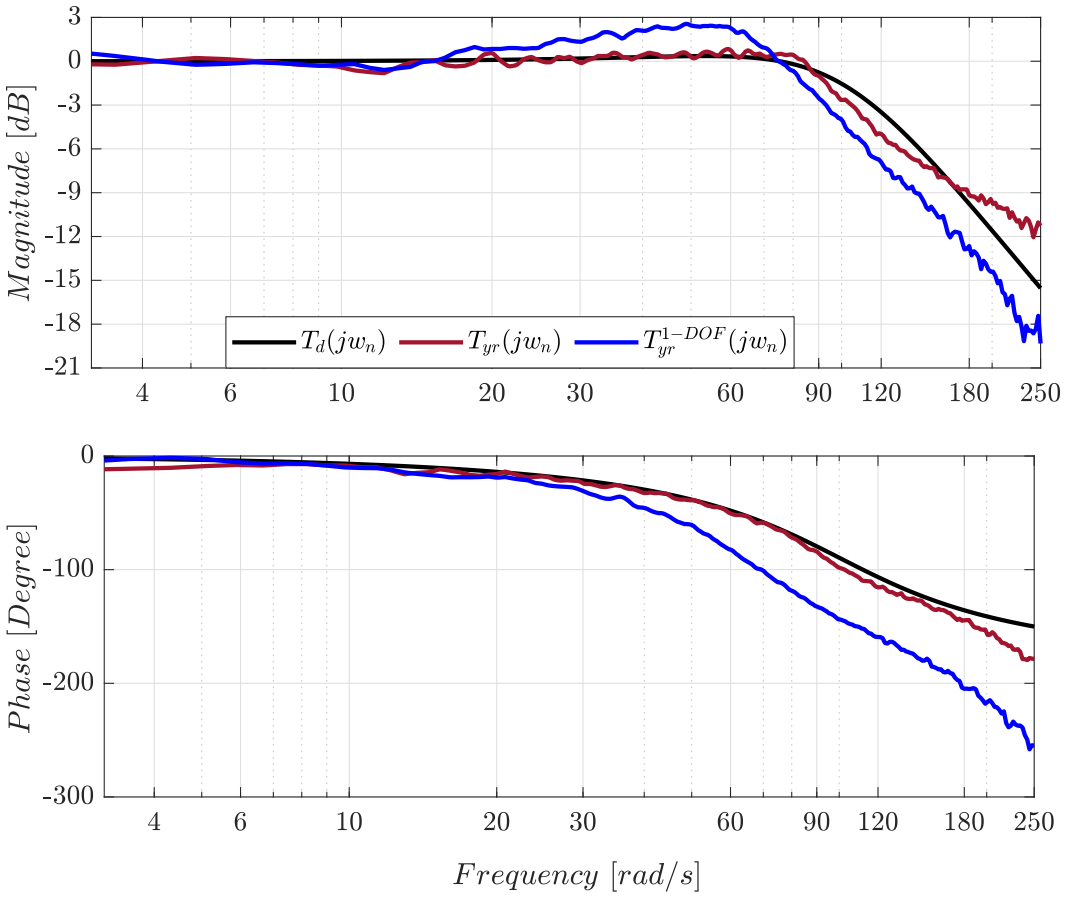

Figure. 4.11. Comparison of model matching achievement of the 2-DOF fixed-order controller with 1-DOF controller.

The obtained 2-DOF controller and the 1-DOF controller satisfy the control input constraints, where $\tilde{u}_{max} = 120,\ W_u = 1$, as shown in Figure. 4.12. Obtained worst-case $\tilde{Q}$-parameter transfer function with the 1-DOF controller design approach, i.e., $\tilde{Q}_{max}^{1-DOF}$, is similar to those obtained with the proposed method, i.e., $\tilde{Q}_{max}$, as shown in Figure. 4.12.

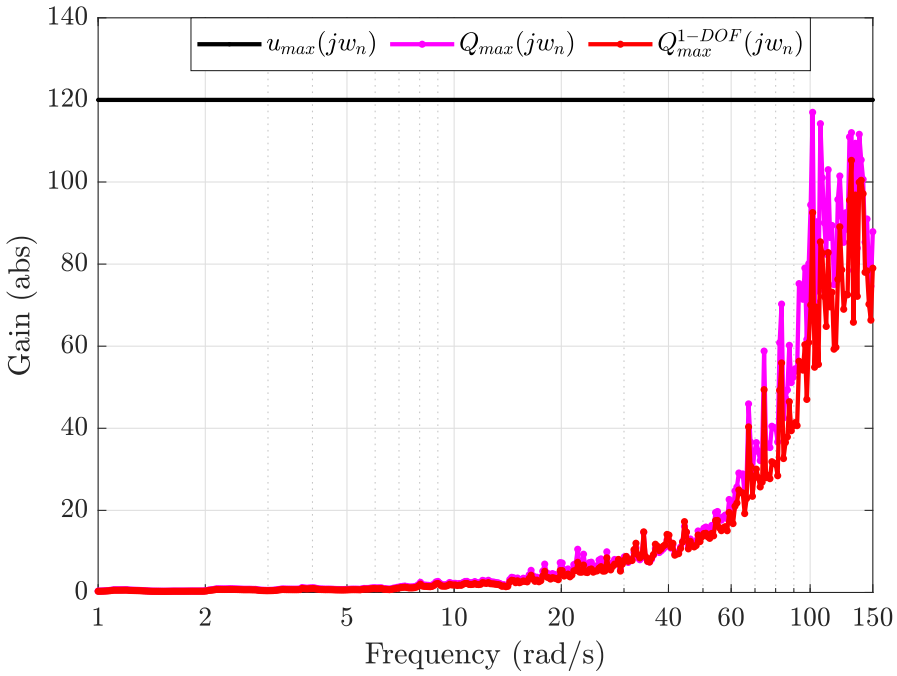

Figure. 4.12. Obtained worst-case $\tilde{Q}$-parameter transfer functions for control input constraints.

Real-time hardware in the loop tests were carried out to verify the performance of the synthesized fixed-order 2-DOF and 1-DOF H_∞ controllers. These controllers were applied to the experimental system in the real-time hardware in the loop tests. An increasing frequency sinusoidal chirp signal up to 20 Hz was applied as reference input to the system in order to determine the bandwidth of the closed loop system and to test the reference tracking performance. The response of the real system in time-domain is given in Figure. 4.13 with 2-DOF controller and 1-DOF controller. The response of the reference model T_{yr}^d is also shown in this figure. As can be seen from this figure, the synthesized data-driven fixed-order 2-DOF H_∞ position controller satisfies the defined model matching objective. Therefore, the objective of designing a data-driven, fixed-order (low-order) controller in frequency domain for position control of the CAS system, which requires precise positioning, could be achieved by using proposed approach. Moreover, the designed 2-DOF robust controller provides improvement in the tracking performance when compared to the 1-DOF design method as shown in Figure. 4.13.

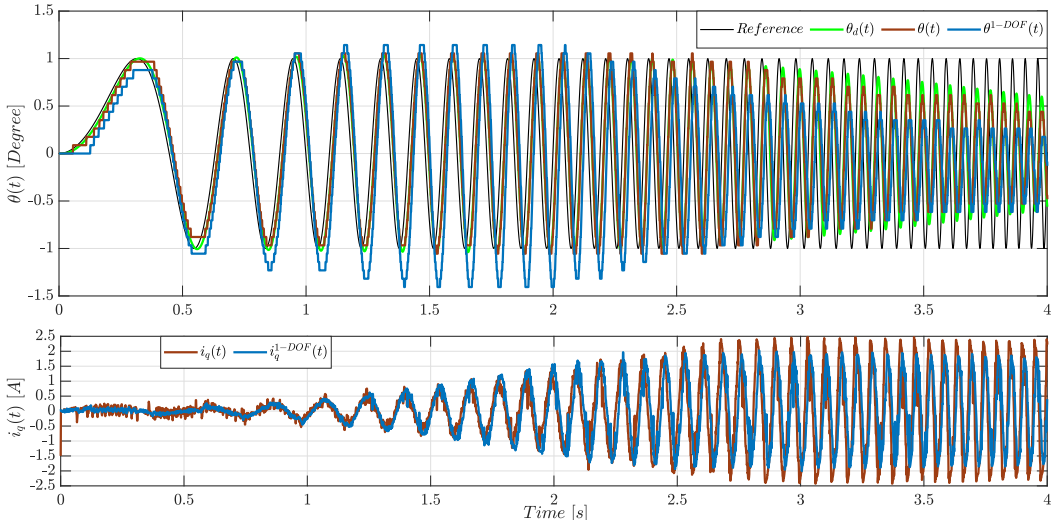

Figure. 4.13. Experimentally obtained output $\theta(t)$ angle with applied control input (current) signal $i_q(t)$.

4.8 Comments

In this chapter, a novel data-driven controller design approach to synthesize two degree of freedom robust fixed-order H_∞ controller for reference tracking based on convex optimization has been presented. The proposed method combines the model-free feature of the non-parametric frequency domain data-driven control methods and the practicality of the fixed-order methods within the H_∞ control framework for 2-DOF controllers. A fixed-order 2-DOF robust controller design algorithm based on constrained convex optimization problem has been introduced with closed loop model matching objective and control input constraints for non-parametric perturbed model in the frequency domain. The proposed controller synthesis method can be applied to any affinely parameterized controller structure such as PID controllers. The theoretical design approach has been experimentally verified on the full-closed loop feedback position control of an electromechanical control actuation system. Experimental results reveal that the proposed 2-DOF feedforward controller design approach improves the reference tracking performance when compared to data-driven fixed-order 1-DOF (feedback only) H_∞ controller design method, under the same performance requirements.

5. DATA-DRIVEN FIXED-ORDER H_∞ CONTROLLER SYNTHESIS IN FREQUENCY DOMAIN: CLOSED-LOOP SYSTEM APPROACH

This chapter aims to design a data-driven fixed-order H_∞ controller in the frequency domain and to apply it for the position control of an electromechanical control actuation system with proportional-derivative (PD) type controller using data obtained from closed loop tests. Coefficients of the fixed-order linearly parametrized H_∞ controller are calculated using closed-loop input-output data without the need of a parametric model of the system. In place of high-order controllers that are obtained by using the classical H_∞ control theory, low-order controllers can be synthesized with the same design constraints with the proposed method. Closed-loop identification of the generalized plant makes our method very useful for systems that are unstable, motion constrained or system with high safety requirements or unreachable feedback loop. The proposed method has been verified using an experimental system where the position control of an electromechanical CAS is performed where a PD type position controller synthesis implemented with the developed method.

5.1 Derivation of the Nominal Performance Conditions

Linearly parameterized fixed-order controllers can also be written as

$$K(s,k) = k\psi(s) \tag{5.1}$$

with the vector of parameters of structured controller defined as

$$k = diag([k_0, k_1, k_2, \ldots, k_n]) \in \mathbb{R}^{(n+1)\times(n+1)} \tag{5.2}$$

and the vectors of stable orthogonal basis functions defined as

$$\psi(s) = diag([1, \psi_1(s), \psi_2(s), \ldots, \psi_n(s)]). \tag{5.3}$$

The continuous-time PID controller is realized in linearly parameterized form as fol-

lows:

$$K_{PID}(s) = \begin{bmatrix} K_p & 0 & 0 \\ 0 & K_i & 0 \\ 0 & 0 & K_d \end{bmatrix} \begin{bmatrix} 1 & 0 & 0 \\ 0 & \frac{1}{s} & 0 \\ 0 & 0 & \frac{s}{1+\tau_d s} \end{bmatrix}, \tag{5.4}$$

where $\tau_d \in \mathbb{R}_+$ and assumed to be known. Based on these linear parameterized controller assumption, the control signal may be defined as follows.

$$u = \begin{bmatrix} k_0 & 0 & \dots & 0 \\ 0 & k_1\psi_1(s) & \dots & 0 \\ \vdots & \vdots & \ddots & \vdots \\ 0 & 0 & \dots & k_n\psi_n(s) \end{bmatrix} e \tag{5.5}$$

The general control configuration can be modified as in Figure. 5.1, with the generalized plant given in (2.46).

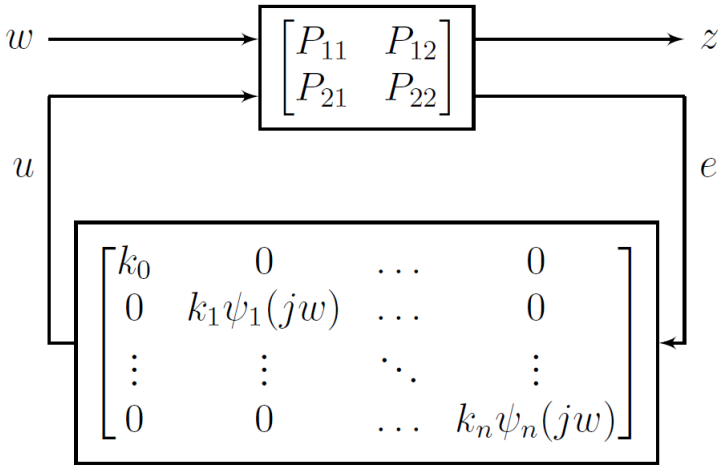

Figure. 5.1. General control configuration with the diagonal control matrix.

Definition 5.1. ***(Nominal stability)*** *The closed-loop SISO system in Figure. 5.1 with the given set of generalized plant P in (2.46) and the diagonally parameterized controller K is nominally stable if and only if*

$$Q_s(k, jw) = det\left(I - P_{22} \begin{bmatrix} k_0 & \dots & 0 \\ \vdots & \ddots & \vdots \\ 0 & \dots & k_n\psi_n \end{bmatrix} \right) \tag{5.6}$$

function does not encircle the origin of the complex plane for $\forall w$.

Definition 5.2. ***(Nominal performance)*** *The closed-loop SISO system in Figure. 5.2 with the given set of generalized plant* P *in (2.46) and the diagonally parameterized controller* K *and* $\|\Delta_P(jw)\|_\infty \leq 1$ *satisfies the nominal performance requirement if and only if*

$$Q_p(k, \Delta_P, jw) = det\left(I - \begin{bmatrix} P_{11} & P_{12} \\ P_{21} & P_{22} \end{bmatrix} \left[\begin{array}{c|ccc} \Delta_P & & 0 & \\ \hline & k_0 & \dots & 0 \\ 0 & \vdots & \ddots & \vdots \\ & 0 & \dots & k_n\psi_n \end{array}\right] \right) \tag{5.7}$$

function does not encircle the origin of the complex plane for $\forall w, \forall \Delta_P(jw) \in \mathbb{C}^{n_w \times n_z}$ *[32].*

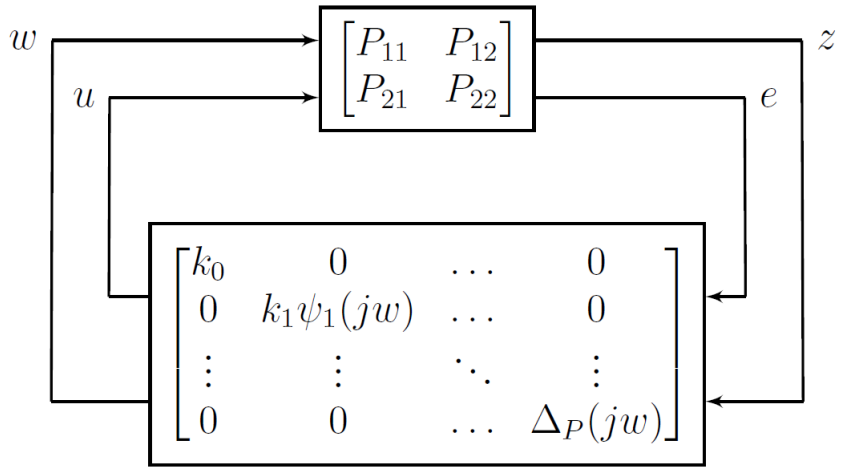

Figure. 5.2. Control configuration with performance channel.

5.2 Optimization Problem

Based on nominal stability and performance requirements, the fixed-order H_∞ control problem can be formulated on the Nyquist plot to calculate the parameters of the controller. The fact that polynomials $Q_s(k, jw)$ and $Q_p(k, jw)$ do not encircle the origins of the Nyquist plot constitutes the constraint function of the optimization problem. This constraint function can be adapted to the control problem by preventing the critical point of the Nyquist curve with a frequency dependent line.

The closed-loop SISO feedback system in Figure. 2.8 satisfies the nominal stability condition if $Q_s(k, jw)$ lies below the line $y = \alpha x + \beta$ on the Nyquist plot, Figure. 5.3.

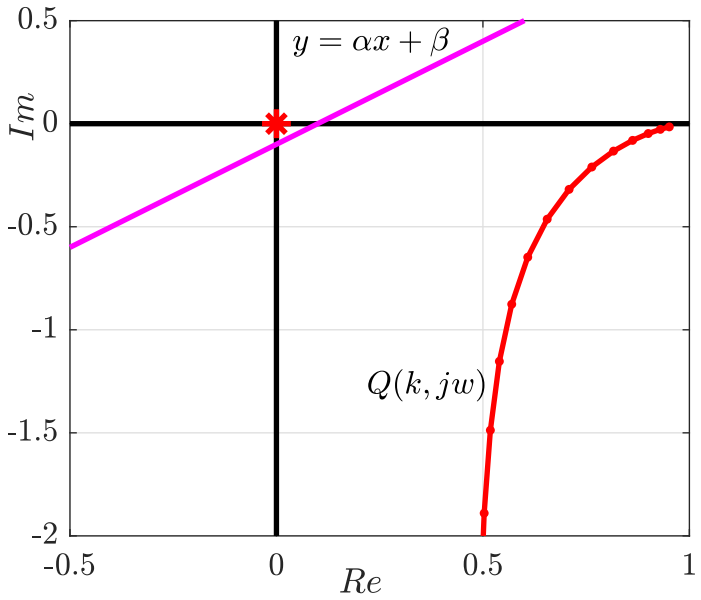

Figure. 5.3. Nyquist plot for $Q_s(k, jw)$.

Parameters of this line may be defined with respect to the requirements of the gain margin and phase margin [65]. Choosing the α and β parameters affects the stability and performance characteristics of the system. For example, if $\alpha = 1$ and $\beta = -0.1$, a gain of approximately 2 dB gain margin and 45 degree phase margin is guaranteed. Controller design optimization problem with this constraint function is given by

$$\begin{aligned} \min_{k} \quad & \|T_{z\omega}(k, jw)\|_\infty \\ \text{s.t.} \quad & \Im(Q_s(k, jw)) - \alpha_s \Re(Q_s(k, jw)) - \beta_s \quad \leq \quad 0. \end{aligned} \tag{5.8}$$

Similarly, this system satisfies the nominal performance condition if $Q_p(k, jw)$ below the line $y = \alpha x + \beta$ in the Nyquist plot. In this case, controller design optimization problem defined as

$$\begin{aligned} \min_{k} \quad & \|T_{z\omega}(k, jw)\|_\infty \\ \text{s.t.} \quad & \Im(Q_p(k, jw)) - \alpha_p \Re(Q_p(k, jw)) - \beta_p \quad \leq \quad 0 \end{aligned} \tag{5.9}$$

where $\Im, \Re$ represent the imaginary and real parts of the complex numbers, respec-

tively.

These optimization problems are non-convex and contain an infinite number constraints which is known as SIP. To convert the data-driven fixed-order H_∞ control design problem, (5.8), (5.9), into SDP problem, which can be solved numerically with available solvers, finite number of frequencies $w_i (i = 1, 2, \dots m)$ are considered. Hence, control design problem may be defined in the following equations for stability and performance requirements, respectively.

$$\begin{aligned} \min_{k} \max_{i} \quad & |T_{z\omega}(k, jw_i)| \\ \text{s.t.} \quad & \Im(Q_s(k, jw_i)) - \alpha_s \Re(Q_s(k, jw_i)) - \beta_s \quad \leq \quad 0 \end{aligned} \tag{5.10}$$

$$\begin{aligned} \min_{k} \max_{i} \quad & |T_{z\omega}(k, jw_i)| \\ \text{s.t.} \quad & \Im(Q_p(k, jw_i)) - \alpha_p \Re(Q_p(k, jw_i)) - \beta_p \quad \leq \quad 0 \end{aligned} \tag{5.11}$$

5.3 Experimental implementation

In this section, the position control of an electromechanical CAS is performed in order to experimentally verify the proposed closed-loop system identification and control synthesis methods are discussed.

5.3.1 Non-parametric Identification of CAS

In the present study, the initial K controller which is used in closed-loop system identification studies, is a 4^{th} order model based H_∞ controller designed and explained in [59] with transfer function given by

$$K(s) = \frac{10^6(1.11s^3 + 25.7s^2 + 172s + 33.4)}{s^4 + 10^8(0.2s^3 + 114s^2 + 182s + 884)} \tag{5.12}$$

with H_∞ cost $\gamma = 0.95$. The experimental test setup is the same as Figure. 3.8. During the experiments, the width of Hanning window is designed as a function of frequency and is chosen as 2.4 up to 15 Hz and 3.8 for higher frequencies. Controller is digitalized by using bilinear transformation method and implemented to the real time system by operated at 1 kHz frequency. For the closed-loop identification of

CAS, a chirp input signal with frequency value between 0.01 Hz and 40 Hz is used. A time domain portion of the chirp reference input signal and the measured output signal are presented in Figure. 5.4. The generated control input signal by the initial H_∞ controller in the closed-loop system is also shown in the same figure.

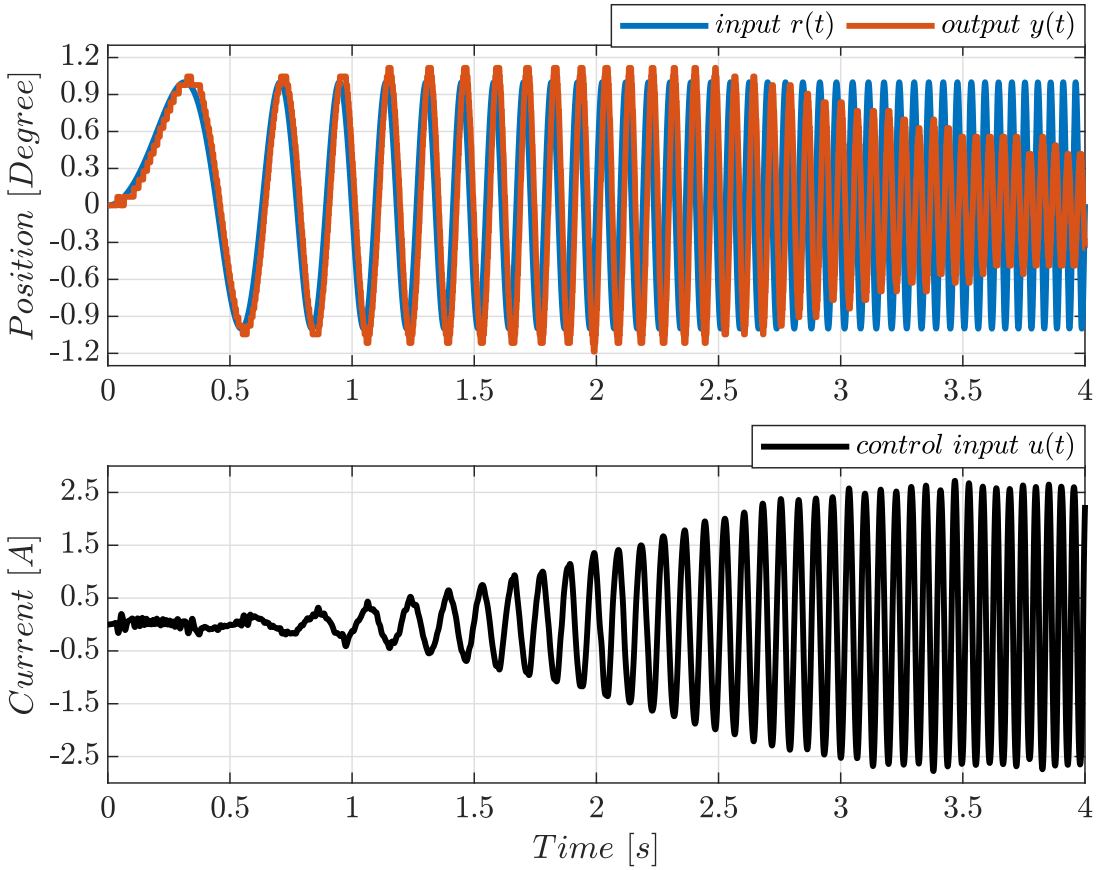

Figure. 5.4. Input, measured output and control signal.

Calculated magnitude and phase plots of $G(jw)$ via direct approach of closed-loop identification method are shown in Figure Figure. 5.5, respectively.

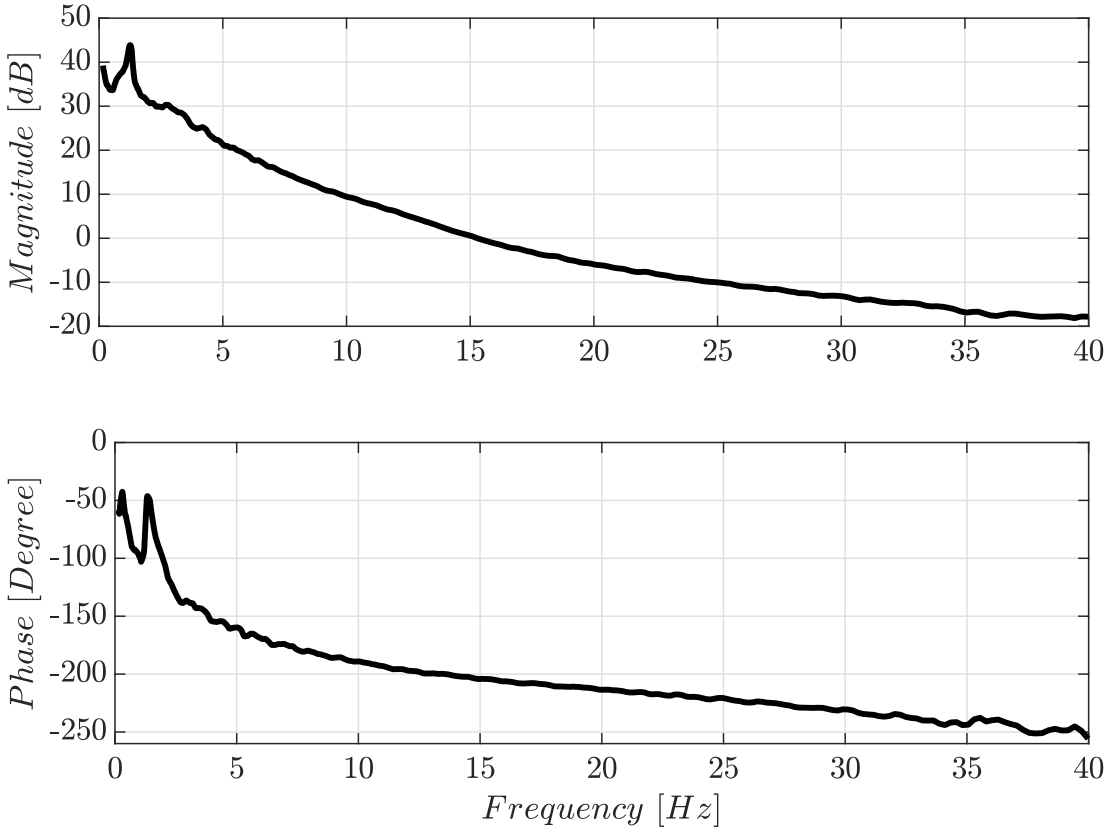

Figure. 5.5. Obtained Bode plot of the CAS.

5.3.2 PD Controller Synthesis for CAS

In this subsection, the presented approach in previous sections is applied on the position control of CAS to calculate PD type controller parameters using the obtained data from closed-loop tests.

The block diagram of the closed loop system that is used for the data-driven PD controller synthesis for the CAS is shown in Figure. 5.6. The control objective is to track the reference position command with admissible error bound and also with actuator limit constraint.

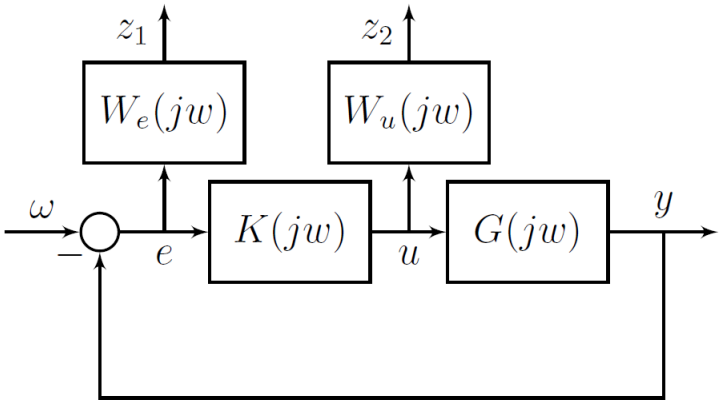

Figure. 5.6. Configuration of the control problem for the CAS.

The PD controller is generated using the proportional and derivative parts in (5.4) as

$$K(k, jw) = \begin{bmatrix} K_p & 0 \\ 0 & K_d \end{bmatrix} \begin{bmatrix} 1 & 0 \\ 0 & \dfrac{jw}{1 + jw\tau_d} \end{bmatrix} \tag{5.13}$$

where K_p and K_d are the controller parameters to be calculated by optimization methods. The parameter τ_d, which is in the denominator of the controller equation, is fixed as 100.

The data-driven fixed-order H_∞ control design problem for the CAS is configured using the block diagram given in Figure. 5.7.

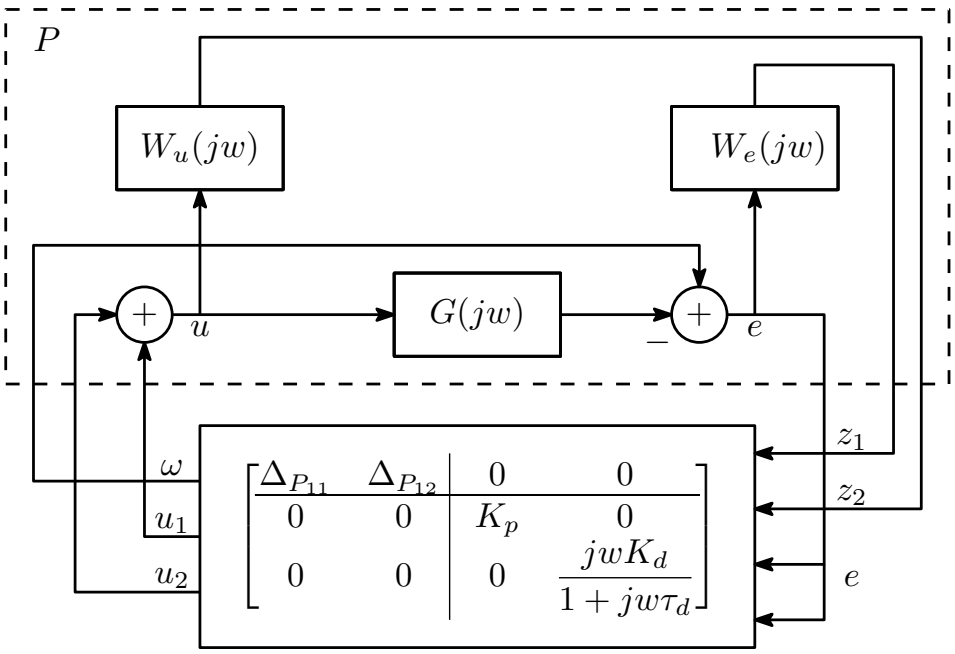

Figure. 5.7. Modification of the control problem for nominal performance criterion.

In this figure, the generalized plant P represents the transfer function from $\begin{bmatrix}\omega & u_1 & u_2\end{bmatrix}^{\mathrm{T}}$ to $\begin{bmatrix}z_1 & z_2 & e & e\end{bmatrix}^{\mathrm{T}}$ and can be partitioned as follows,

$$P(k,jw)=\left[\begin{array}{c|cc}P_{11}&P_{12}\\\hline P_{21}&P_{22}\end{array}\right]=\left[\begin{array}{c|cc}We&-GW_e&-GW_e\\\hline 0&W_u&W_u\\I&-G&-G\\I&-G&-G\end{array}\right]. \tag{5.14}$$

$W_e(jw)$ and $W_u(jw)$ shown in these figures are the frequency-dependent weighting functions representing the performance requirements defined on the error and control signal outputs, respectively. A proper selection of these performance weighting filters are given by

$$W_e(jw)=\frac{0.71jw+50.27}{jw+87.73} \tag{5.15}$$

$$W_u(jw)=\frac{0.11jw+85.96}{jw+175.92}. \tag{5.16}$$

The $K_\Delta(k,jw)$ matrix consisting of the Δ_P components between the inputs and

outputs in the performance channel and the diagonal control matrix is formed as follows.

$$K_{\Delta}(k,jw) = \left[\begin{array}{cc|cc} \Delta_{P_{11}} & \Delta_{P_{12}} & 0 & 0 \\ \hline 0 & 0 & K_p & 0 \\ 0 & 0 & 0 & \dfrac{jwK_d}{1+jw\tau_d} \end{array}\right] \tag{5.17}$$

The transfer function of $T_{z\omega}$ that represents the transfer function from reference input $[\omega]$ to performance outputs $\begin{bmatrix} z_1 & z_2 \end{bmatrix}^{\mathrm{T}}$ of the system, can be calculated with the LFT of $P(k,jw)$ and $K(k,jw)$ matrices and using (2.47) as

$$\begin{aligned} T_{z\omega}(k,jw) = &\begin{bmatrix} W_e \\ 0 \end{bmatrix} + \begin{bmatrix} -GW_e & -GW_e \\ W_u & W_u \end{bmatrix} \begin{bmatrix} K_p & 0 \\ 0 & \dfrac{jwK_d}{1+jw\tau_d} \end{bmatrix} \\ &\left[I_{2\times 2} - \begin{bmatrix} -G & -G \\ -G & -G \end{bmatrix} \begin{bmatrix} K_p & 0 \\ 0 & \dfrac{jwK_d}{1+jw\tau_d} \end{bmatrix} \right]^{-1} \begin{bmatrix} I \\ I \end{bmatrix} \end{aligned} \tag{5.18}$$

and given by

$$T_{z\omega}(k,jw) = \begin{bmatrix} W_e S \\ W_u K S \end{bmatrix} \tag{5.19}$$

where

$$\begin{aligned} S &= 1/(1 + GK_p + G\frac{jwK_d}{1+jw\tau_d}) \\ KS &= (K_p + \frac{jwK_d}{1+jw\tau_d}) \end{aligned} \tag{5.20}$$

The frequency-dependent expression of the closed-loop performance constrain function $Q_p(k,\Delta_P,jw)$ for two controller parameters, an exogenous input and two perfor-

mance outputs can be obtained by using (5.7) as follows.

$$\begin{aligned} Q_p(k,\Delta_P,jw) &= 1 + GK_p + G\frac{jwK_d}{1+jw\tau_d} \\ &-\Delta_{P_{11}}W_e - \Delta_{P_{12}}W_uK_p - \Delta_{P_{12}}W_u\frac{jwK_d}{1+jw\tau_d} \end{aligned} \tag{5.21}$$

During the controller synthesis, the Nyquist plot of $Q_p(k,\Delta_P,jw)$ is forced to lie beneath by the line $y=\alpha x+\beta$, where $\alpha=1,\beta=-0.1$. Controller design optimization problem with this constraint is formulated as

$$\begin{aligned} \min_k \max_i \quad & |T_{zw}(k,jw_i)| \\ \text{s.t.} \quad & \Im(Q_p(k,jw)) - \Re(Q_p(k,jw)) + 0.1 \quad \leq \quad 0 \end{aligned} \tag{5.22}$$

for a finite number of logarithmically separated frequencies $w_i = \begin{bmatrix} 0.1 & 200 \end{bmatrix} rad/s$ where $i=1,2,\ldots 200$. In this optimization problem, the performance part of $K_\Delta(k,jw)$ is realized by $n_p=40$ samples for each iteration of w_i with

$$\left\| \begin{bmatrix} \Delta_{P_{11}} & \Delta_{P_{12}} \end{bmatrix} \right\|_\infty = 1. \tag{5.23}$$

The optimization problem is solved by using the $fminimax$ function of MATLAB and coefficients of PD controller are obtained as $K_p=0.0278,\ K_d=0.0041$. The transfer function of the controller is given explicitly by

$$K(k,jw) = 0.0278 + 0.0041\frac{jw}{1+jw100}. \tag{5.24}$$

Transfer function of the $T_{zw}(k,jw)$ is calculated for each frequency point using (5.19) together with controller parameters. The Nyquist plot of the $Q_p(k,jw)$ function with obtained PD controller that is verify the nominal performance H_∞ cost with $\gamma = 0.82$, is shown in Figure. 5.8. As seen in this figure, the $Q_p(k,jw)$ function does not encircle the origin of the Nyquist plot. The $\gamma = 0.82$ value indicates that the closed-loop system together with the controller provides the nominal stability and performance requirements determined by the weighting functions.

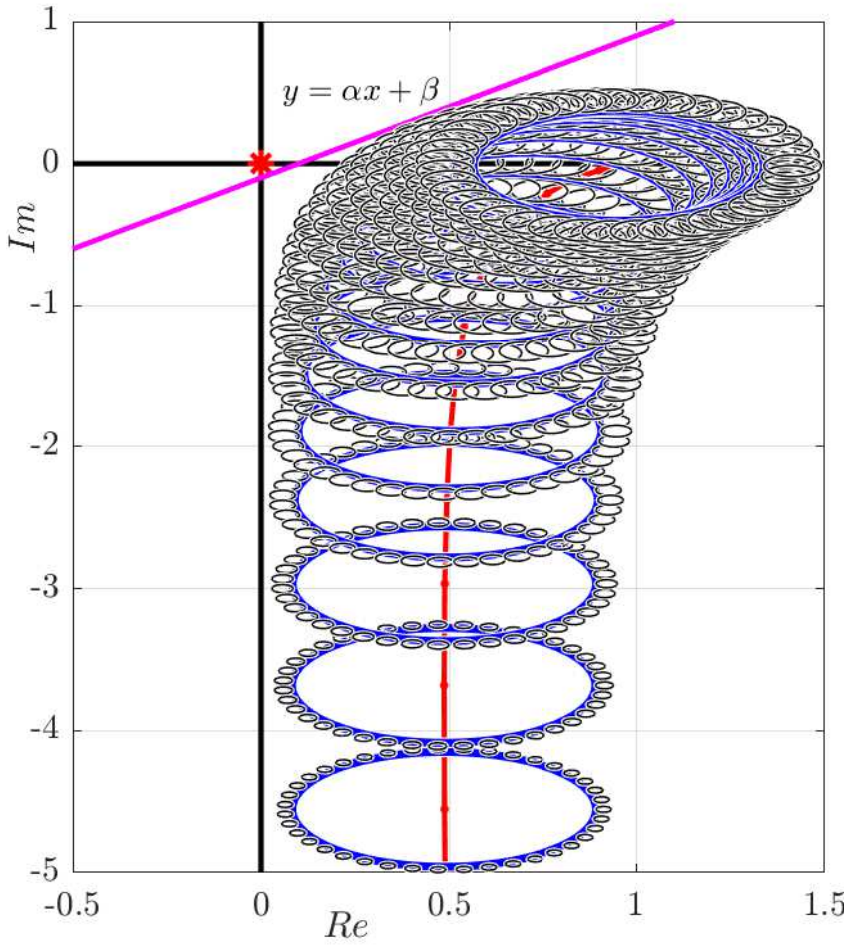

Figure. 5.8. Obtained Nyquist plot of $Q_p(k, jw)$ (green) and $Q_s(k, jw)$ (red).

Real-time hardware in the loop tests have been performed to verify the performance of the synthesized fixed-order H_∞ controller. This controller is applied to the experimental system in the real-time hardware in the loop tests. The step response of the system in time-domain is given in Figure. 5.9. As can be seen from this figure, the synthesized data-driven fixed-order PD type position controller provides the requirements specified by the weighting functions. In these tests the filtered step function is applied to the system to prevent sudden current consumption. As can be seen that the CAS position control, which requires precise positioning, indeed be designed in the frequency domain using a model-free, fixed-order, low-order PD controller.

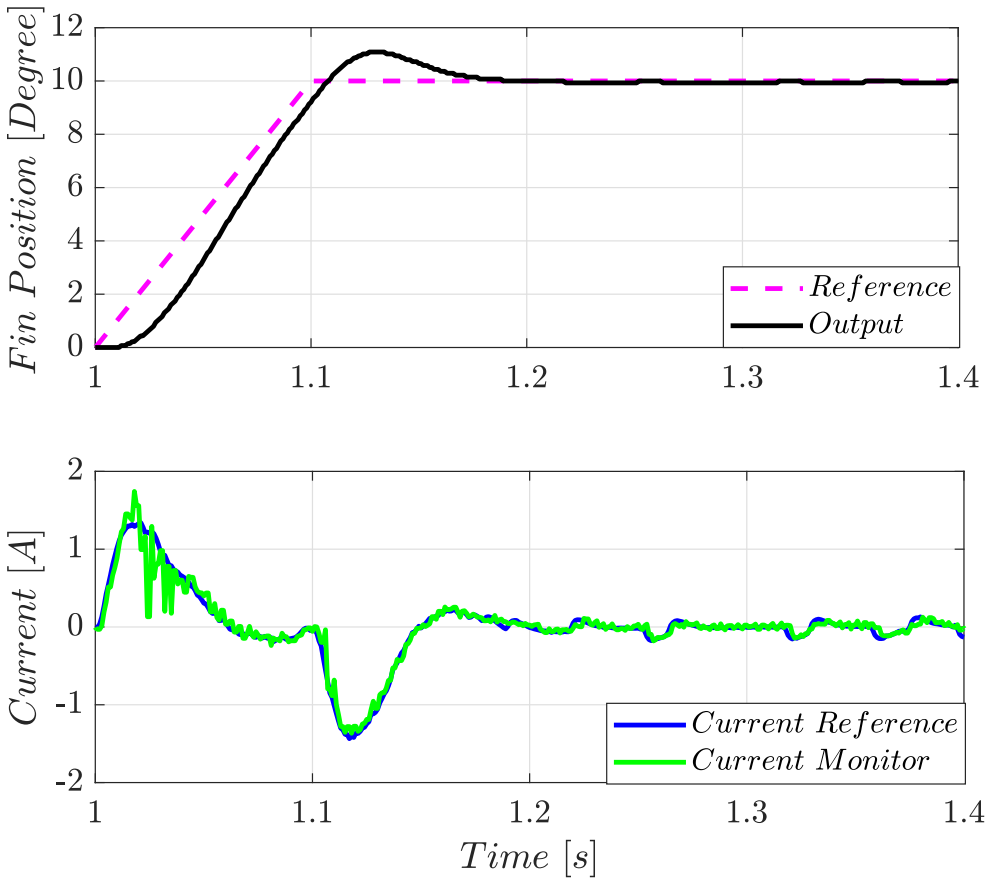

Figure. 5.9. Experimentally obtained CAS fin angle and applied control input (current) signal.

In order to determine the bandwidth of the closed loop system and to test the reference tracking performance, an increasing frequency sinusoidal chirp signal up to 20 Hz is applied as reference input to the system. The response of the system and applied control signal for this input with the synthesized PD controller is given in Figure. 5.10. As seen in this figure, the output position of the fin value is reaches 0.707 times the position command after about 3 seconds later. The bandwidth of the system is calculated as 15 Hz since each second interval corresponds to 5 Hz.

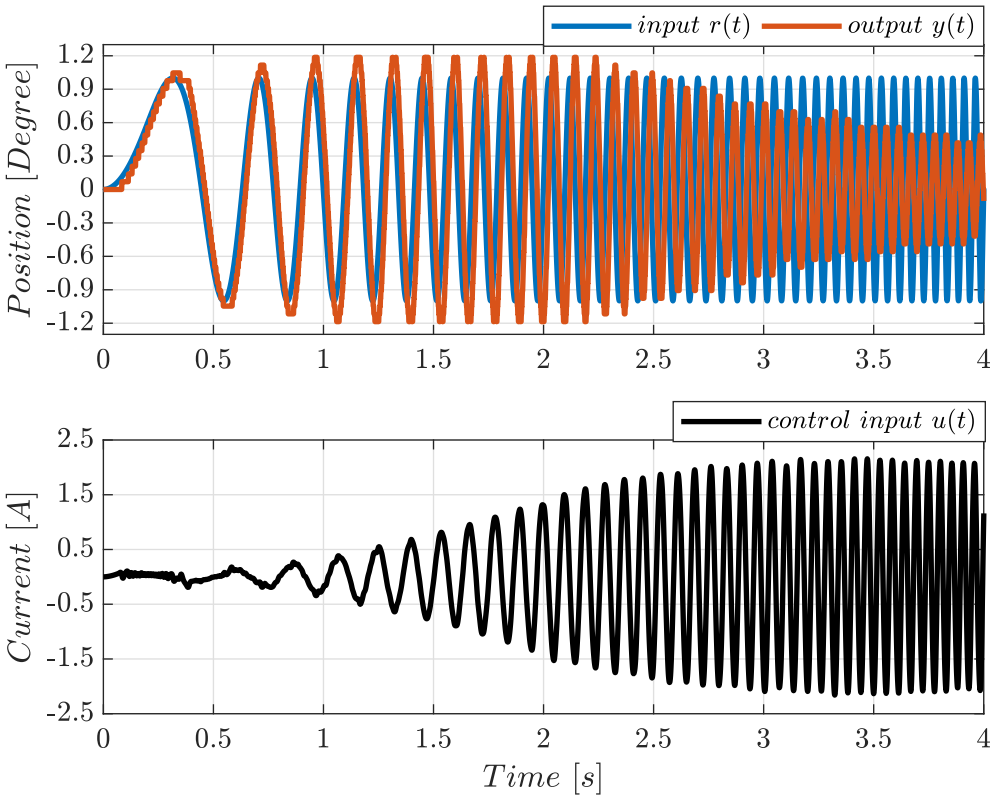

Figure. 5.10. Reference input, measured output and control input signal.

5.4 Comments

A new method to design data-driven fixed-order H_∞ controller for SISO systems with generalized plant obtained from closed-loop test and control parameters written in diagonal form is presented. In this method, the system to be controlled is represented with FRF data of the plant in the operating range of interest instead of a transfer function. The nominal stability and nominal performance conditions are derived together with the identified generalized plant and the linearly parameterized fixed-order controller structure. These design requirements are described on the Nyquist plot. Based on the user defined weighting functions, the fixed-order H_∞ controller design optimization problem is formulated on the Nyquist plot to calculate the parameters of the controller. The objective and constraint functions of this non-convex optimization problem are reduced to SDP form. Since adverse factors such as modelling errors, time delay are contained within the frequency-dependent data, the system representation is more accurate than the model-based approach. The effectiveness of the proposed method is verified using real-time hardware in the loop

test set-up where the position control of an electromechanical CAS is performed. PD type position controller synthesis for this system is realized by the developed method.

6. CONCLUSIONS AND FUTURE WORK SUGGESTIONS

In this section, the results obtained in the thesis, the main topics covered by the study and the future works are explained.

6.1 Conclusions

This thesis combines the model-free feature of the non-parametric frequency domain data-driven control methods and the practicality of the fixed-order methods within the convex optimization based H_∞ control problem for the design of linearly parameterized 1-DOF and 2-DOF controllers. Within the framework of data-driven control systems, robust fixed-order H_∞ controller synthesis problems have been addressed in this thesis. Convex optimization has been chosen as the optimization method and has been summarized in the second chapter of the thesis.

As already mentioned, classical unstructured uncertainty models are generally calculated from a set of frequency response data and resulting models may be considerably conservative. In order to represent the variations in the system dynamics by minimal uncertainty circle around the optimal nominal model for the corresponding frequency points, an SDP algorithm has been proposed. Since the modelling of unstructured uncertainty depends on a nominal model, this algorithm simultaneously computes a minimal uncertainty model while finding an optimal nominal model from the frequency domain experimental data. Therefore, variations in the system dynamics can be represented by minimal uncertainty circle around the optimal nominal model for the corresponding frequency points on the Nyquist diagram. Furthermore, since the frequency domain multiple model set includes the time delay, time-delay systems can be considered without any approximation in the proposed robust controller synthesis method by this algorithm.

The optimal nominal model and optimal multiplicative uncertainty function have been calculated using a semi-definite convex optimization method for electromechanical systems. This convex optimization problem has been solved using CVX solver. For comparison purposes, another nominal model has been calculated by the classical method. The classical uncertainty modelling approach has produced a considerably

more conservative weighting function model than the proposed optimal uncertainty modelling method. The obtained experimental results demonstrate that the proposed convex optimization based algorithm reduces the conservatism of uncertainty bound and consequently improves the robustness and performance of the closed-loop control system.

In this thesis, the cost function of the convex optimization problem has been formulated as a closed-loop model matching objective. The closed-loop model matching cost function has been approximated to a convex function using the FRF of the system and the linearly parameterized controllers. Therefore, experimental closed-loop frequency response matches a frequency response of the predefined reference model in the H_∞ norm sense. The linearly parameterized controllers for fixed-order controller structure have been modelled with stable orthogonal Laguerre basis functions. Thus, closed-loop transfer functions such as sensitivity function, complementary sensitivity function, Q-parameter transfer function have been modified as affine functions with respect to the Laguerre coefficients.

In this study, the saturation characteristics of the actuators have been included mathematically in the controller design algorithm. Therefore, the robust data-driven fixed-order H_∞ control design methodologies have been applied for linear systems with weighted control input constraints. Two inequality constraints have been added to the optimization based control design problem to account for actuator constraints in the convex optimization framework.

Since the model matching does not guarantee internal stability, a novel sufficient condition for robust performance constraints of 1-DOF and 2-DOF control systems using Nyquist stability theorem and μ synthesis methods has been derived and has been represented by a convex constraint on the Nyquist plot. The robust performance constraint has been adapted to the data-driven robust H_∞ control problem by preventing the intersection of performance and uncertainty circles via a frequency dependent line. In order to represent the robust performance condition as a convex constraint in the optimization problem, parameters of this line have been defined with respect to the desired loop gain model. The robust stability, nominal performance and nominal stability conditions have also been modified using this

approximation. This approach is the most important contribution of this thesis study to the literature.

The choice of a predefined reference model for closed-loop model matching objective and performance weighting function is a crucial step of the proposed controller design algorithm. Therefore, a practical approximation to a feasible choice of this user-defined functions has been suggested. The formulated optimization problem has involved an infinite number of constraints, i.e., SIP problem. In order to transform this SIP problem into SDP problem, a finite number of frequency points have been considered. Moreover, a randomized scenario approach has been adapted to compute the minimum number of frequency point to guarantee the constraints with a chosen probability level.

In the third chapter of this thesis, a path has been charted out on how to implement data-driven control method and controller design problem has been turned into an algorithm step by step. In this context, a 1-DOF robust data-driven fixed-order H_∞ controller synthesis method based on convex optimization has been presented. This method has consisted of two main steps. First, the non-parametric frequency response identification of system with minimal unstructured uncertainty model has been obtained from multiple measurement data. Second, the formulation of a fixed-order H_∞ controller design algorithm by using linearly parameterized controller structure have been given. Proposed controller design methodology has been applied to the position control of an electromechanical TVC system. The resulting robust controller has been shown to satisfy the robust performance condition and control input constraints. For comparison purpose, the performance of the presented method is compared with the available FDRC toolbox on the experimental TVC system test setup. The robust performance achievement of the controller obtained by this toolbox has been worse than the robust performance achievement of the proposed data-driven controller.

An extension of the 1-DOF controller design algorithm has been proposed in Chapter 4 to synthesize 2-DOF controllers for reference tracking of the non-parametric systems. A fixed-order 2-DOF robust controller design framework based on constrained convex optimization problem has been introduced with a closed-loop model

matching objective and control input constraints for the non-parametric perturbed model in the frequency domain. The theoretical design approach has been experimentally verified on the full-closed loop feedback position control of an electromechanical CAS system. The synthesized data-driven fixed-order position controllers for CAS has achieved the required model matching objective. Experimental results have revealed that the goal of designing a robust 2-DOF data-driven fixed-order controller in the frequency domain for precise positioning systems can be achieved by using the proposed approach, under the same performance requirements. Moreover, the designed 2-DOF robust controller has improved the tracking performance and closed-loop system bandwidth of the TVC system when compared to the 1-DOF design method. The obtained 2-DOF controller has also satisfied the weighted control input constraints.

In Chapter 5, a new non-convex optimization based method to design data-driven fixed-order H_∞ controller for non-parametric SISO systems has been presented. This method does not depend on any approximation of objective function and the generalized plant is identified by using experimental data obtained from closed-loop tests which are not treated in other data-driven controller synthesis methods. The coefficients of the linearly parametrized controller have been written in diagonal form. Multiple desired performance specifications such as weighted error shaping and weighted control input constraints have been considered as constraint functions in the optimization problem. In order to satisfy the stability and performance requirements, an SDP non-convex optimization problem has been formulated. The proposed algorithm has been verified experimentally with application to the control of electromechanical TVC system and CAS. A closed-loop system identification technique has been applied to FRF estimation of the experimental CAS. This identified model has been used to synthesize a data-driven PD controller using proposed fixed-order H_∞ controller design approach. The obtained PD controller has been implemented on the position control of electromechanical CAS. This controller has achieved the requirements specified by the weighting functions. The obtained test results have shown that the position control of the CAS, which requires precise positioning, can be designed in the frequency domain using a model-free PD controller.

6.2 Future Works

There are future research work directions that can be proposed as extensions to the presented controller synthesis approach:

- In this thesis, a fixed-order H_∞ controller synthesis algorithm for non-parametric SISO systems is introduced by using linearly parameterized controllers. To make the data-driven structured H_∞ approach more applicable, the presented methods can be extended to rational controllers, i.e., numerator and denominators having coefficients as decision variables. Moreover, the development of a new necessary and sufficient conditions for robust performance criteria would be useful.

- In this study, the pole of the Laguerre basis function is chosen by a linear search. Therefore, the optimal choice of this basis functions is an important extension of presented controller synthesis approaches.

- The defined optimization problems involve an infinite number of constraints which constitute an SIP problem. To transform this SIP problem into and SDP problem, which can be solved numerically using available convex optimization techniques and solvers, another frequency gridding method solving the fixed-order control problem with a finite number of frequency points can be considered as an alternative method to scenario approach.

- All of the proposed data-driven controller synthesis methods in this thesis are based on frequency domain data. Thus, an extension of these methods to time-domain data-driven fixed-order robust controller design methods would be useful.

- In order to reduce conservatism of the H_∞ controller, data-driven fixed-order H_∞ controller with gain scheduling can be considered as future work.

- In this study, we assume that the systems are stable. Therefore, the development of the proposed methods that can be useful for unstable systems would be a prospective study.

- Additionally, the presented approach can be extended to MIMO systems. Especially, the proposed approach in Chapter 5 can be applied to MIMO systems with some modifications.

REFERENCES

[1] Nyquist, Harry, Regeneration theory, *Bell system technical journal*, 11, 1, 126–147, 1932.

[2] Zames, George, Feedback and optimal sensitivity: Model reference transformations, multiplicative seminorms, and approximate inverses, *IEEE Transactions on automatic control*, 26, 2, 301–320, 1981.

[3] Mayr, Otto, The origins of feedback control, *Scientific American*, 223, 4, 110–119, 1970.

[4] Hou, Zhong-Sheng, Wang, Zhuo, From model-based control to data-driven control: Survey, classification and perspective, *Information Sciences*, 235, 3–35, 2013.

[5] Doyle, John C, Glover, Keith, Khargonekar, Pramod P, Francis, Bruce A, State-space solutions to standard H_2 and H_∞ control problems, *IEEE Transactions on Automatic control*, 34, 8, 831–847, 1989.

[6] Gahinet, Pascal, Apkarian, Pierre, A linear matrix inequality approach to H_∞ control, *International journal of robust and nonlinear control*, 4, 4, 421–448, 1994.

[7] Skogestad, Sigurd, Postlethwaite, Ian, *Multivariable feedback control: Analysis and design*, 2, Wiley New York, 2007.

[8] Lee, Chibum, Salapaka, Srinivasa M, Voulgaris, Petros G, Two degree of freedom robust optimal control design using a linear matrix inequality optimization, in *Proceedings of the 48h IEEE Conference on Decision and Control (CDC) held jointly with 2009 28th Chinese Control Conference*. IEEE, 714–719, 2009.

[9] Yin, Shen, Li, Xianwei, Gao, Huijun, Kaynak, Okyay, Data-based techniques focused on modern industry: An overview, *IEEE Transactions on Industrial Electronics*, 62, 1, 657–667, 2015.

[10] Hou, Zhongsheng, Jin, Shangtai, *Model free adaptive control: Theory and applications*, CRC press, 2013.

[11] Safonov, Michael G, Tsao, Tung-Ching, The unfalsified control concept and learning, in *Decision and Control, 1994., Proceedings of the 33rd IEEE Conference on*. IEEE, 3, 2819–2824, 1994.

[12] Hjalmarsson, Håkan, Iterative feedback tuning-an overview, *International journal of adaptive control and signal processing*, 16, 5, 373–395, 2002.

[13] Karimi, A, Mišković, L, Bonvin, D, Iterative correlation-based controller tuning, *International journal of adaptive control and signal processing*, 18, 8, 645–664, 2004.

[14] Campi, Marco C, Lecchini, Andrea, Savaresi, Sergio M, Virtual reference feedback tuning: a direct method for the design of feedback controllers, *Automatica*, 38, 8, 1337–1346, 2002.

[15] Van Heusden, Klaske, Karimi, Alireza, Bonvin, Dominique, Data-driven model reference control with asymptotically guaranteed stability, *International Journal of Adaptive Control and Signal Processing*, 25, 4, 331–351, 2011.

[16] Bristow, Douglas A, Tharayil, Marina, Alleyne, Andrew G, A survey of iterative learning control, *IEEE Control Systems*, 26, 3, 96–114, 2006.

[17] Bontempi, Gianluca, Birattari, Mauro, Bersini, Hugues, Lazy learning for local modelling and control design, *International Journal of Control*, 72, 7-8, 643–658, 1999.

[18] Erol, Bilal, Delibaşı, Akın, Proportional–integral–derivative type H_∞ controller for quarter car active suspension system, *Journal of Vibration and Control*, 24, 10, 1951–1966, 2018.

[19] Menezes, Eduardo FM, Aguiar, Raquel SS, Simões, Alberto M, Apkarian, Pierre, Structured robust controller design via non-smooth mixed μ synthesis, *IET Control Theory & Applications*, 10, 17, 2186–2193, 2016.

[20] Maruta, Ichiro, Kim, Tae-Hyoung, Sugie, Toshiharu, Fixed-structure H_∞ controller synthesis: A meta-heuristic approach using simple constrained particle swarm optimization, *Automatica*, 45, 2, 553–559, 2009.

[21] Hara, Shinji, Iwasaki, Tetsuya, Shiokata, Daisuke, Robust PID control using generalized KYP synthesis: Direct open-loop shaping in multiple frequency ranges, *IEEE Control systems magazine*, 26, 1, 80–91, 2006.

[22] Lim, Jae Sik, Ryoo, Jung Rae, Lee, Young Il, Son, Sung Yong, Design of a fixed-order controller for the track-following control of optical disc drives, *IEEE Transactions on Control Systems Technology*, 20, 1, 205–213, 2011.

[23] Wang, Shaopeng, Chow, Joe H, Low-order controller design for SISO systems using coprime factors and LMI, *IEEE Transactions on Automatic Control*, 45, 6, 1166–1169, 2000.

[24] Boyd, Stephen, Hast, Martin, Åström, Karl Johan, MIMO PID tuning via iterated LMI restriction, *International Journal of Robust and Nonlinear Control*, 26, 8, 1718–1731, 2016.

[25] Yang, Fuwen, Gani, Mahbub, Henrion, Didier, Fixed-order robust H_∞ controller design with regional pole assignment, *IEEE Transactions on Automatic Control*, 52, 10, 1959–1963, 2007.

[26] Grimholt, Chriss, Skogestad, Sigurd, Optimization of fixed-order controllers using exact gradients, *Journal of Process Control*, 71, 130–138, 2018.

[27] Gahinet, Pascal, Apkarian, Pierre, Structured H_∞ synthesis in matlab, *IFAC Proceedings Volumes*, 44, 1, 1435–1440, 2011.

[28] Burke, James V, Henrion, Didier, Lewis, Adrian S, Overton, Micheal L, Hifoo-a matlab package for fixed-order controller design and H_∞ optimization, *IFAC Proceedings Volumes*, 39, 9, 339–344, 2006.

[29] Horowitz, Isaac, Survey of quantitative feedback theory (QFT), *International Journal of Robust and Nonlinear Control: IFAC-Affiliated Journal*, 11, 10, 887–921, 2001.

[30] Karimi, Alireza, Kunze, Marc, Longchamp, Roland, Robust controller design by linear programming with application to a double-axis positioning system, *Control Engineering Practice*, 15, 2, 197–208, 2007.

[31] Karimi, Alireza, Galdos, Gorka, Fixed-order H_∞ controller design for non-parametric models by convex optimization, *Automatica*, 46, 8, 1388–1394, 2010.

[32] van Solingen, E, van Wingerden, JW, Oomen, Tom, Frequency-domain optimization of fixed-structure controllers, *International Journal of Robust and Nonlinear Control*, 28, 12, 3784–3805, 2018.

[33] Khadraoui, Sofiane, Nounou, Hazem, Nounou, Mohamed, Datta, Aniruddha, Bhattacharyya, Shankar P, A model-free design of reduced-order controllers and application to a DC servomotor, *Automatica*, 50, 8, 2142–2149, 2014.

[34] Khadraoui, Sofiane, Nounou, Hazem N, Nounou, Mohamed N, Datta, Aniruddha, Bhattacharyya, Shankar P, A measurement-based approach for designing fixed-order controllers for unknown closed-loop architecture, *Asian Journal of Control*, 18, 2, 686–698, 2016.

[35] Mercader, Pedro, Åström, Karl Johan, Banos, Alfonso, Hägglund, Tore, Robust PID design based on QFT and convex–concave optimization, *IEEE Transactions on Control Systems Technology*, 25, 2, 441–452, 2016.

[36] Nicoletti, Achille, Martino, Michele, Karimi, Alireza, A robust data-driven controller design methodology with applications to particle accelerator power converters, *IEEE Transactions on Control Systems Technology*, 27, 2, 814–821, 2018.

[37] Xie, Yangmin, Wang, Chao, Shi, Hang, Shi, Junwei, A data driven control method for structure vibration suppression, *Acta Astronautica*, 143, 302–309, 2018.

[38] Xie, Yangmin, Shi, Hang, Bi, Fengxia, Shi, Junwei, A MIMO data driven control to suppress structural vibrations, *Aerospace Science and Technology*, 77, 429–438, 2018.

[39] Khadraoui, Sofiane, Nounou, Hazem, A nonparametric approach to design fixed-order controllers for systems with constrained input, *International Journal of Control, Automation and Systems*, 16, 6, 2870–2877, 2018.

[40] Apkarian, P, Noll, D, Structured H_∞-control of infinite-dimensional systems, *International Journal of Robust and Nonlinear Control*, 28, 9, 3212–3238, 2018.

[41] Zhou, Kemin, Doyle, John Comstock, *Essentials of robust control*, 104, Prentice hall Upper Saddle River, NJ, 1998.

[42] Poussot-Vassal, Charles, *Large-scale dynamical model approximation and its applications*, Ph.D. thesis, 2019.

[43] Nalbantoglu, Volkan, Robust control and system identification for flexible structures., 1999.

[44] Akçay, Hüseyin, Ninness, Brett, Orthonormal basis functions for modelling continuous-time systems, *Signal processing*, 77, 3, 261–274, 1999.

[45] Wang, Liuping, Discrete model predictive controller design using Laguerre functions, *Journal of process control*, 14, 2, 131–142, 2004.

[46] Ljung, Lennart, System identification," in *Signal analysis and prediction*, 163–173. Springer, 1998.

[47] Forssell, Urban, Ljung, Lennart, Closed-loop identification revisited, *Automatica*, 35, 7, 1215–1241, 1999.

[48] Nalbantoğlu, Volkan, Bokor, Jozsef, Balas, Gary, Gaspar, Peter, System identification with generalized orthonormal basis functions: an application to flexible structures, *Control Engineering Practice*, 11, 3, 245–259, 2003.

[49] Boyd, Stephen, Vandenberghe, Lieven, *Convex optimization*, Cambridge university press, 2004.

[50] Beck, Amir, *Introduction to nonlinear optimization: Theory, algorithms, and applications with MATLAB*, 19, Siam, 2014.

[51] Venkataraman, Panchapakesan, *Applied optimization with MATLAB programming*, John Wiley & Sons, 2009.

[52] Toscano, Rosario, *Structured controllers for uncertain systems*, Springer, 2013.

[53] Karimi, Alireza, Frequency-domain robust control toolbox, in *52nd IEEE Conference on Decision and Control*. IEEE, 3744–3749, 2013.

[54] Doyle, John C, Francis, Bruce A, Tannenbaum, Allen R, *Feedback control theory*, Courier Corporation, 2013.

[55] Tu, Yi-Wei, Ho, Ming-Tzu, Robust second-order controller synthesis for model matching of interval plants and its application to servo motor control, *IEEE Transactions on Control Systems Technology*, 20, 2, 530–537, 2011.

[56] Campi, Marco C, Garatti, Simone, *Introduction to the Scenario Approach*, 26, SIAM, 2018.

[57] Lu, Hao, Li, Yunhua, Zhu, Chenglin, Robust synthesized control of electromechanical actuator for thrust vector system in spacecraft, *Computers & Mathematics with Applications*, 64, 5, 699–708, 2012.

[58] Baskin, Mehmet, Leblebicioğlu, Mehmet Kemal, Robust control for line-of-sight stabilization of a two-axis gimbal system, *Turkish Journal of Electrical Engineering & Computer Sciences*, 25, 5, 3839–3853, 2017.

[59] Daş, Ersin, Delice, İsmail İlker, Keleş, Murat, Analysis and robust position control of an electromechanical control actuation system, *Transactions of the Institute of Measurement and Control*, 0142331218813421, 2018.

[60] Wang, Can, Yang, Ming, Zheng, Weilong, Hu, Kun, Xu, Dianguo, Analysis and suppression of limit cycle oscillation for transmission system with backlash nonlinearity, *IEEE transactions on Industrial Electronics*, 64, 12, 9261–9270, 2017.

[61] Kim, Sang Hwa, Tahk, Min-Jea, Modeling and experimental study on the dynamic stiffness of an electromechanical actuator, *Journal of Spacecraft and Rockets*, 708–719, 2016.

[62] Grant, Michael, Boyd, Stephen, CVX: Mablab software for disciplined convex programming, version 2.1, 2014.

[63] Lee, Chibum, Mohan, Gayathri, Salapaka, Srinivasa, 2DOF control design for nanopositioning," in *Control Technologies for Emerging Micro and Nanoscale Systems*, 67–82. Springer, 2011.

[64] Peng, Chao, Han, Chongwei, Zou, Jianxiao, Zhang, Guanghui, H_∞ optimal inversion feedforward and robust feedback based 2DOF control approach for high speed-precision positioning systems, *Journal of Control Science and Engineering*, 2016, 3, 2016.

[65] Daş, Ersin, Çağlar Başlamışlı, Selahattin, Data-driven fixed-order H_∞ controller synthesis in frequency domain: Closed-loop system approach, *Transactions of the Institute of Measurement and Control*, 0142331219847741, 2019.